ENVIRONMENTAL HEALTH SERIES
Air Pollution

PILOT STUDY OF ULTRAVIOLET RADIATION IN LOS ANGELES OCTOBER 1965

U. S. DEPARTMENT OF HEALTH, EDUCATION, AND WELFARE
Public Health Service

PILOT STUDY OF ULTRAVIOLET RADIATION IN LOS ANGELES OCTOBER 1965

A Report on Concurrent Measurements Made by
Cooperating Organizations by Various Methods

Edited by John S. Nader

Control Technology Research and Development Programs

U. S. DEPARTMENT OF HEALTH, EDUCATION, AND WELFARE

Public Health Service
National Center for Air Pollution Control
Cincinnati, Ohio
1967

The ENVIRONMENTAL HEALTH SERIES of reports was established to report the results of scientific and engineering studies of man's environment: The community, whether urban, suburban, or rural, where he lives, works, and plays; the air, water and earth he uses and reuses; and the wastes he produces and must dispose of in a way that preserves these natural resources. This SERIES of reports provides for professional users a central source of information on the intramural research activities of the Centers in the Bureau of Disease Prevention and Environmental Control, and on their cooperative activities with State and local agencies, research institutions, and industrial organizations. The general subject area of each report is indicated by the letters that appear in the publication number; the indicators are

AP - Air Pollution

RH - Radiological Health

UIH Urban and Industrial Health

Triplicate tear-out abstract cards are provided with reports in the SERIES to facilitate information retrieval. Space is provided on the cards for the user's accession number and additional key words.

Reports in the SERIES will be distributed to requesters, as supplies permit. Requests should be directed to the Center identified on the title page.

Public Health Service Publication No. 999-AP-38

ACKNOWLEDGMENT

The Public Health Service acknowledges the contributions of the cooperating participants to this study of ultraviolet radiation in Los Angeles. Appreciation for assistance in executing the study is expressed to the Los Angeles County Air Pollution Control District for the use of their facilities both on the laboratory rooftop and within the laboratory; to the Mt. Wilson Resort for use of grounds as nonurban sampling site; to station KCET for access to their facilities on Mt. Wilson and to Mr. James Mead, the station engineer; to Mr. Ralph Keith, Senior Meteorologist with LACAPCD, for his work in forecasting and calling the flight days; to Mr. George Kalstrom, Meteorologist, Los Angeles Weather Bureau, for assistance in locating a nonurban sampling site; and in particular, to Mr. C. Frederick Smith, Public Health Service, who coordinated the efforts of the participants and made many of the decisions required for the successful execution of the study involving concurrent measurements coordinated with special flight days.

Mr. J. S. Nader acknowledges the advice and comments of Drs. J. H. Ludwig, B. J. Steigerwald, and A. P. Altshuller, and Mr. R. A. McCormick, Public Health Service, in the planning, coordination, and execution of this study.

COOPERATING PARTICIPANTS

Organization	Responsible Individual
Vehicle Pollution Laboratory Bureau of Air Sanitation Division of Environmental Sanitation California Department of Public Health 434 South San Pedro Street Los Angeles, Calif. 90013	Dr. Robert J. Gordon Supervisory Physicist
Los Angeles Country Air Pollution Control District 434 South San Pedro Street Los Angeles, Calif. 90013	Mr. Robert J. Bryan Director of Technical Services
National Bureau of Standards Meteorology Division Gaithersburg Maryland 20760	Mr. Ralph Stair Physicist
Pennsylvania State University College of Earth and Mineral Sciences University Park, Pa. 16802	Dr. Hans Neuberger Chairman Dept. of Meteorology
Public Health Service National Center for Air Pollution Control Chemical and Physical Research and Development Program 4676 Columbia Parkway Cincinnati, Ohio 45226	Mr. John S. Nader, Chief Physical Measurements
University of California, Riverside Riverside, Calif.	Dr. J. N. Pitts Professor of Chemistry

PREFACE

To our knowledge, this pilot study represents the first field effort of several research groups to obtain simultaneous data on available ultraviolet (UV) radiation in the atmosphere of a large urban community under representative environmental conditions. This study was initiated to evaluate possible methods of measuring the UV important in photochemical reactions, in the range from 300 to 400 nanometers, under realistic field conditions. At the same time some preliminary data were obtained on the UV energy available with respect to location, elevation, and time of day for various levels of air pollution.

Los Angeles was selected for the study because its smog environment is primarly associated with photochemical reactions. October was selected because a wide range of air pollution conditions, particularly those associated with photochemical smog, are usually experienced at that time.

Organizations who had developed methods of UV measurements were invited to participate in this study as a means of evaluating their techniques against those of others. The Public Health Service investigators used physical detection methods (filter photocell and photochromic glass); the National Bureau of Standards and Pennsylvania State University also used physical methods (filter phototube and photosensitive plastic, respectively); the University of California at Riverside and California State Department of Health used chemical methods (actinometers involving gas, liquid, and solid reactions). The Los Angeles County Air Pollution Control District conducted chemical analyses and provided meteorological and air quality data as supporting information.

The rooftop of the laboratory of the Los Angeles County Air Pollution Control District in downtown Los Angeles was the site for measurements of incoming UV radiation at ground level below the urban smog envelope. A clearing near the KCET transmission tower on Mt. Wilson at an elevation of 5,700 feet was the site for measurements of incoming radiation representative of that incident on top of the Los Angeles smog envelope.

Aircraft flights were made over downtown Los Angeles to measure the outgoing radiation reflected from the ground and from smog layers. Within the 4 weeks of the study, flights were made on 5 days to encompass environmental conditions ranging from clear atmospheres to relatively heavy smog. On all 5 days the skies were essentially free of cloud cover. During these flights simultaneous measurements were made of meteorological parameters, air quality relative to pollutants, and ultraviolet radiation incident on a horizontal plane surface and on a volumetric actinometer. Four flights were made on each of the 5 flight days. Measurements in the aircraft were made in each flight at eleva-

tions ranging from 5,700 feet, corresponding to the elevation of the Mt. Wilson site, to a minimum of about 1,300 feet.

This report is a compilation of the data obtained on the 5 flight days by the various participants. The contribution of each participant is presented as a separate section, intact, with a brief explanation of the instrumentation and procedure used to obtain the data together with a tabulation of the data reduced to a format permitting convenient use of information by interested researchers. Both the PHS and NBS continuous recorder data have been put on punch cards and are available as relatively instantaneous values throughout the day as well as in the summary form presented in this report.

In the final section related data from the various contributor sections are discussed. Some limited effort is made to relate concurrent data of measurements by different methods and at various locations and to summarize some of the conclusions.

As a result of this study, the National Center for Air Pollution Control plans to pursue the measurement of the UV incident on a volume in space in addition to the horizontal-plane technique currently available, which represents only the UV component normal to the plane of incidence. This study also provides the basis on which plans will be formulated for a large-scale systematic study of available UV radiation and its reduction in atmospheres of several large cities and the relationship of UV intensity levels to potential photochemical smog.

John S. Nader

Cincinnati, Ohio
1967

CONTENTS

ABSTRACT

Several research groups combined efforts to measure simultaneously the available ultraviolet radiation of the urban atmosphere of Los Angeles under representative environmental conditions. The study was planned to permit evaluation of possible methods of measuring the UV radiation important in photochemical reactions (in the range from 300 to 400 nanometers) and to obtain preliminary data on the UV radiation energy with respect to location, elevation, and time of day. Measurements were made on five days at various levels of air pollution ranging from no smog to moderate-to-heavy smog.

This report is a compilation of data obtained by the several participants, with brief accounts of instrumentation and procedures. The instrumental sensors used to detect the UV radiation were filter photocell, filter phototube, photochemical sensors, photosensitive plastic, and photochromic glass. Air quality and meteorological data for the sampling periods are also presented. A discussion and summary relates the data obtained in measurements by the different methods and at the various locations.

INTRODUCTION

The Los Angeles measurement site on the rooftop of the laboratory building was about 350 feet above sea level. Measurements of incoming UV radiation were made with the filter-photocell and filter-phototube sensors, photochromic glass and photosensitive plastic, photochemically treated filter paper, and photochemical gas and liquid reaction cells (Figures 1 and 2). Supporting data on air quality and meteorology were also obtained at this site.

At the Mt. Wilson site the instrumentation was on ground level at an elevation of 5,700 feet. This site was located in a clearing about 200 feet to the right of the KCET television station building (Figure 3). The only measurements at this site were of incoming UV radiation made with the filter-phototube sensor, which was a duplicate of that at the Los Angeles site.

The measurements of outgoing radiation were made in a Cessna 180 aircraft. Figure 4 shows the wing mounting of the sensor for the outgoing radiation. This radiation was measured with a filter-photocell sensor, which was a duplicate of that at the Los Angeles site. Both incoming and outgoing radiation were also measured by photochemically treated filter paper. Air quality measurements were made on air samples collected only on the first flight of each scheduled flight day at three elevations. Temperature readings were also taken at all times.

The 5 flight days were October 6 (Wednesday), 12 (Tuesday), 16 (Saturday), 18 (Monday), and 20 (Wednesday), 1965. These 5 days were classified by the Air Pollution Control District according to a rating based on observed smog effects: moderate to heavy (M-H), light to moderate (L-M), none (N), light (L), and light (L). The observed smog effects were one or more of the following three: ozone concentration, visibility, and eye irritation.

The wavelengths are given in nanometers (nm = 10^{-9}m). Irradiance (incident flux density) is in watts per square meter (w/m^2), consistent with the MKS system of basic units and the internationally recognized system of prefix notation for multiples and submultiples of basic units. Calculations of time of day were based on an average approximation that true solar time (TST) is equal to Pacific daylight time (PDT) minus 40 minutes. Thus, 12:00 noon (TST) is 12:40 p.m. (PDT).

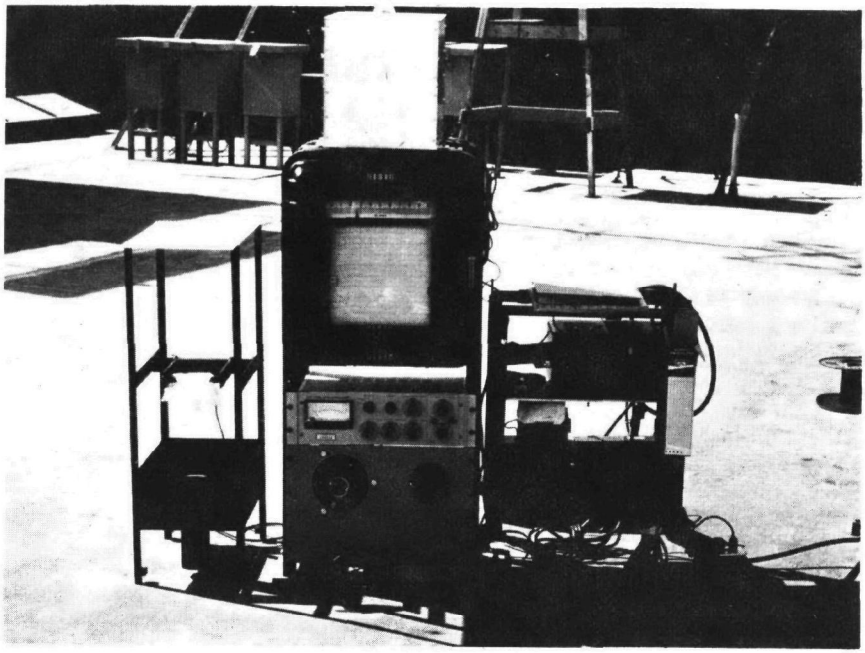

Figure 1. Instruments on rooftop at Los Angeles measurement site.

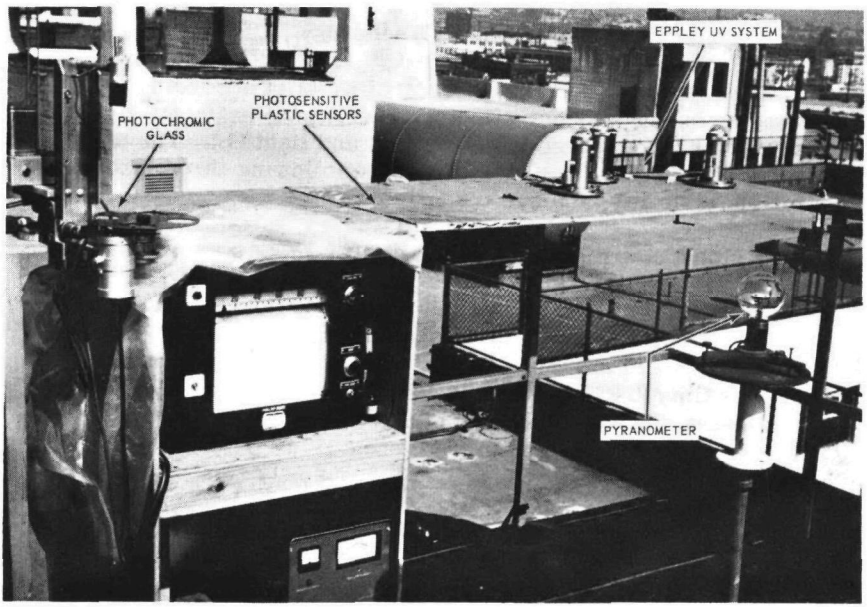

Figure 2. NBS filter-phototube equipment at Los Angeles site.

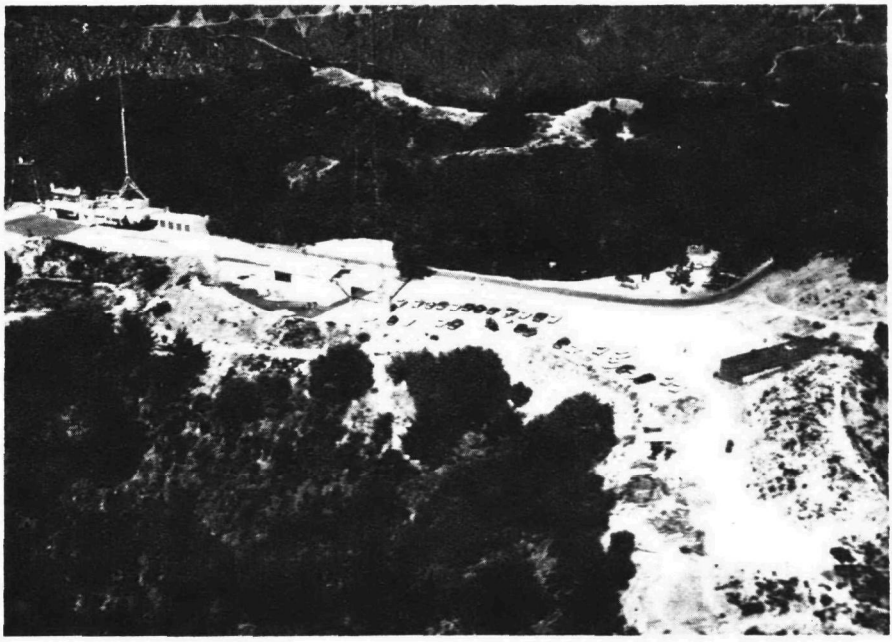

Figure 3. Aerial view of Mt. Wilson measurement site.

Figure 4. Wing-mounted sensor for measurements from aircraft.

Public Health Service

1: FILTER-PHOTOCELL MEASUREMENTS

John S. Nader and C. Frederick Smith

National Center for Air Pollution Control

INSTRUMENTATION AND METHOD*

The Eppley sensors used in surface measurements were designed by and constructed at the Eppley Laboratory for the Public Health Service. The sensor used in the aircraft was constructed by the National Bureau of Standards in accordance with the Eppley filter-photocell design. The filter-photocell sensor (Figure 1-1) consisted of a Weston selenium barrier-layer photovoltaic detector cell with a sealed-in quartz window, a bandpass interference filter to restrict the ultraviolet radiation incident on the photocell to the range of interest, a diffusing disc of opaque quartz protected from weathering effects by a quartz hemispherical envelope (2-mm wall thickness), and a circular spirit level mounted on the sensor stand with levelling screws.

The diffusing disc was designed and constructed to reduce the light intensity at the photocell for improved stability with exposure time and also to optimize the response of the sensor in accordance with the Lambert cosine Law (Table 1-1). The disc is nearly uniformly diffusing over the wavelength of interest as well as geometrically within the system. The terminals of the photocell are connected through a precision resistor (1,500 ohms), across which a voltage signal is developed. This arrangement restricts light flux to the order of 1 to 2 footcandles and the resulting current in the circuit to a few mircroamperes at most, thus maintaining photocell stability.

Three Eppley instrument systems were used to isolate the wide band, 300 to 380 nm, and two narrow bands within this range, namely, 315 to 330 nm (low) and 357 to 372 nm (high). Each narrow-band system, in addition to its sensor included a d-c amplifier with full-scale input ranges of 50, 100, 200, 500, 1000, and 2000 microvolts and constant full-scale output range of 10 millivolts. All systems used in downtown Los Angeles to measure the incoming radiation continuously incorporated recording millivolt potentiometers with adjustable full-scale

* Mention of commercial products throughout this report does not constitute endorsement by the Public Health Service.

settings within the ranges of 3 and 30 millivolts. The wide-band system used on the aircraft to measure outgoing radiation incorporated an indicating microvoltmeter, from which the attending technician observed and recorded the electrical readings at prescribed elevations.

These systems were calibrated by the Eppley Laboratory to convert the detected electrical signal into absolute energy values for the UV flux incident on the horizontal plane sensor. Calibration of the wide-band system *(1)* involved the use of a calibrated differential thermopile detector as a standard reference sensor and exposure of both test and reference instruments simultaneously to solar radiation. The outdoor exposure method referred to above could not be used for calibration of the narrow-band filters because the thermopile detector lacked the sensitivity required for the low energy levels involved. In this case, exposure to an NBS lamp standard of spectral irradiance *(2)* was made in the laboratory. From knowledge of the energy at the photocell and the factor for the diffuser (determined through exposure to the sun and sky), the first approximation of the required calibration was obtained. From consideration of: (1) the specific UV band being isolated; (2) the shape of the transmission curve of the filter defining this region (Figure 1-2); (3) the shape of the spectral response curve of the photocell (Figure 1-3); and (4) the deviation between the relative spectral emission curves of the calibrating lamp and natural daylight in the wavelength region of interest (Figure 1-4), appropriate corrections were applied as deemed necessary *(1)*. The adopted calibration values given in Table 1-2 include the value for the wide-band sensor used on the aircraft.

A test unit was provided to verify the calibration stability of each system during field use. It consisted of a 45-watt quartz tungsten-iodine lamp as a light source and a regulated power supply from a 12-volt automobile battery.

The Eppley sensor for the aircraft measurements was mounted underneath the wing of the aircraft, and a signal cable transmitted the sensor output voltage to an indicating microvoltmeter in the cabin of the aircraft.

RESULTS

Instantaneous values of the incoming radiation in downtown Los Angeles at 5-minute intervals were taken from the continuous chart records and put on punch cards. These recorder values were reduced to absolute energy values and averaged for 30-minute intervals. Tabulated results are given for the incoming radiation in the two narrow-band ranges and in the wide-band range in Tables 1-3, 1-4, and 1-5, respectively. Figures 1-5, 1-6, and 1-7 give graphic representations of these data as a function of time of day for the 5 flight days.

Measurements of the outgoing UV radiation taken from the aircraft over downtown Los Angeles were instantaneous values taken at different

elevations over a span of time. Since these measurements did not correspond exactly either for the same elevation in different flights or for the same time of day on different days, the results, reduced to absolute energy values, were tabulated to correspond both to identical elevation intervals and to identical intervals of time. Thus, the data are given in Table 1-6 in a cell array of radiation energy values as a function of time and of elevation intervals. In the graphical representations of the data the midpoints of these intervals were plotted to give two sets of curves. Figures 1-8 and 1-9 give the outgoing radiation as a function of elevation for various flight-time intervals. Figures 1-10 and 1-11 give the outgoing radiation as a function of time of day for various elevation intervals.

The outgoing radiation as a function of elevation was plotted on semilog paper with the elevation on log scale. Initially, a rectilinear plot showed a trend toward an exponential relationship similar to that in lightscatter measurements from a turbid medium wherein lightscatter increases with increased turbidity and increased medium thickness. If this is the case, a semilog plot should give a linear relationship with elevation except when a sharp change in the turbidity of the medium may occur, as may be the situation in going through the bottom or top of an inversion layer.

The experimental points for the plot of outgoing radiation as a function of time of day were limited to four values corresponding to the four flight trips per day. Nonetheless, a relatively smooth curve was anticipated relating to the sine function of the sun's elevation. Accordingly, points between the experimental values were calculated on the basis of a least-squares best-fit equation (3rd order) to give the curves shown.

Data on outgoing radiation were plotted only for the two extreme smog conditions, the no-smog day (October 16) and the moderate-to-heavy-smog day (October 6). These graphs adequately encompass what would be portrayed by the data for the remaining 3 days, on which smog conditions were within the range of the two extremes.

The temperature data taken at various elevations during all of the flights were used to determine the temperature profiles (Figure 1-12) from which the location of the ground inversion layer was determined. Since the lowest elevation at which the temperature measurements were made was about 1,300 feet, information about location of inversion layer boundaries was limited to those between 1,300 and 6,000 feet. Table 1-7 gives the elevation of the top of the inversion layer nearest ground level, based on the elevation at which the temperature ceases to increase with further increase in elevation.

REFERENCES

1. Drummond, A. J. Instrumentation for Measurement of Ultraviolet Radiation. In: Proceedings of the Fourth International Congress of Biometeorology, August 1966, Rutgers University (in press).

2. Stair, R., W. E. Schneider, and J. K. Jackson. A New Standard of Spectral Irradiance. Appl. Optics. 2:1151 (1963).

Table 1-1. COSINE RESPONSE OF THE EPPLEY FILTER-PHOTOCELL SENSOR

Zenith angle, degrees	Equivalent elevation angle, degrees	Relative response[a]
Total (300-380 nm)	High (357-372 nm)	
20	70	1.02
30	60	1.00
40	50	1.00
50	40	1.06
60	30	1.02
70	20	1.09
Low (315-330 nm)		
20	70	1.32
30	60	1.11
40	50	1.00
50	40	0.96
60	30	0.96
70	20	1.00

[a]Values are normalized to 45-degree angle; range of solar elevation at Los Angeles from 0800 to 1600 TST during experiment was 20 to 55 degrees.

Table 1-2. ABSOLUTE CALIBRATION VALUES FOR EPPLEY-DESIGNED SENSORS

Photocell sensor	Range, nm	Serial No.	Conversion factor, $w\text{-}m^{-2}/mv$
Eppley wide-band UV	300-380	E-7368	10.7
Eppley High UV	357-372	E-7369	25.0
Eppley Low UV	315-330	E-7370	149.0
NBS wide-band UV	300-380		17.8

Table 1-3. AVERAGE INCOMING 315- TO 330-nm RADIATION FOR 30-MINUTE INTERVALS, DOWNTOWN LOS ANGELES

(w/m^2)

Midpoint of time interval (TST)	Oct 6	Oct 12	Oct 16	Oct 18
0545	0.0268	0.0223	0.0044	0.0268
0615	0.0424	0.0252	0.0163	0.0275
0645	0.206	0.119	0.142	0.147
0715	0.558	0.380	0.451	0.430
0745	0.922	0.686	0.882	0.795
0815	1.30	0.917	1.44	1.29
0845	1.65	1.18	2.03	1.66
0915	2.07	1.47	2.61	2.20
0945	2.31	1.83	3.19	2.71
1015	2.37	2.21	3.58	3.18
1045	2.38	2.63	3.95	3.43
1115	3.09	2.90	4.26	3.37
1145	3.52	2.93	4.22	3.12
1215	3.65	3.13	4.07	2.73
1245	3.57	3.27	3.94	2.37
1315	3.41	3.08	3.67	2.41
1345	3.16	2.90	3.30	2.11
1415	2.80	2.51	2.82	1.85
1445	2.10	2.04	2.30	1.71
1515	1.58	1.59	1.77	1.40
1545	1.26	1.11	1.19	0.945
1615	0.729	0.620	0.697	0.521
1645	0.331	0.258	0.326	0.191
1715	0.0781		0.122	
1745	0.0275		0.0521	

Table 1-4. AVERAGE INCOMING 357- TO 372-nm RADIATION FOR 30-MINUTE INTERVALS, DOWNTOWN LOS ANGELES

(w/m^2)

Midpoint of time interval (TST)	Oct 6	Oct 12	Oct 16	Oct 18
0545	0.0225	0.0075	0.0075	0.0150
0615	0.0962	0.0275	0.0462	0.0287
0645	0.590	0.350	0.534	0.441
0715	1.31	0.888	1.48	1.26
0745	2.08	1.52	2.65	2.17
0815	2.84	1.98	3.92	3.24
0845	3.56	2.41	5.16	3.98
0915	4.28	2.87	6.31	5.12
0945	4.69	3.50	7.31	6.16
1015	4.67	4.34		6.95
1045	4.72	5.13	8.41	7.16
1115	6.30	5.65	8.90	6.97
1145	6.99	5.72	8.80	6.43
1215	7.16	6.27	8.48	5.55
1245	7.22	6.68	8.32	5.19
1315	6.97	6.42	8.00	5.41
1345	6.59	6.22	7.39	4.78
1415	6.04	5.54	6.58	4.21
1445	4.64	4.60	5.63	4.11
1515	3.52	3.78	4.55	3.51
1545	3.01	2.89	3.32	2.65
1615	1.99	1.83	2.21	1.70
1645	1.14	1.03	1.24	0.950
1715	0.520	0.396	0.538	0.400
1745	0.120	0.0825	0.070	0.075

Table 1-5. AVERAGE INCOMING 300- TO 380-nm RADIATION FOR 30-MINUTE INTERVALS, DOWNTOWN LOS ANGELES

(w/m^2)

Midpoint of time interval (TST)	Oct 6	Oct 12	Oct 16	Oct 18	Oct 20
0545	0.374	0.321	0.365	0.428	0.277
0615	0.641	0.606	0.623	0.588	0.434
0645	2.27	2.02	2.63	2.26	1.97
0715	4.84	4.09	6.18	5.24	5.02
0745	7.99	6.43	10.6	8.68	9.06
0815	11.5	8.35	15.5	12.8	13.6
0845	14.4	10.0	20.2	15.8	17.8
0915	17.4	12.1	24.7	20.7	21.5
0945	19.0	14.6	28.8	24.8	24.7
1015	19.0	18.2	31.5	28.3	25.9
1045	19.1	21.3	33.9	29.6	26.7
1115	25.3	23.4	36.0	29.3	30.5
1145	28.8	23.9	36.0	27.0	33.4
1215	29.9	26.2	34.7	23.3	32.9
1245	30.1	27.9	34.2	21.9	29.8
1315	28.8	26.9	32.8	22.5	27.3
1345	27.1	26.1	30.2	19.9	23.7
1415	24.8	22.9	26.5	17.5	21.4
1445	19.2	19.0	22.6	17.0	18.6
1515	14.9	15.6	18.2	14.2	14.4
1545	12.4	11.7	13.3	10.7	10.7
1615	8.30	7.55	8.66	7.04	7.30
1645	4.82	4.37	4.86	3.83	3.66
1715	2.38	1.97	1.94	1.46	1.27
1745	0.677	0.552	0.507	0.419	0.291

Table 1-6. INSTANTANEOUS OUTGOING 300- TO 380-nm RADIATION MEASURED FROM AIRCRAFT
(w/m^2)

Time interval (TST)	Elevation, thousands of feet						
	1.0-1.5	1.6-2.0	2.6-3.0	3.6-4.0	4.6-5.0	5.6-6.0	6.1-6.5
Oct 6							
0830-0930	4.09	4.45	5.07	5.34	5.87	5.87	5.70
1030-1130		5.34	6.94		8.19	8.54	8.54
1230-1330	4.45	5.60	6.74	7.30	7.48	8.01	
1430-1530	2.14	2.49	4.19	5.34	5.70	5.70	6.06
Oct 12							
0800-0900	3.56	4.27	5.52	5.34	5.70	5.34	
1000-1100	4.63	5.70	7.12	7.48	8.28	8.19	
1200-1300	5.52	6.23	7.20	7.83	7.95	8.54	
1400-1500	4.18	5.34	5.60	6.05	6.76	6.94	
Oct 16							
0800-0900	1.78	1.96	2.49	2.67	2.84	2.94	
1000-1100	2.49	2.67	3.12	3.92	4.27	4.63	
1200-1300	2.31	2.85	3.38	3.92	4.45	4.81	
1400-1500	1.42	1.96	2.31	3.03	3.56	3.92	
Oct 18							
0800-0900	2.67	3.20	3.20	3.56	3.92	3.83	
1000-1100	2.85	3.92	4.45	5.16	5.43	5.70	
1200-1300	3.12	4.45	6.23	6.76	7.83	8.10	
1400-1500	1.50	2.14	4.27	5.70	6.23	6.76	
Oct 20							
0800-0900	1.78	2.31	2.58	3.03	3.03	3.21	
1000-1100	2.94		3.92	4.45		5.16	
1200-1300	2.49	3.03	3.92	4.81		5.43	
1400-1500	1.96		3.03	4.09	4.09	5.16	

Table 1-7. ELEVATION OF THE TOP OF THE INVERSION LAYER NEAREST GROUND LEVEL
(feet)

Time Interval (TST)	Oct 6	Oct 12	Oct 16	Oct 18	Oct 20
0830-0930	3,150				
1030-1130	3,000				
1230-1330	2,900				
1430-1530	2,500				
0800-0900		3,000		1,300[a]	
1000-1100		2,000		2,900[b]	
1200-1300		2,500	2,000	c	
1400-1500		2,000		d	

[a] Inversion bottom of second layer at 4,000 feet.
[b] Inversion bottom of second layer at 4,500 feet.
[c] Second inversion layer bottom at 4,000 feet and top at 5,000 feet.
[d] Second inversion layer bottom at 3,000 feet and top at 4,000 feet.

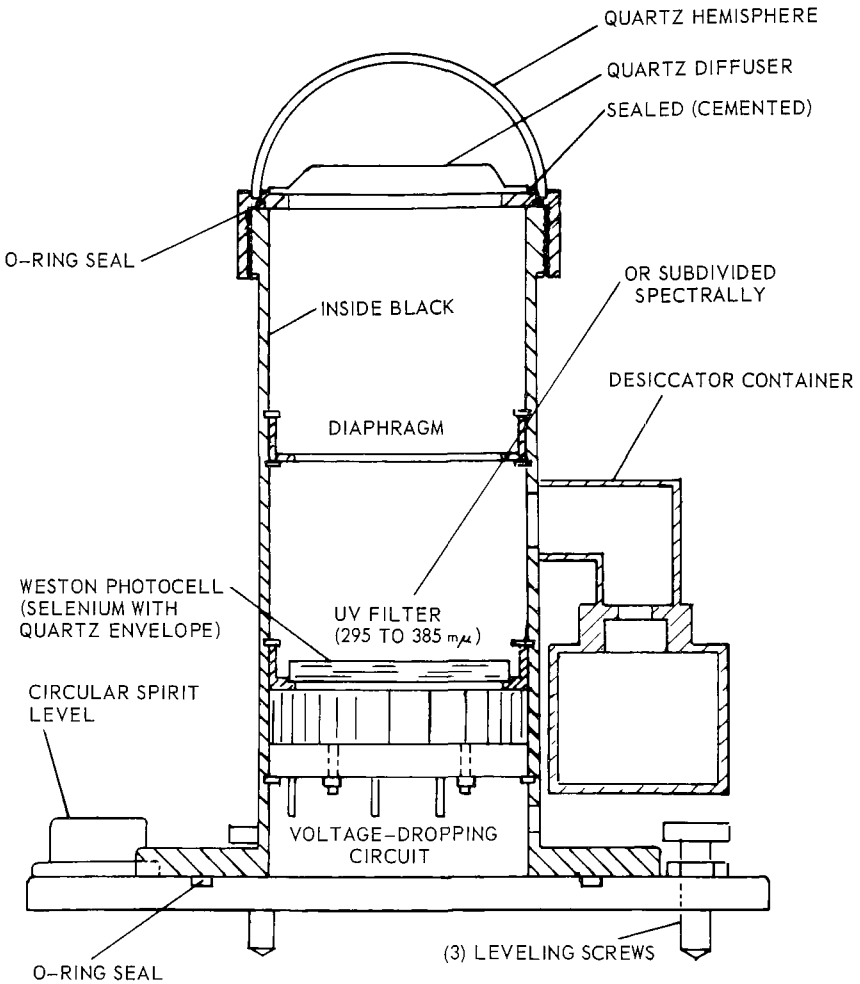

Figure 1-1. Eppley filter-photocell UV sensor.

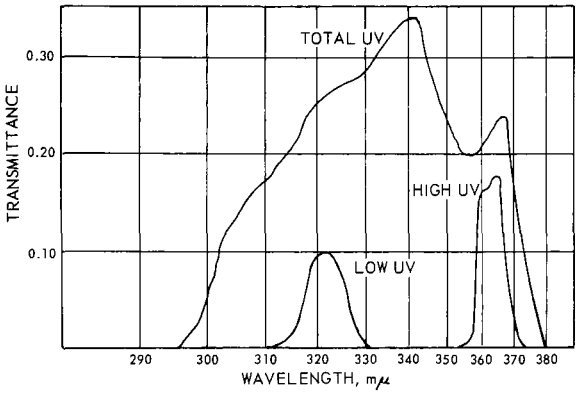

Figure 1-2. Spectral transmission of the interference filters in Eppley sensors.

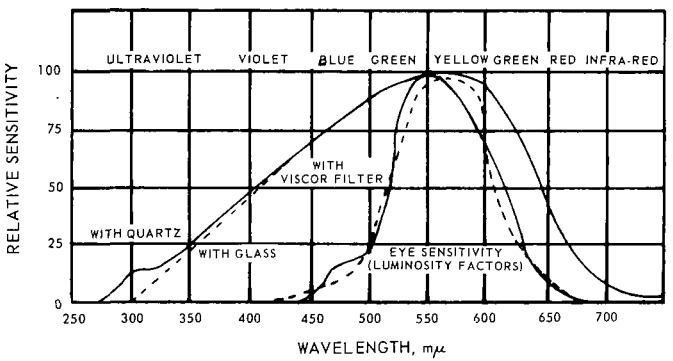

Figure 1-3. Relative spectral response of the selenium photocell in the Eppley UV sensors.

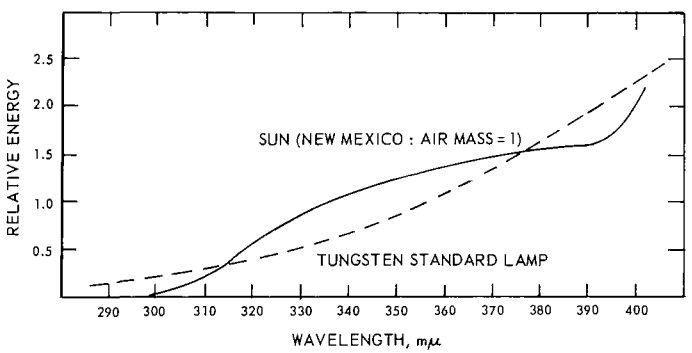

Figure 1-4. Relative spectral emissions of the standard tungsten lamp and of the sun for air mass 1.

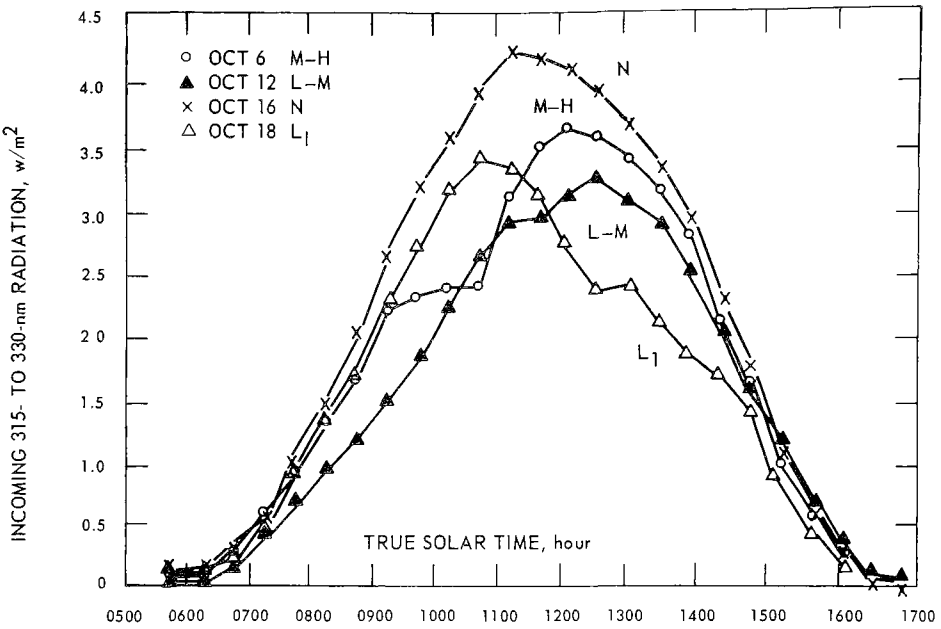

Figure 1-5. Average incoming 315- to 330-nm radiation for 30-minute intervals, as function of time of day on various days of smog in downtown Los.Angeles.

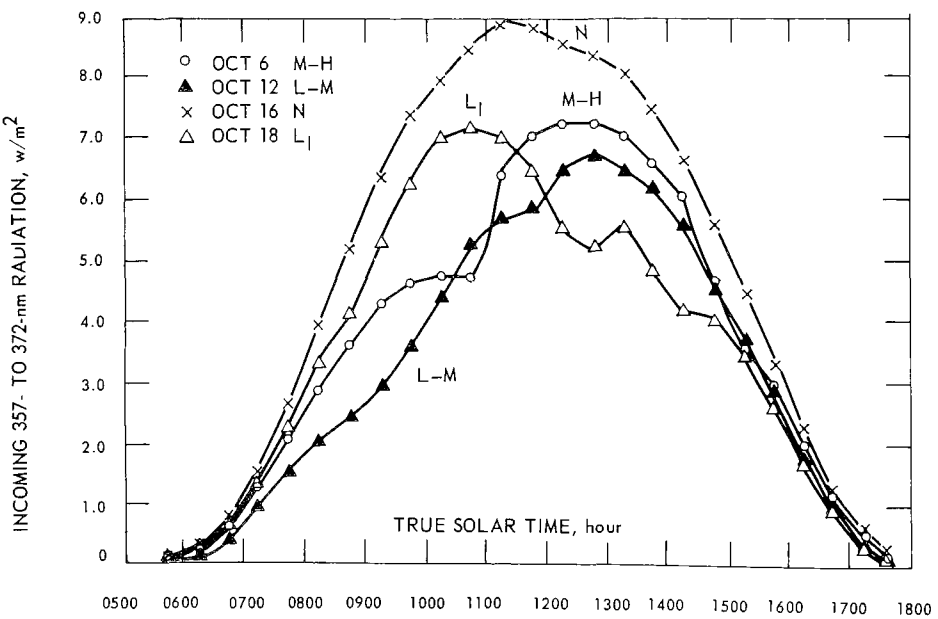

Figure 1-6. Average incoming 357- to 372-nm radiation for 30-minute intervals, as function of time of day on various days of smog in downtown Los Angeles.

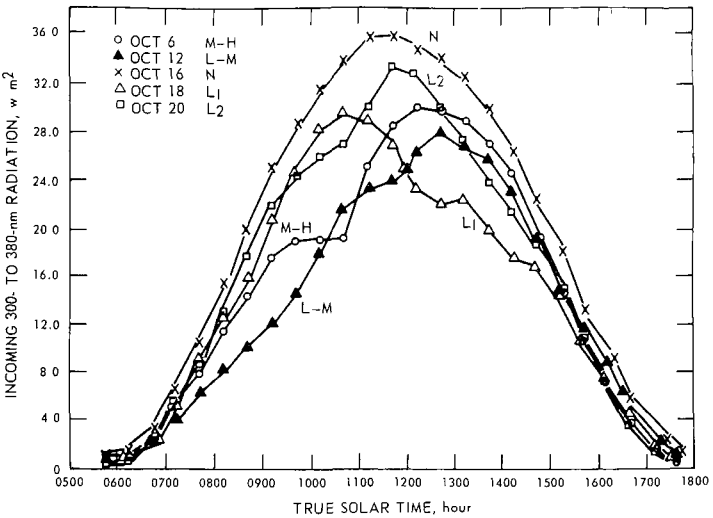

Figure 1-7. Average incoming 300- to 380-nm radiation for 30-minute intervals, as function of time of day on various days of smog in downtown Los Angeles.

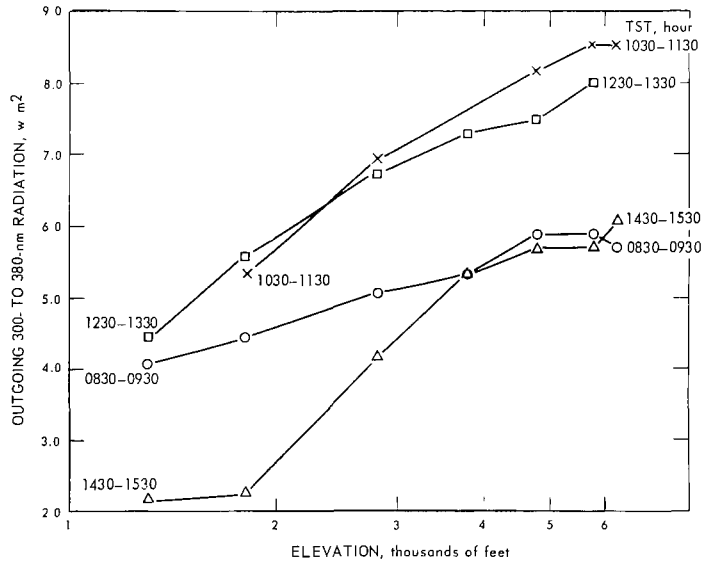

Figure 1-8. Outgoing 300- to 380-nm radiation as function of elevation over Los Angeles at different times of day, October 6 (M-H Smog).

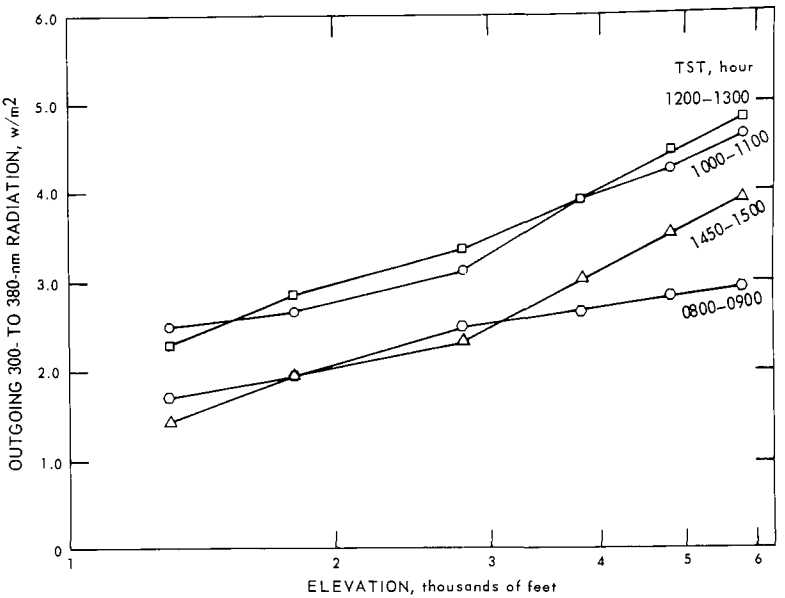

Figure 1-9. 300- to 380-nm radiation as function of elevation over Los Angeles for different times of day, October 16 (no smog).

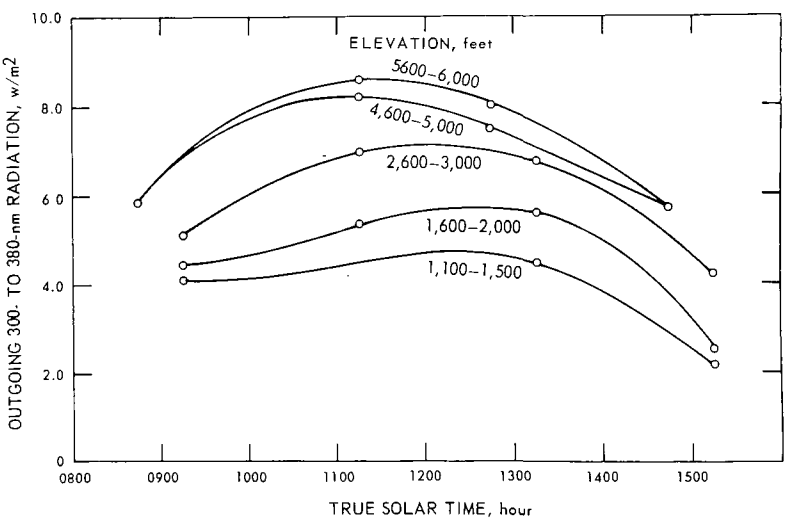

Figure 1-10. Outgoing 300- to 380-nm radiation as function of time of day for various elevations over Los Angeles, October 6 (M-H Smog).

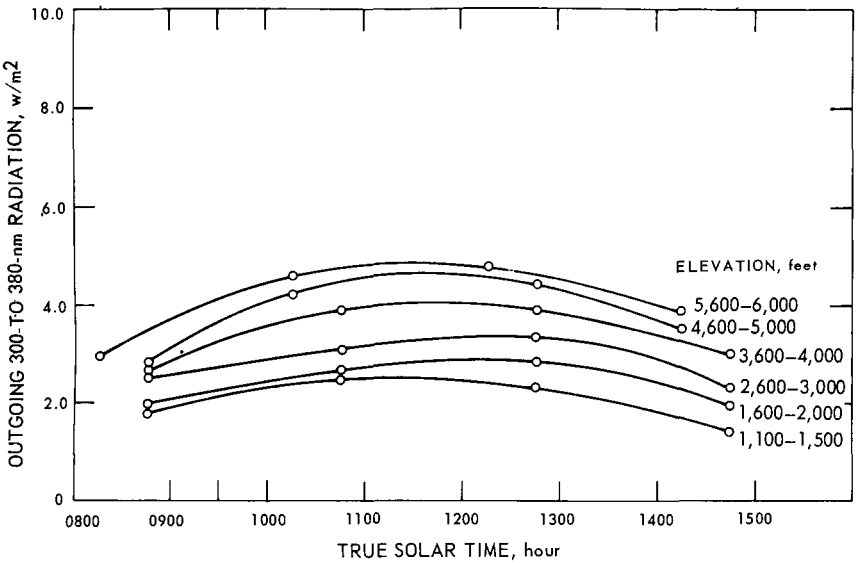

Figure 1-11. Outgoing 300- to 380-nm radiation as function of time of day for various elevations over Los Angeles, October 16 (no smog).

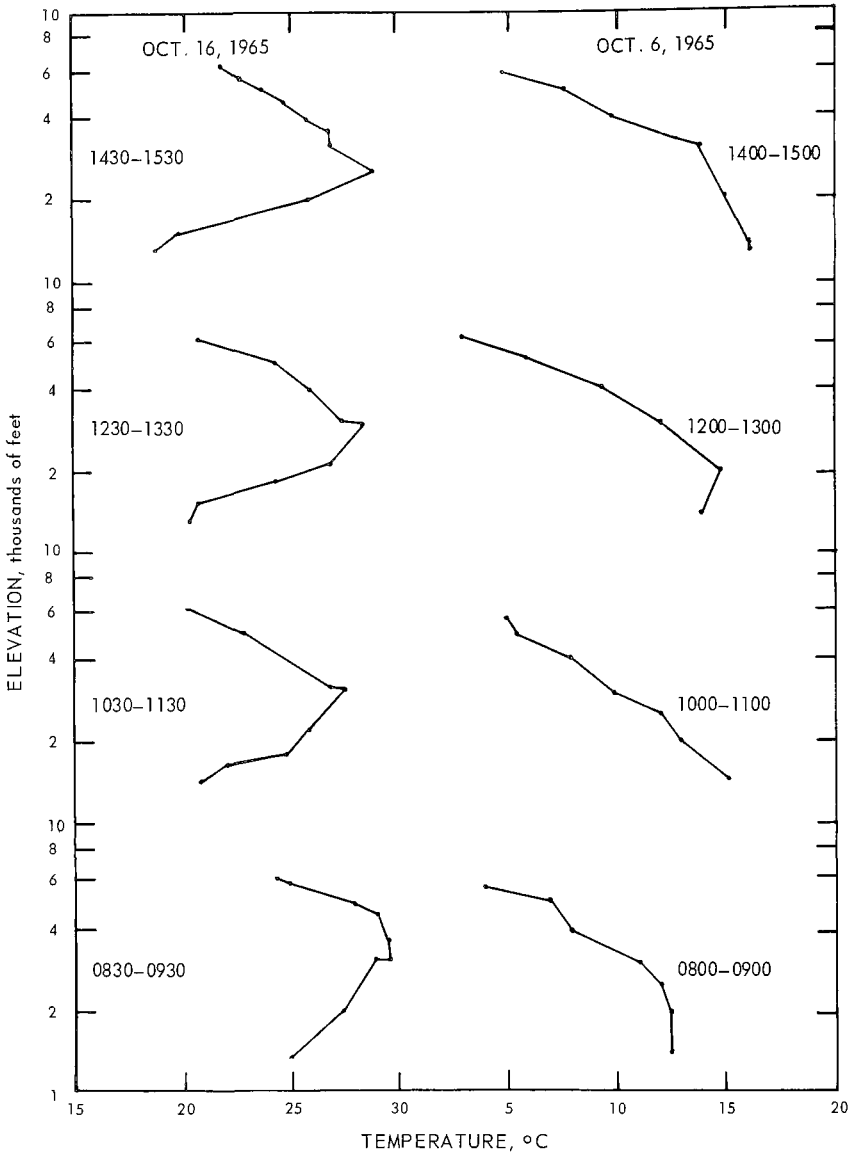

Figure 1-12. Temperature profiles at Los Angeles.

National Bureau of Standards

2: FILTER-PHOTOTUBE MEASUREMENTS*

Ralph Stair

Meteorology Division
National Bureau of Standards

John S. Nader

National Center for Air Pollution Control

INTRODUCTION

The literature of the past 50 years contains many data on the total solar irradiances at various locations and different seasons of the year. These data have usually been obtained with some type of pyrheliometer in the form of a blackened horizontal receiver housed in a glass envelope. As a result, the short-wave ultraviolet and long-wave infrared are not included in the measurements *(1)*. Furthermore, the uncertainty in the measurements has been of the order of a few percent a magnitude approximating that of the total ultraviolet irradiance. Hence, the great amount of available data gives little information concerning the solar ultraviolet irradiance present in any locality. Only in those researches wherein special equipment has been employed are any quantitative ultraviolet data available. Measurements of this type have usually been made at high altitudes or in locations having relatively unpolluted atmospheres. Since the primary purpose of this investigation was to evaluate the available solar ultraviolet irradiation in both a polluted area and a nearby area relatively free of pollution, special instrumentation and techniques were required.

INSTRUMENTATION AND METHOD

There is considerable interest in photochemical processes to which gaseous and particulate material in the atmosphere are subjected. Although these processes are directly related to absorption of radiation incident from any direction (a volume effect), it is to be noted that our instrumentation set up in downtown Los Angeles and on Mt. Wilson measures the solar ultraviolet irradiance (at selected wavelengths) on a horizontal surface. For best results, this measurement requires the use of a detector having sensitivity over its surface in accordance with the cosine law for all angles from 0 degree (the horizon) to 90 degrees

* This section is based on original data collected by the National Bureau of Standards for work sponsored by the U. S. Public Health Service.

(the zenith). Hence, equipment of special design was required and was built to separate narrow spectral bands and at the same time not upset the cosine-law response for angular elevation of source (the sun and sky).

Figure 2-1 is a layout diagram of the photoelectric equipment assembled for this work. The solar irradiance (sun and sky) was collected in an integrating sphere, which was coated with a thick layer of $BaSO_4$. The entrance and exit ports were each 1/2 inch in diameter; the sphere, 4 inches. The entrance port was fashioned with a "knife-edge" opening, which was in the plane of the topmost section of the box and was adjusted precisely to a horizontal position. The exit opening was placed to the east or west, (so that at no time did direct sunlight or the sun's primary reflection fall directly into its view) and was covered by a shield and Corning filter 9863 having high opacity within the visible spectral region.

A filter wheel carrying nine narrow-band and one wide-band interference filter and two blanks (zero transmittance) was set about 6 inches from the sphere exit port so that a narrow beam of ultraviolet flux passed (nearly perpendicular) through each of the filters onto a type RCA-935 phototube as the filter wheel was step-rotated by a synchronous motor and geneva-drive mechanism. In this manner each filter and each blank (zero transmittance) was set in position for a period of about 10 seconds (enough time for the pico-ammeter and recorder to register a definite value on a strip chart). Thus the magnitude of each spectral irradiance was registered once in each interval of approximately 2 minutes (about 30 times per hour). For purposes of calibration at intervals during each day a 1,000-watt quartz iodine lamp, standard of spectral irradiance mounted in a special carriage to eliminate all sun and sky irradiance was placed above the integrating sphere (at a measured distance) and the output through the 10 filters was recorded over a period of several minutes (two to three rotations of the filter disk).

The spectral transmittances of each of the nine narrow-band interference filters used at Mt. Wilson are depicted in Figure 2-2 and of the wide-band in Figure 2-3. Each narrow-band filter has a half-band width of approximately 10 nm, and its centroid is situated near even 10-nm intervals from 310 to 390 nm.

Table 2-1 lists (in column 2) the relative responses of the RCA type 935 phototube (No. 5) when irradiated by a 1,000-watt quartz-iodine lamp standard of spectral irradiance No. 131 through Corning filter 9863 and each interference filter in turn, (in column 3) the wavelength centroid under these same conditions and (in column 4), as an example, the correction that should be applied when the spectral energy distribution of the irradiating source is that of the sun as determined at Sacramento Peak, New Mexico *(2)*, for air mass 1.0 rather than that of lamp standard No. 131. The spectral data on these sources, this detector, and Corning filter 9863 are also included in Figure 2-2. Because

corrections as listed in column 4 of Table 2-1 are smaller than the uncertainties in this type of measurement, they were not applied in computing the values reported in the results of this report. Other small corrections that are worthy of note but are neglected in this report arise from the following considerations: (1) the data herein reported in detail apply to the Mt. Wilson instrumentation, a "duplicate" of which, with filters cut from the same stock, was set up and operated in downtown Los Angeles; the differences between the instruments are considered to be minor; (2) an additional correction of approximately 1 percent could be applied to cover loss of sky irradiance passing directly through the two sphere openings and missing the detector entirely (see Figure 2-1); however, a nearly equal but opposite error occurs for sky irradiance reflected on first reflection from the sphere wall directly onto the detector. (Note that all of the flux from the quartz-iodine standard and nearly all of the sky flux is multiply reflected in the sphere before it is incident on the detector.)

The instrumentation required little attention since all operations, except setting up and operating the standard lamp for calibration, were automated. The usual service consisted of keeping the quartz hemisphere cover clean, keeping the recorder pen cleaned and filled, and recording time indications and other pertinent weather and air pollution information on the recorder strip chart or an associated notebook.

Column 2 of Table 2-1 shows differences of a factor of more than 10 between the highest and lowest integrated instrumental reading at one total irradiance. A similar variation, nearly tenfold, occurred between the early morning (or late afternoon) readings and those obtained near the noon hour. Since it is impractical to change instrumental sensitivity either between the interposition of filters or during the day, another method was employed to keep all data on a reasonable chart scale. This method consisted of placing (permanently) perforated metal screens (of various transmittances) over most of the filters so that in all cases the short-wave spectral regions produced readable deflections while the other spectral regions produced deflections not exceeding the chart limits or the fatigue level for the phototube. The transmittance values for these screens were not required and have not been obtained in reduction of the data.

RESULTS

Ultraviolet spectral solar and sky irradiance on a horizontal surface were made daily over a period of about 1 month between about September 20 and October 20, 1965, at Mt. Wilson and downtown Los Angeles. This report summarizes the data obtained during the 5 flight days with the instrumentation described above. The data obtained with the narrow-band interference filters are summarized in Tables 2-2, a-i, for Mt. Wilson and for downtown Los Angeles. These data are plotted in Figures 2-4 to 2-7 for only the 2 days involving the extreme smog conditions, i.e., no smog (October 16) and moderate-to-heavy smog (October 6).

The summation of energy values for the narrow-band filters in the range from 300 to 380 nm, to give another measure of the wide-band energy in this range, was calculated from the narrow-band filter measurements as follows:

The energy for the narrow-band filters 310 through 370 nm was summed directly, and one-half of the energy value for the 380-nm filter was added together with an extrapolated value for the energy in the range from 300 to 305 nm. This latter value is calculated as 1/8 of the energy for the 310-nm filter. The two sets of data for the spectral region from 300 to 380 nm are given in Table 2-3 and 2-4; results for the wide-band filter are shown graphically in Figures 2-8 and 2-9 for Mt. Wilson and downtown Los Angeles, respectively.

Note that precise values of spectral response of the particular phototube (set up at Mt. Wilson) as well as of the spectral irradiance of the NBS standard lamp and of the spectral transmittance of the wide-band filters used at that station were used in reducing the measurements made on Mt. Wilson with the wide-band filters. Under these conditions the two sets of data for the spectral region of 300 to 380 nm agree within about 1 percent, which may be considered unexpectedly good considering that a solar curve for M = 1 for Sacramento Peak, New Mexico, was used as a basis (rather than the true curve) for reducing the measurements with the wide-band filter.

Wider disagreement (2.5 to 3.0%) occurs in data from the downtown Los Angeles measurements for the wide-band spectral region of 300 to 380 nm. Possibly wider divergencies exist between the true and the solar curve (M = 1.0 for Sacramento Peak) employed. Or the greater discrepancy results because of our assumption that relative spectral responses of the two phototubes were the same. A difference of 2.5 to 3.0 percent is small, but since all measurements fall within the range of 2.5 to 3.0 percent, the indication is that the error is related to some of the basic factors common to all the measurements. Possibly the wide-band filter transmittance was significantly different at Los Angeles from what it was when measured after the work in the field. We know that all the interference filters used in this work solarized significantly during the investigation; however, since lamps were calibrated at least twice daily, any error resulting because of filter solarization is considered insignificant except possibly for the wide-band unit.

ACKNOWLEDGMENT

Development of the instrumentation used in this investigation was sponsored jointly by the United States Public Health Service and the National Aeronautics and Space Administration. Operation of the field equipment and collection of data were conducted with the help of Messrs. William R. Waters and John K. Jackson of NBS. Reduction of data and calculation of results were done with the help of Thomas A. Ante of the Public Health Service.

MISCELLANEOUS NOTES ON WEATHER AND SMOG

October 6 Sky clear on Mt. Wilson during most of the day but with very slight haze. Little or no wind at both stations. Smog layer appearing early over basin. Overcast and smoggy in downtown Los Angeles all day. Some clouds on Mt. Wilson after 2:00 p.m. A very smoggy day.

October 12 Sky very clear on Mt. Wilson in early morning. Thin layer of reddish-brown smog present at about 1,000 feet below Mt. Wilson station. No wind. By 2:30 p.m. smog layer reached Mt. Wilson station. Ozone meter responds to incoming oxidants. Downtown overcast all day. Intermediate smog.

October 16 Sky clear on Mt. Wilson all day. Good visibility downtown. Northwest wind at both stations, about 30 mph on Mt. Wilson. A clear and windy day. Little smog.

October 18 - Sky clear on Mt. Wilson all day. Light haze and smog over basin. Little or no wind at both stations. A relatively clear and calm day.

October 20 Sky clear on Mt. Wilson all day except for a few thin scattered clouds in afternoon. Some cloudiness and haze over basin all day. Little or no wind at either station. Light to moderate smog in downtown Los Angeles.

REFERENCES

1. IGY Instruction Manual, Part VI, Radiation Instruments and Measurement. Pergamon Press, New York, N. Y. (1958). (The glass envelope of pyrheliometers is opaque to the infrared of wavelengths longer than about 4 microns and to some of the ultraviolet; new instruments have higher transmittances at 300 nm.)

2. Stair, R., and R. G. Johnston. Preliminary Spectroradiometric Measurements of the Solar Constant. J. Research Nat. Bur. Standards. 57: 205 (1956).

Table 2-1. FILTER PHOTOTUBE DATA

Interference filter	Relative response of the combined lamp and detection system	Wavelength centroid, nm	Correction for measuring solar irradiance, percent (air mass 1.0)
310 nm	1,172	309.42	+2.9
320	3,345	322.29	−3.0
330	4,663	331.58	+1.4
340	5,145	340.65	+0.8
350	9,759	352.70	+3.2
360	12,500	360.22	+0.2
370	10,539	371.80	+2.5
380	8,805	381.33	+1.9
390	7,609	392.10	−2.7

Table 2-2A. AVERAGE INCOMING 305- TO 315-nm RADIATION FOR 30-MINUTE INTERVALS

(w/m^2)

Midpoint of time interval (TST)	Mt. Wilson					Downtown Los Angeles				
	Oct 6	Oct 12	Oct 16	Oct 18	Oct 20	Oct 6	Oct 12	Oct 16	Oct 18	Oct 20
0715	0.055					0.045		0.038	0.151	
0745	0.168	0.103	0.117	0.248	0.132	0.090	0.102	0.121	0.133	0.170
0815	0.281	0.236	0.234	0.361	0.748	0.165	0.153	0.214	0.154	0.182
0845	0.490	0.422	0.427	0.402	0.406	0.235	0.170	0.317	0.223	0.277
0915	0.683	0.630	0.616	0.589	0.599	0.343	0.228	0.455	0.385	0.420
0945	0.924	0.873	0.860	0.824	0.784	0.410	0.325	0.614	0.533	0.537
1015	1.22	1.060	0.985	0.941	0.971	0.464	0.438	0.772	0.661	0.622
1045	1.36	1.22	1.11	1.08	1.08	0.497	0.547	0.802	0.749	0.696
1115	1.40	1.30	1.23	1.18	1.24	0.672	0.629	0.914	0.765	0.812
1145	1.44	1.39	1.17	1.22	1.20	0.784	0.633	0.933	0.691	0.916
1215	1 48	1.40	1.29	1.18	1.21	0.855	0.698	0.903	0.596	0.899
1245	1.44	1.38	1.19	1.13	1.10	0.861	0.750	0.887	0.518	0.781
1315	1.31	1.20	1.12	1.01	0.966	0.816	0.705	0.829	0.516	0.668
1345	1.04	1.07	1.02	0.865	0.822	0.644	0.657	0.721	0.453	0.554
1415	0.950	0.897	0.833	0.710	0.800	0.596	0.535	0.602	0.354	0.451
1445	0.580	0.672	0.599	0.512	0.467	0.436	0.417	0.436	0.298	0.338
1515	0.439	0.455	0.404	0.507	0.510	0.294	0.315	0.295	0.214	0.225
1545	0.246	0.247	0.245	0.231	.0.231	0.191	0.185	0.158	0.174	0.135

Table 2-2B. AVERAGE INCOMING 315- TO 325-nm RADIATION FOR 30-MINUTE INTERVALS

(w/m^2)

Midpoint of time interval (TST)	Mt. Wilson					Downtown Los Angeles				
	Oct 6	Oct 12	Oct 16	Oct 18	Oct 20	Oct 6	Oct 12	Oct 16	Oct 18	Oct 20
0715	0.408					0.274		0.256	0.517	
0745	0.789	0.685	0.627	0.684	0.616	0.479	0.353	0.465	0.471	0.485
0815	1.24	1.12	1.03	1.06	1.11	0.702	0.491	0.830	0.738	0.805
0845	1.70	1.57	1.48	1.44	1.43	0.930	0.638	1.21	0.978	1.12
0915	2.17	2.02	1.93	1.88	1.87	1.19	0.745	1.56	1.33	1.45
0945	2.45	2.23	2.08	2.29	2.27	1.18	1.00	1.92	1.66	1.73
1015	2.87	2.71	2.57	2.63	2.62	1.29	1.25	2.22	1.98	1.90
1045	3.26	3.11	2.96	2.89	2.88	1.37	1.52	2.44	2.15	2.03
1115	3.47	3.29	3.16	3.05	3.07	1.82	1.70	2.63	2.17	2.33
1145	3.50	3.37	3.21	3.14	3.07	2.10	1.74	2.65	1.98	2.54
1215	3.53	3.42	3.21	3.09	3.06	2.25	1.89	2.55	1.71	2.49
1245	3.50	3.37	3.16	3.04	2.93	2.28	2.06	2.54	1.54	2.26
1315	3.31	3.15	2.99	2.83	2.71	2.17	1.98	2.43	1.57	2.02
1345	2.58	2.63	2.43	2.58	2.37	1.77	1.91	2.20	1.41	1.75
1415	2.66	2.40	2.26	2.21	2.01	1.70	1.67	1.89	1.23	1.50
1445	1.77	2.13	1.94	1.82	1.60	1.38	1.37	1.55	1.13	1.25
1515	1.68	1.65	1.49	1.46	1.19	1.04	0.991	1.20	0.913	0.952
1545	1.23	1.19	1.04	0.944	0.841	0.827	0.732	0.663	0.590	1.10

Table 2-2C. AVERAGE INCOMING 325- TO 335-nm RADIATION FOR 30-MINUTE INTERVALS

(w/m^2)

Midpoint of time interval (TST)	Mt. Wilson					Downtown Los Angeles				
	Oct 6	Oct 12	Oct 16	Oct 18	Oct 20	Oct 6	Oct 12	Oct 16	Oct 18	Oct 20
0715	0.864					0.552		0.545	1.04	
0745	1.49	1.35	1.27	1.21	1.22	0.877	0.619	0.817	0.855	0.816
0815	2.19	2.02	1.92	1.91	1.84	1.24	0.907	1.47	1.31	1.41
0845	2.92	2.72	2.61	2.55	2.52	1.57	1.08	2.07	1.67	1.91
0915	3.59	3.41	3.29	3.22	3.20	1.97	1.28	2.63	2.04	2.38
0945	3.97	3.64	3.39	3.85	3.80	1.91	1.62	3.16	2.70	2.80
1015	4.58	4.40	4.23	4.36	4.33	2.08	2.03	3.60	3.19	3.05
1045	5.21	5.03	4.84	4.72	4.73	2.20	2.41	3.90	3.42	3.20
1115	5.50	5.30	5.13	4.97	5.01	2.92	2.70	4.18	3.43	3.65
1145	5.53	5.39	5.20	5.09	5.01	3.35	2.74	4.18	2.99	3.97
1215	5.61	5.47	5.19	5.05	4.97	3.58	3.00	4.03	2.73	3.87
1245	5.55	5.41	5.11	4.94	4.79	3.64	3.27	4.03	2.48	3.54
1315	5.29	5.10	4.89	4.66	4.09	3.48	3.42	3.87	2.55	3.20
1345	4.13	4.23	3.92	4.29	3.96	2.84	3.07	3.53	2.29	2.59
1415	4.29	3.94	3.75	3.75	3.38	2.78	2.72	3.09	2.01	2.44
1445	2.92	3.59	3.33	3.14	2.78	2.28	2.24	2.58	1.89	2.06
1515	2.88	2.85	2.64	2.48	2.18	1.73	1.63	2.05	1.57	1.61
1545	2.18	2.13	1.94	1.73	1.53	1.44	1.26	1.15	1.10	1.52

Table 2-2D. AVERAGE INCOMING 335- TO 345-nm RADIATION FOR 30-MINUTE INTERVALS

(w/m^2)

Midpoint of time interval (TST)	Mt. Wilson					Downtown Los Angeles				
	Oct 6	Oct 12	Oct 16	Oct 18	Oct 20	Oct 6	Oct 12	Oct 16	Oct 18	Oct 20
0715	1.02					0.690		0.672	1.28	
0745	1.70	1.52	1.53	1.53	1.42	0.992	0.749	1.03	1.02	0.989
0815	2.44	2.22	2.23	2.22	2.25	1.36	1.04	1.70	1.50	1.61
0845	3.17	2.94	2.97	2.85	2.79	1.71	1.19	2.37	1.87	2.14
0915	3.89	3.64	3.68	3.55	3.50	2.11	1.43	2.94	2.45	2.64
0945	4.29	3.94	3.85	4.18	4.10	2.05	1.77	3.51	3.00	3.07
1015	4.93	4.67	4.68	4.68	4.64	2.21	2.18	3.93	3.51	3.31
1045	5.55	5.30	5.29	5.03	5.05	2.34	2.61	4.29	3.73	3.45
1115	5.82	5.54	5.60	5.28	5.32	3.12	2.91	4.58	3.73	3.94
1145	5.84	5.63	5.65	5.39	5.31	3.57	2.96	4.57	3.41	4.26
1215	5.91	5.72	5.64	5.36	5.27	3.54	3.25	4.41	2.95	4.16
1245	5.88	5.68	5.56	5.26	5.08	3.86	3.55	4.40	2.72	3.82
1315	5.61	5.36	5.30	4.98	4.74	3.72	3.43	4.23	2.80	3.52
1345	4.44	4.54	4.37	4.60	4.22	3.06	3.32	3.88	2.52	2.79
1415	4.64	4.22	4.15	4.05	3.62	3.01	2.95	3.47	2.22	2.64
1445	3.11	3.82	3.68	3.41	3.02	2.44	2.45	2.86	2.11	2.24
1515	3.14	3.06	2.95	2.81	2.50	1.88	1.81	2.15	1.76	1.76
1545	2.39	2.31	2.21	1.97	1.73	1.57	1.41	1.32	1.27	1.78

Table 2-2E. AVERAGE INCOMING 345- TO 335-nm RADIATION FOR 30- MINUTE INTERVALS

(w/m^2)

Midpoint of time interval (TST)	Mt. Wilson					Downtown Los Angeles				
	Oct 6	Oct 12	Oct 16	Oct 18	Oct 20	Oct 6	Oct 12	Oct 16	Oct 18	Oct 20
0715	1.04					0.674		0.729	1.41	
0745	1.72	1.56	1.51	1.62	1.43	1.05	0.827	1.12	1.11	1.13
0815	2.47	2.27	2.20	2.27	2.32	1.44	1.05	1.83	1.60	1.74
0845	3.21	3.00	2.93	2.87	2.84	1.81	1.26	2.54	2.00	2.31
0915	3.94	3.70	3.84	3.58	3.56	2.23	1.52	3.16	2.62	2.84
0945	4.39	4.18	3.97	4.20	4.17	2.19	1.85	3.75	3.22	3.30
1015	5.03	4.79	4.69	4.71	4.71	2.36	2.32	4.20	3.77	3.55
1045	5.59	5.36	5.25	5.06	5.12	2.51	2.77	4.58	3.98	3.78
1115	5.86	5.61	5.55	5.30	5.39	3.36	3.11	4.89	3.98	4.28
1145	5.86	5.68	5.58	5.40	5.38	3.82	3.16	4.87	3.65	4.60
1215	5.97	5.78	5.59	5.36	5.34	4.10	3.48	4.69	3.19	4.49
1245	5.92	5.74	5.52	5.28	5.15	4.12	3.79	4.68	2.97	4.14
1315	5.68	5.43	5.26	5.02	4.82	3.96	3.68	4.49	3.07	3.79
1345	4.65	4.69	4.49	4.66	4.32	3.11	3.55	4.13	2.72	3.05
1415	4.75	4.34	4.17	4.11	3.69	3.21	3.15	3.63	2.39	2.90
1445	3.24	3.87	3.64	3.47	3.10	2.59	2.61	3.05	2.28	2.43
1515	3.18	3.12	2.94	2.97	2.73	1.99	1.96	2.31	1.90	1.90
1545	2.44	2.36	2.22	2.06	1.83	1.68	1.51	1.45	1.39	1.36

Table 2-2F. AVERAGE INCOMING 355- TO 365-nm RADIATION FOR 30-MINUTE INTERVALS

(w/m^2)

Midpoint of time interval (TST)	Mt. Wilson					Downtown Los Angeles				
	Oct 6	Oct 12	Oct 16	Oct 18	Oct 20	Oct 6	Oct 12	Oct 16	Oct 18	Oct 20
0715	1.04					0.700		0.747	1.72	
0745	1.73	1.58	1.57	1.79	1.49	1.07	0.894	1.21	1.20	1.29
0815	2.51	2.31	2.30	2.42	2.63	1.47	1.12	1.94	1.68	1.84
0845	3.30	3.07	3.07	2.98	2.94	1.85	1.31	2.64	2.09	2.36
0915	4.03	3.80	3.83	3.71	3.64	2.27	1.57	3.27	2.75	2.99
0945	4.56	4.27	4.28	4.36	4.33	2.24	1.92	3.92	3.38	3.49
1015	5.20	4.97	4.97	4.88	4.88	2.44	2.42	4.45	3.95	3.72
1045	5.72	5.49	5.52	5.26	5.31	2.60	2.88	4.79	4.26	3.91
1115	6.00	5.78	5.83	5.51	5.60	3.50	3.22	5.11	4.18	4.54
1145	6.00	5.85	5.85	5.63	5.56	3.97	3.27	5.08	3.81	4.71
1215	6.11	5.95	5.87	5.56	5.54	4.24	3.62	4.89	3.34	4.77
1245	6.08	5.91	5.79	5.48	5.34	4.25	3.94	4.88	3.16	4.39
1315	5.80	5.57	5.53	5.18	4.98	4.09	3.82	4.69	3.26	4.03
1345	4.90	4.90	4.87	4.82	4.45	3.24	3.67	4.29	2.85	3.23
1415	4.95	4.48	4.44	4.22	3.85	3.49	3.24	3.78	2.51	3.07
1445	3.17	3.95	3.82	3.57	3.20	2.63	2.69	3.16	2.38	2.56
1515	3.25	3.17	3.04	3.15	2.99	2.05	2.06	2.41	1.93	2.00
1545	2.47	2.38	2.27	2.14	1.92	1.72	1.56	1.54	1.47	1.46

Table 2-2G. AVERAGE INCOMING 365- TO 375-nm RADIATION FOR 30-MINUTE INTERVALS

(w/m^2)

Midpoint of time interval (TST)	Mt. Wilson					Downtown Los Angeles				
	Oct 6	Oct 12	Oct 16	Oct 18	Oct 20	Oct 6	Oct 12	Oct 16	Oct 18	Oct 20
0715	1.21					0.828		0.866	1.98	
0745	2.01	1.84	1.77	2.09	1.69	1.26	1.05	1.43	1.38	1.47
0815	2.90	2.67	2.61	2.79	3.22	1.72	1.32	2.26	1.94	2.12
0845	3.76	3.55	3.50	3.39	3.34	2.18	1.53	3.08	2.41	2.75
0915	4.60	4.37	4.34	4.22	4.17	2 68	1.83	3.81	3.18	3.37
0945	5.22	4.97	4.90	4.94	4.89	2.65	2.24	4.57	3.89	3.97
1015	5.95	5.73	5.60	5.51	5.50	2.88	2.81	5.08	4.54	4.18
1045	6.49	6.29	6.15	5.93	5.97	3.09	3.36	5.51	4.79	4.44
1115	6.80	6.60	6.49	6.20	6.27	4.16	3.68	5.89	4.79	5.09
1145	6.80	6.65	6.49	6.30	6.22	4.70	3.83	5.84	4.39	5.48
1215	6.89	6.78	6.52	6.24	6.21	4.99	4.24	5.62	3.84	5.43
1245	6.86	6.74	6.45	6.18	5.99	5.00	4.62	5.61	3.65	4.93
1315	6.56	6.36	6.16	5.84	5.58	4.82	4.45	5.41	3.79	4.54
1345	5.54	5.69	5.53	5.43	5.03	3.85	4.26	5.03	3.40	3.68
1415	5.62	5.16	5.02	4.79	4.36	4.18	3.77	4.36	2.90	3.47
1445	3.56	4.54	4.31	4.04	3.63	3.14	3.14	3.65	2.75	2.92
1515	3.71	3.64	3.46	3.68	3.52	2.39	2.41	2.77	2.29	2.24
1545	2.78	2.75	2.59	2.74	2.21	2.02	1.82	1.80	1.72	1.64

Table 2-2H. AVERAGE INCOMING 375- TO 385-nm RADIATION FOR 30-MINUTE INTERVALS

(w/m^2)

Midpoint of time interval (TST)	Mt. Wilson					Downtown Los Angeles				
	Oct 6	Oct 12	Oct 16	Oct 18	Oct 20	Oct 6	Oct 12	Oct 16	Oct 18	Oct 20
0715	1.22					0.809		0.848	1 95	
0745	2.05	1.82	1.77	2.27	1.68	1.23	1.09	1.46	1.36	1.60
0815	2.95	2.66	2.59	2 88	3.33	1.69	1.34	2.23	1.89	2.06
0845	3.81	3.52	3.44	3.38	3.32	2.13	1.50	3.02	2.36	2.72
0915	4.65	4.33	4.26	4.18	4.15	2.64	1.79	3.74	3.11	3.35
0945	5.36	5.17	5.14	4.90	4.87	2.67	2.19	4.44	3.82	3.89
1015	6.11	5.78	5.65	5.48	5.48	2.87	2.77	4.94	4.42	4.15
1045	6.59	6.23	6.08	5.88	5.94	3.09	3.30	5.37	4.67	4.32
1115	6.84	6.54	6.41	6.15	6.24	4.23	3.70	5.73	4.68	5.03
1145	6.84	6.55	6.39	6.24	6.18	4 28	3.78	5.67	4.36	5.38
1215	6.96	6.69	6.43	6.17	6.17	4.91	4.18	5.49	3.78	5.25
1245	6.93	6.68	6.37	6.12	5.96	4.93	4.54	5.47	3.61	4.86
1315	6.65	6.31	6.07	5.80	5.55	4.75	4.37	5.27	3.74	4.48
1345	5.75	5 86	5.76	5.40	5.01	3.88	4.19	4.82	3.26	3.60
1415	5.86	5.21	5.04	4.76	4.31	4.18	3.69	4.19	2.84	3.43
1445	3.52	4 52	4.25	4.02	3.61	3.04	3.06	3.56	2.69	2.83
1515	3 77	3 62	3.44	3.85	3.81	2.34	2.39	2.72	2.23	2.19
1545	2.84	2.72	2.57	2.56	2.30	1.98	1.80	1.83	1.72	1.65

Table 2-2I. AVERAGE INCOMING 385- TO 395-nm RADIATION FOR 30-MINUTE INTERVALS

(w/m^2)

Midpoint of time interval (TST)	Mt. Wilson					Downtown Los Angeles				
	Oct 6	Oct 12	Oct 16	Oct 18	Oct 20	Oct 6	Oct 12	Oct 16	Oct 18	Oct 20
0715	1.25					0.819		0.856	2.11	
0745	2.11	1.89	1.84	2.53	1 72	1.26	1 16	1.55	1.42	1.76
0815	3.05	2.77	2.71	3.10	3.83	1.71	1.41	2.28	1.94	2.11
0845	3.95	3.64	3.62	3.50	3.43	2.16	1.51	3.06	2.40	2.78
0915	4.79	4 49	4.49	4.34	4.28	2.67	1.80	3.78	3.16	3.39
0945	5.64	5.51	5.66	5.09	5.44	2.77	2 22	4.47	3.89	3.93
1015	6 38	6 07	5.99	5.63	5.61	2.84	2.81	4.94	4.47	4.16
1045	6 74	6 40	6.35	6.02	6.09	3.16	3.35	5 38	4.71	4.34
1115	6 99	6.69	6 69	6 31	6.39	4.24	3 74	5.77	4.72	5.40
1145	7.01	6 73	6 66	6.39	6.30	4.39	3.80	5.69	4.34	5.40
1215	7.14	6.87	6.71	6 36	6.27	4.99	4 21	5.50	3.85	5.28
1245	7.10	6.88	6.64	6 26	6.08	4 99	4.55	5.47	3.72	4 88
1315	6.80	6.48	6 33	5.96	5.66	4.82	4.38	5.27	3.83	4.51
1345	6.05	6 23	6.25	5.56	5.11	3.98	4.20	4.81	3.32	3.63
1415	6.11	5.46	5 36	4 88	4.46	4.28	3.71	4.26	2.91	3.47
1445	3.46	4 67	4.42	4 12	3.68	3 08	2.48	3.59	2.75	2.85
1515	3.86	3.71	3.56	4.15	4.19	2.39	2.48	2.76	2.28	2.22
1545		2.81	2.67	2.69		2.02	1.84	1.90	1.81	1.71

Table 2-3. AVERAGE INCOMING 300- TO 380-nm RADIATION FOR 30-MINUTE INTERVALS, WIDE-BAND FILTER

(w/m^2)

Midpoint of time interval (TST)	Mt. Wilson					Downtown Los Angeles				
	Oct 6	Oct 12	Oct 16	Oct 18	Oct 20	Oct 6	Oct 12	Oct 16	Oct 18	Oct 20
0715	6.47					4.44		4.67	10.3	
0745	10.9	9.80	9.46	10.2	9.08	6.87	5.31	7.21	7.29	7.33
0815	15.8	14.4	14.0	14.5	14.5	9.38	6.83	11.9	10.5	11.3
0845	20.7	19.1	18.7	18.3	18.1	11.8	8.28	16.4	13.0	15.0
0915	24.4	23.7	23.3	22.8	22.8	14.6	9.94	20.3	17.1	18.6
0945	28.1	26.1	25.1	27.0	26.8	14.3	12.2	24.5	21.0	21.5
1015	32.5	30.9	30.2	30.3	30.3	15.4	15.5	27.5	24.5	23.0
1045	36.7	34.6	33.9	32.6	33.0	16.5	18.2	29.9	26.2	24.0
1115	37.9	36.3	35.8	34.4	34.8	22.1	20.2	31.9	26.0	28.1
1145	38.1	36.7	36.0	35.0	34.6	25.2	20.6	31.7	23.5	27.9
1215	38.7	37.5	36.1	34.7	34.4	26.7	22.7	30.7	20.4	29.4
1245	38.3	37.0	35.5	34.0	33.1	27.0	25.4	30.8	19.3	26.6
1315	36.6	34.8	33.8	32.0	30.7	25.9	23.8	29.3	19.9	24.4
1345	29.0	29.9	29.2	30.0	27.4	20.1	22.9	26.7	17.6	19.7
1415	30.4	27.4	26.5	26.0	23.4	22.6	20.1	23.3	15.4	18.7
1445	19.6	24.5	23.0	21.8	19.3	16.8	16.8	19.6	14.6	15.6
1515	19.9	19.5	18.5	18.5	17.1	13.1	12.6	14.2	12.1	12.1
1545	15.1	14.7	13.6	12 5	11.3	10.7	9.62	9.23	8.76	8.51

Table 2-4. AVERAGE INCOMING 300- TO 380-nm RADIATION FOR 30-MIHUTE INTERVALS, SUM OF VALUES FROM NARROW-BAND FILTERS

(w/m^2)

Midpoint of time interval (TST)	Mt. Wilson					Downtown Los Angeles				
	Oct 6	Oct 12	Oct 16	Oct 18	Oct 20	Oct 6	Oct 12	Oct 16	Oct 18	Oct 20
0715	6.26					4.17		4.28	9.09	
0745	10.7	9.56	9.30	10.3	8.86	6.44	5.15	6.94	6.87	7.17
0815	15.6	14.2	13.9	14.5	15.9	8.96	6.77	11.4	9.89	10.8
0845	20.5	19.1	18.8	18.2	18.0	11.4	7.95	15.8	12.4	14.3
0915	25.3	23.8	23.7	22.9	22.7	14.2	9.53	19.8	16.4	17.8
0945	28.6	26.8	26.0	27.2	26.9	14.0	11.9	23.7	20.4	20.9
1015	33.0	31.4	30.7	30.6	30.5	15.2	14.9	26.8	23.9	22.5
1045	36.7	35.1	34.3	33.0	33.2	16.2	17.8	29.1	25.5	23.8
1115	38.5	36.9	36.4	34.7	35.1	21.8	19.9	31.2	25.5	27.3
1145	38.6	37.4	36.5	35.4	35.0	24.5	20.3	31.1	23.2	29.3
1215	39.2	38.1	36.7	35.1	34.8	26.1	22.4	30.0	20.3	28.8
1245	38.9	37.7	36.1	34.5	33.5	26.6	24.3	29.9	18.9	26.4
1315	37.1	35.5	33.4	32.5	30.8	25.5	23.8	28.7	19.5	24.1
1345	30.3	30.8	29.6	30.1	27.8	20.5	22.6	26.3	17.3	19.5
1415	30.9	28.2	27.2	26.3	24.0	21.1	19.9	23.0	15.1	18.2
1445	20.2	24.9	23.5	22.0	19.7	16 5	16.5	19.1	13.0	15.3
1515	20.2	19.8	18.7	19.0	17.6	12.6	12.4	14.6	11.7	11.8
1545	15.2	14.8	13.8	13.1	11.5	10.5	9.40	9.02	8.60	9.84

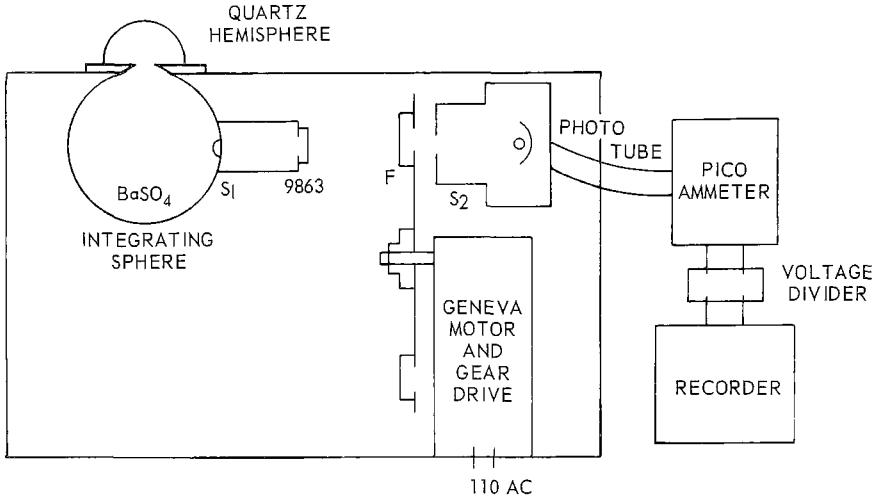

Figure 2-1. NBS filter-phototube UV system.

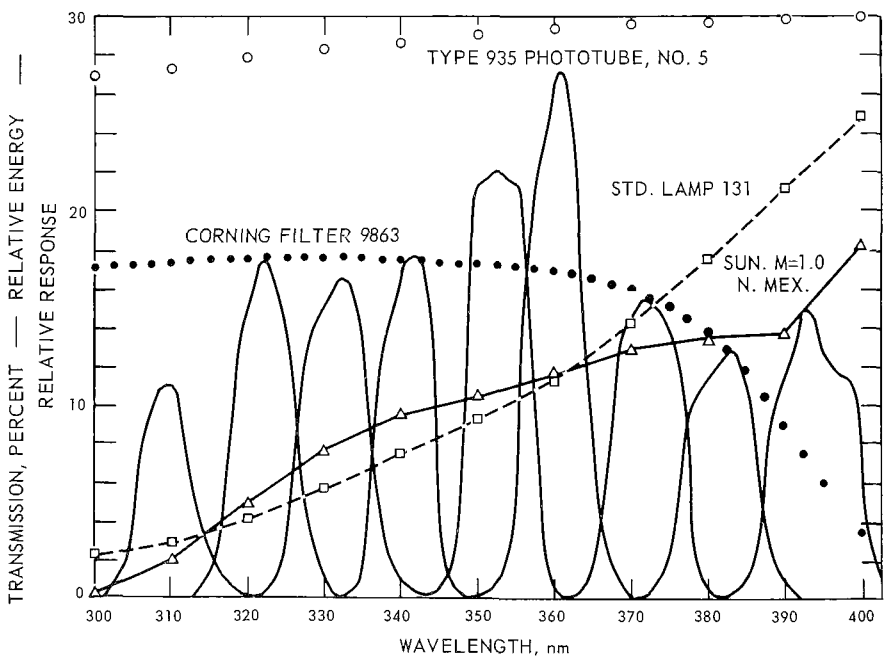

Figure 2-2. Spectral characteristics of the filters, phototube, 1000-watt quartz-iodine lamp standards of spectral irradiance, and the sun. The ordinates are exact for the nine interference filters, divided by 5 for Corning glass No. 9863, and relative only for the phototube, standard lamp, and the sun.

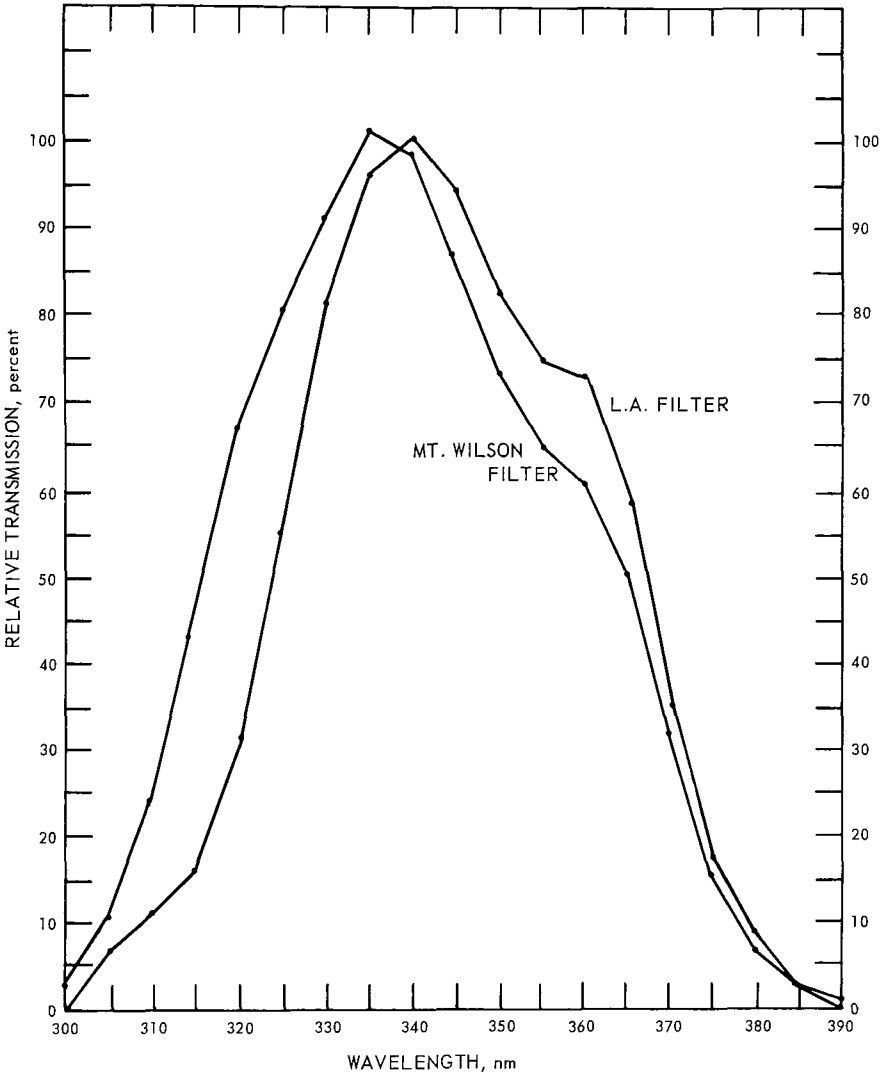

Figure 2-3. Relative spectral response of wide-band filter in filter photometers at Mt. Wilson and in Los Angeles.

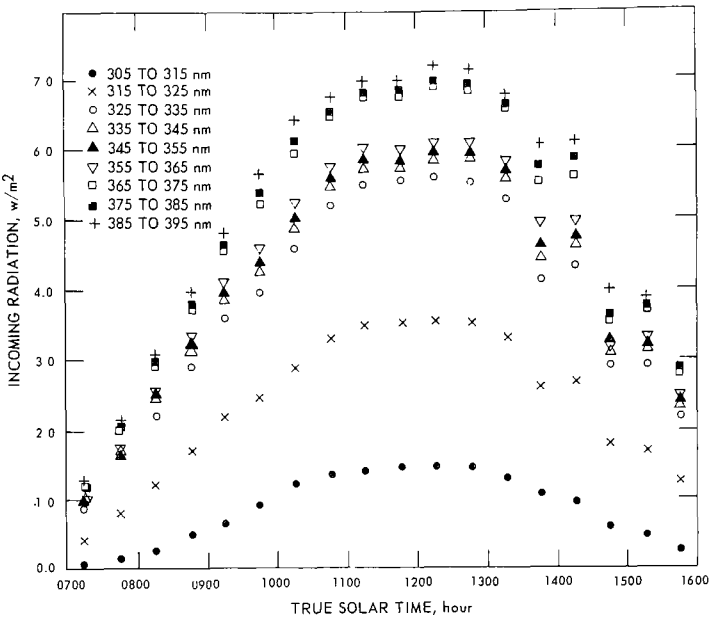

Figure 2-4. Average incoming radiation on Mt. Wilson, for 30-minute intervals as function of time, October 6.

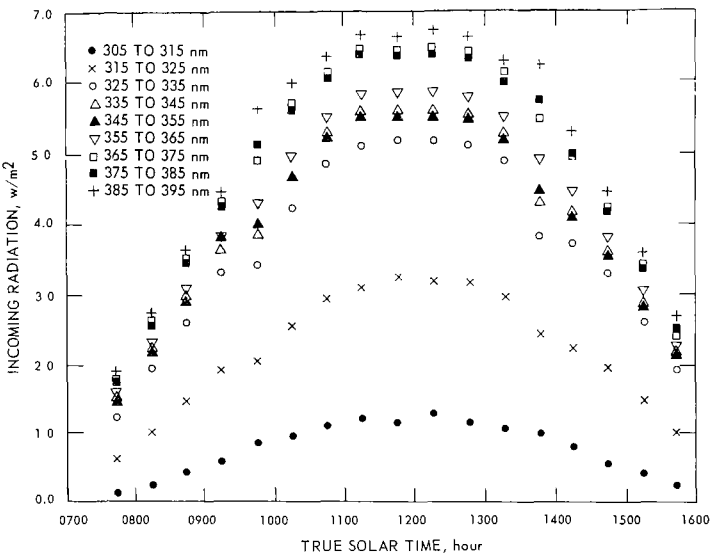

Figure 2-5. Average incoming radiation on Mt. Wilson, for 30-minute intervals as function of time, October 16.

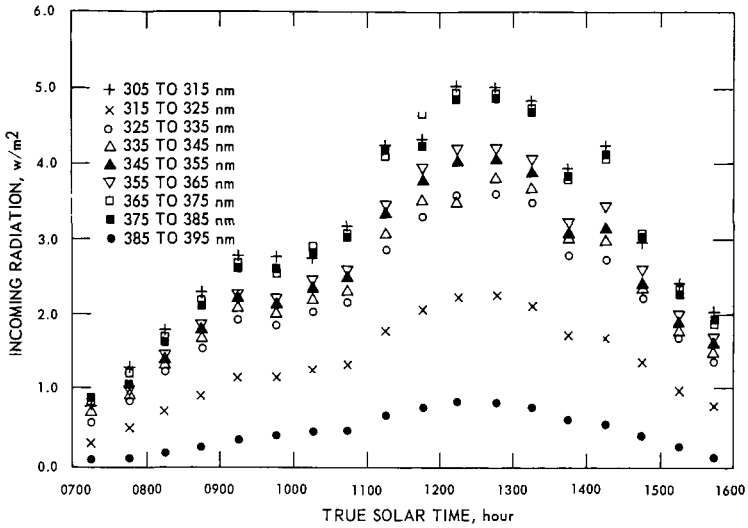

Figure 2-6. Average incoming radiation at Los Angeles for 30-minute intervals as function of time, October 6.

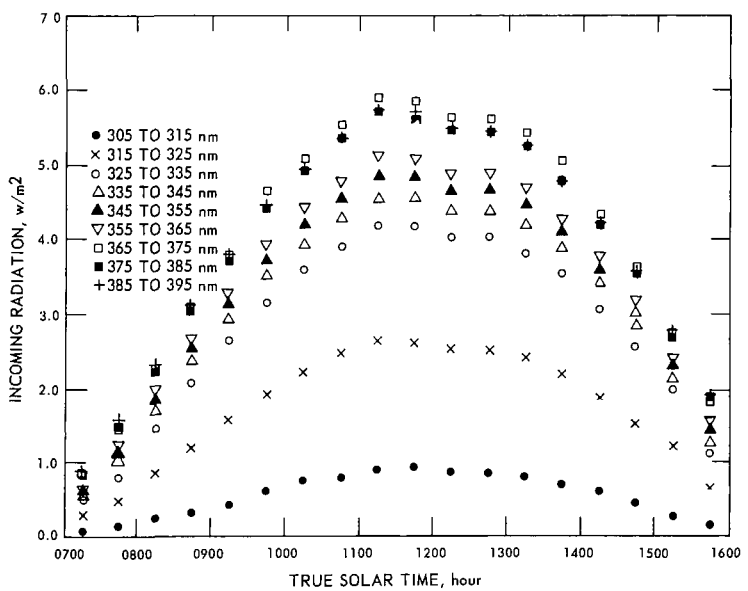

Figure 2-7. Average incoming radiation in downtown Los Angeles for 30-minute intervals as function of time, October 16.

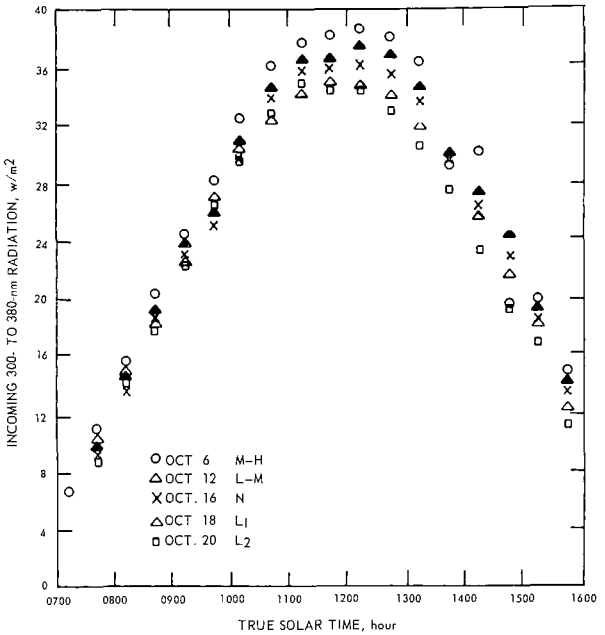

Figure 2-8. NBS wide-band filter measurements of average incoming radiation at Mt. Wilson for 30-minute intervals as function of time of day.

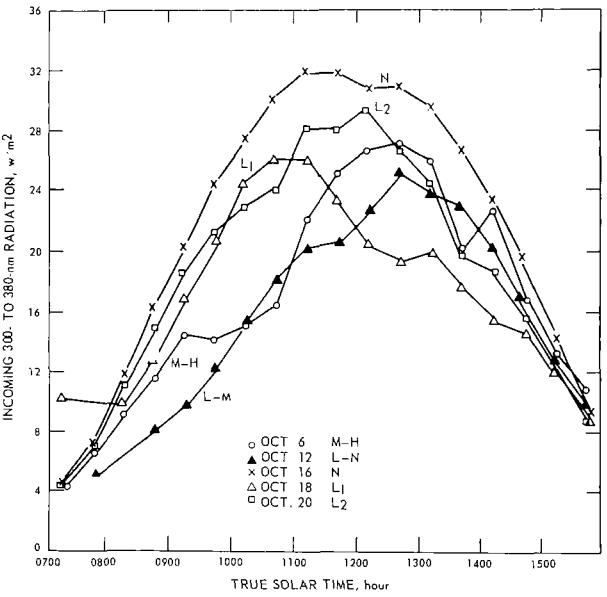

Figure 2-9. NBS wide-band filter measurements of average incoming radiation in downtown Los Angeles for 30-minute intervals as function of time of day; October 1965.

3: PHOTOCHEMICAL MEASUREMENTS

Robert J. Gordon
California Department of Public Health

INTRODUCTION

It is well recognized that the intensity of ultraviolet sunlight in the lower atmosphere figures importantly in determining the progress of photochemical smog reactions. Our Laboratory collaborated with PHS by making a number of measurements with chemical actinometers. These instruments were situated on the laboratory rooftop of the Los Angeles County Air Pollution Control District adjacent to the instruments used for physical measurements. The measurements were made at the indicated times on the scheduled flight days except for October 12 (an official holiday, for state and local government employees).

Two types of chemical actinometers were used. One was that of Tuesday *(1)*, in which the photolysis of nitrogen dioxide in nitrogen is determined by analysis before and after exposure to light. The reaction is

$$NO_2 + h_v \qquad NO + 0$$

The other system was the photoisomerization of o-nitrobenzaldehyde to o-nitrosobenzoic acid proposed for ultraviolet actinometry by Pitts and co-workers *(2)*.

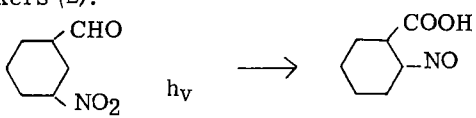

In this latter system liquid solutions were used. Isomerization was followed by pH measurement. This system was later elaborated into a trial model of a continuous recording actinometer.

EXPERIMENTAL PROCEDURE

NO_2 Photolysis - For NO_2 exposures a pillow-shaped bag of 0.001-inch Mylar film having an inflated capacity of about 90 liters was used. The dimensions flat were 60 by 104 centimeters; inflated, approximately 20 by 50 by 90 centimeters. The bag was heat-sealed and was equipped with a half-inch bulkhead fitting of stainless steel. A short Tygon connection closed with a Hoffman clamp was attached. The bag was en-

closed for darkness in a fiber drum with an opaque cloth under the metal lid. For about a minute before exposure the cloth served as light protection when the lid was removed during that interval.

The bag was evacuated and purged with 10 to 20 liters of prepurified nitrogen, then evacuated again. The bag was half-filled with nitrogen at 20 liters per minute through a Kel-F lubricated glass system. NO_2 from a cylinder was passed through a heated section of the system, closed off by stopcocks, and expanded into an evacuated bulb. The original volume, now at reduced pressure, was then swept into the bag with the remaining half of the nitrogen. Concentrations varied from 0.5 to 4.1 ppm NO_2.

After standing 30 to 45 minutes, the bag was attached to a continuous nitrogen oxides analyzer (Saltzman reagent) *(3)*. This analyzer requires about a half liter of sample per minute and reaches a level reading in about 20 minutes. The bag was left on the instrument for 30 minutes. Within a few minutes after exposure the bag was attached again to the analyzer for another 30 minutes. The same bag was used for all measurements.

Exposure was made by attaching the exposed fitting of the covered bag to a halyard, then uncovering and running the bag quickly up a 20-foot mast. At completion of the exposure the bag was quickly brought down into the drum and recovered with the cloth. It is estimated that time required for covering and uncovering the bag was about 5 seconds. All exposures were for 2 minutes.

o-Nitrobenzaldehyde (ONBA) Photolysis Solutions of o-nitrobenzaldehyde (Matheson-Coleman and Bell) were made in foil-covered vessels under subdued light. The procedure was to dissolve 0.01 mole of the material in 50 milliliters of chemically pure methanol, add slowly with stirring to 800 to 900 milliliters of water in a liter volumetric flask, rinse the weighing container with another 50 milliliters of methanol, and make up to volume with water. This procedure gave a 0.01 M solution in 10 percent aqueous methanol.

Exposures were made in 100-milliliter spherical Pyrex flasks filled just to the neck and closed with rubber stoppers. The outer diameter of the flasks was 6.3 centimeters with wall thickness of 0.15 centimeter. A flask was attached by a wire loop under the lip to the halyard. For exposure the foil covering was removed and the flask was hoisted up the mast. Exposures were for 10 minutes. Since the same halyard was used for NO_2 bag exposures, the flask was brought down (but not covered) briefly when the NO_2 bag was sent up and again when it was brought down. This changed the elevation of the flask, but not the length of exposure, for an estimated 1 minute of the total 10 minutes.

Conversion of the ONBA to acid was estimated by pH measurement on a Beckman Zeromatic pH meter. The pH of the unexposed solution was essentially that of deionized water, approximately 5.5. (The

limiting pH for prolonged exposure to UV light in one example was 2.77.) All flasks from a day of exposure were kept well-covered through the day. The pH levels of the solutions were measured in succession in a covered beaker at the end of the day. The meter was zeroed on pH 7 buffer reference. Corrections to the measured pH of exposed ONBA solutions were made as required, based on the reading for a pH 3 buffer reference.

Determinations by potentiometric titration were made of the dissociation constant for o-nitrosobenzoic acid (obtained by photolysis of ONBA solution). A set of triplicate runs using freshly boiled water and a nitrogen blanket gave $k_a = 2.8 \pm 0.3 \times 10^{-4}$.

TREATMENT OF DATA

NO_2 Photolysis - Tuesday's *(1)* method permits determination of the apparent decomposition rate constant for NO_2, k_d, from the following expression:

$$k_d = \frac{2.303}{t} \log \frac{(NO_2)_0}{(NO_2)_t}$$

where t is the exposure time (120 seconds in this case), $(NO_2)_0$ the initial NO_2 concentration, and $(NO_2)_t$ the final NO_2 concentration. The rate constant k_d is composite, involving three reactions *(4)*. To convert it to the primary k_a for the photolytic step itself, k_d must be multiplied by 1.45.

In order to infer from k_a the intensity of incident radiation, I_0, in the wavelength region absorbed by NO_2, the absorption coefficients for NO_2 *(5)* over 10-nm intervals were weighted and averaged as follows. The transmission of the Mylar bag in each interval was estimated from reference *(6)* (recalculated from 0.003 to 0.001 inch thickness). The quantum yield estimated for each interval *(7)* transmissivities of the Mylar, and the weighted distribution of solar ultraviolet for typical conditions *(8)* were used to weight the NO_2 absorption coefficients for averaging. (The solar distribution used was not necessarily that prevailing on the days of exposure, but it is closer to the actual than the assumption of uniform distribution would be. The correction resulting from its use is less than 5%.) The resultant average coefficient over the 300-to-410-nm range was

$$\bar{\alpha} = 1.47 \times 10^{-19} \text{ cm}^2 \text{/molecule}$$

For weak absorption, as in this case, $\bar{\alpha}$, k_a and I_0 are related by the expression *(9)*

$$K_a = 2.303 \alpha I_0$$

$$I_0 = 4.28 \times 10^{18} \text{ photons/sec-cm}^2$$

since the use of consistent units and the quantum yield factors relate molecules reacted to incident photons. Values calculated from this

expression are given in Table 3-1. Assuming an average wavelength of absorption of 350 nm, we converted the results to watts per square meter and plotted the data for various days of smog (Figures 3-1, 3-2.)

ONBA Data Treatment From the dissociation constant for o-nitroso-benzoic acid, the known concentration of the ONBA solution, and the pH before and after exposure to light, the total acid produced could be calculated. This is taken as equivalent to the amount of ONBA photo-isomerized. To derive from this the light intensity entering the solution, an expression similar to that of Pitts, Vernon and Wan *(10)* is used. This expression is based on the assumption of complete absorption. For the system used in the present work the transmission at 390 nm would be about 1 percent, at 400 nm about 15 percent, and at 410 nm about 60 percent *(10)*. No correction has been attempted for this. The flasks were assumed to be perfect spheres, although the peak partially obscured about 3 percent of the surface area.

$$I_S = \frac{NV}{\phi A t}\left[(Acid)_t - (Acid)_o\right] \times 10^{-3}$$

I_S = light intensity entering the solution, photons/sec-cm^2

N = Avegadro number = 6.02×10^{23}

$\frac{V}{A}$ = $\frac{\text{Volume of flask}}{\text{Cross-sectional area of flask}} = \frac{4\pi r^3/3}{\pi r^2} = \frac{4}{3}r = 4.0$ cm

o = Quantum yield, molecules / photon = 0.5

t = Exposure time, sec = 600

$(Acid)_t$ = Acid concentration at time t, moles/liter

$(Acid)_o$ = Acid concentration at start, moles/liter

Numerically this reduces to

$$I_S = 8.03 \times 10^{18} (Acid)_t$$

for the conditions used, where $(Acid)_o$ was negligible.

To infer from I_o the intensity of exterior radiation one must make corrections for reflection, absorption, and variation in angle of incidence at the wall of the Pyrex flask. The reflectance of Pyrex was calculated from Fressel's formula for equal 10 percent increments in incident flux. The absorbence of the Pyrex varies as a function of the length of the path through it, which is a function of the angle of incidence. The effect of wavelength, weighted for reported solar intensity distribution, *(8)*, on Pyrex absorption was also considered. Details of this treatment are given in Appendix 3A, in which the over-all average transmittance of the flask wall is derived. From this the expression for incident intensity is:

$$I_o = \frac{I_s}{\overline{T}_a \ \overline{T}_r}$$

where I_o = incident light intensity, photons/sec-cm^2

T_a = average transmission relative to absorption

T_r = average transmission relative to reflection

As shown in the Appendix, $T_a = 0.775$ and $T_r = 0.883$. Thus

$$I_o = 1.173 \times 10^{19} \times (\text{Acid})_t, \text{ photons/sec-cm}^2$$

Values derived from this expression are given in Table 3-1. Assuming an average wavelength of absorption of 350 nm, we converted the results to watts per square meter and plotted the data for various days of smog (Figure 3-2).

DISCUSSION

Table 3-1 shows the results of the two methods of measurement in comparable terms. Pitts, Wan, and Schuck *(2)* proposed the use of ONBA for actinometry of this sort because it absorbs with uniform quantum yield throughout the wavelength range that is effective in NO_2 photolysis. As pointed out by Pitts, Vernon, and Wan *(10)* the fall-off in photodissociation of NO_2 around 400 nm is at least roughly paralleled by the fall-off in ONBA absorptivity in the same region.

The short wavelength cut-offs for Mylar and Pyrex are also roughly parallel. Since the incident sunlight falls off rapidly in the same region, any difference in transmissivity of the two materials is not thought to be significant. The difference is in the direction of greater transmissivity of Pyrex.

Examination of Table 3-1 shows that although results obtained by the two methods are generally similar, the NO_2 values seem to be erratic. Since this method is quite reliable with rigid vessels (such as a spectrometer cell), the scatter may be related to the use of bags. One possibility is the variation in orientation of the bag during exposure as determined by the direction of the wind.

Another potential cause of difference between the two sets of readings is that NO_2 in this region has some vibrational structure *(11)*, whereas the ONBA in solution does not. Consequently if there is any NO_2 in the atmosphere, it will selectively absorb at wavelength maxima that are exactly those to which the NO_2 actinometer responds. The ONBA actinometer, however, responds alike to light at wavelengths of adjacent NO_2 maxima and minima, and therefore gives a better idea of radiation entering the upper levels of a polluted atmospheric layer.

The NO_2 actinometer corresponds to radiation, effective in NO_2 photolysis, which has survivied passage through the whole polluted layer. The differences in the two sets of readings were shown to be significantly correlated with the atmospheric NO_2 level by the t test (95% confidence limits). This effect may not be small, since the correlation suggests that 10 pphm NO_2 would increase the difference by about 0.5 x 10^{16} photons per second per square centimeter.

Another limitation on accuracy is the factor 1.45 used to convert k_d (NO_2) to k_a values. This factor is derived *(4)* from elementary rate constants in the literature that are not known with high precision.

It appears that either method is potentially suitable for solar UV measurements in a relative sense, the ONBA method being considerably simpler in execution. Several sources of uncertainty and approximation are involved in reducing absolute values of light intensity by either method, as discussed above. Since much of this relates to the containers, the uncertainty might be reduced somewhat by use of a container of special properties, such as a thin-walled quartz bulb for the ONBA. In any case the chemical methods are adequate for relative measurements and have the useful property as applied of integrating radiation from all directions.

APPENDIX 3A: OPTICAL PROPERTIES OF SPHERICAL PYREX FLASK

The ultraviolet absorption characteristics of Pyrex were obtained from catalog information of the Corning Glass Company. These are given in Table 3-2. The refractive index was reported to be $n_D = 1.474$. From known refractive index - wavelength variations for several other types of glass, the index for Pyrex at 350 nm was estimated to be 1.494. This value was used in computation.

Reflectances at the air-Pyrex interface were calculated. For normal incidence ($i = 0^o$)

$$R = \left(\frac{n-1}{n+1}\right)^2$$

where R = reflectance, n = refractive index of Pyrex, 1 = refractive index of air. From this formula R = 0.0392. For other angles of incidence Fresnel's formula was used:

$$R = 1/2 \left[\frac{\sin^2 (i-r)}{\sin^2 (i+r)} + \frac{\tan^2 (i-r)}{\tan^2 (i+r)}\right]$$

where i = angle of incidence and r = angle of refraction. The angle of refraction r was obtained from the relation

$$n = \frac{\sin i}{\sin r}$$

Values of transmittance, (relative to reflection) $T_r = 1-R$, are given in Table 3-3 for 10 percent annular increments in flux area (see below).

The reflection at the second surface between Pyrex and water was considered in a similar way. For the worst case (i = 90 degrees from Table 3-3) the reflectance at the glass-water interface is only 0.0072. This effect was therefore neglected.

The distribution of light flux over various angles of incidence was deduced as follows. For light from any particular direction, rays striking the flask at angle i lie on a circle of diameter D sin i, where D is the diameter of the flask. This circle projected on a plane normal to the direction of the rays has an area $A = \frac{\pi}{4} (D \sin i)^2$. Incremental areas of annular rings on the plane of projection are given by

$$dA = \frac{\pi}{2} D^2 \sin i \cos i \, di.$$

To obtain values for the area between circles for given values of i, the above expression is integrated:

$$A = \int_{i_1}^{i_2} \frac{\pi}{2} D^2 \sin i \cos i \, di$$

$$= \frac{\pi}{4} D^2 (\sin^2 i_2 - \sin^2 i_1)$$

Values of i have been tabulated for 10 percent increments in $\sin^2 i$ (Table 3-4). These relative areas were used to weight $\overline{T}_r$ to arrive at the average over-all $\overline{T}_r$. Similarly the path length through the glass, $w = w_o/\cos r$ (where w_o is the normal thickness of the flask wall) was weighted for relative areas to derive the over-all $\overline{w}$.

In Table 3-2 the absorbances A_λ for Pyrex at various wavelengths are weighted by factors derived for solar intensities in the lower atmosphere (8). Multiplied by the average path-length $\overline{w}$ these allow the value for the over-all average transmittance (relative to absorption), $\overline{T}_a$, to be derived.

$$\overline{A} = 0.0647 \text{ (1 mm path)}$$

$$\overline{w}\overline{A} = 0.1111 = -\log \overline{T}_a$$

$$\overline{T}_a = 0.775$$

Although the solar irradiance values used for weighting are estimated for typical conditions, not necessarily the same as those prevailing on the days of exposure, they represent a closer approach to the accurate value of $\overline{T}_a$ than does no weighting at all. Without weighting, $\overline{T}_a$ would be approximately 0.65 for the interval 300 to 400 nm, a 16 percent difference.

In Table 3-4 the solar intensity (8) weighting factors are used to derive the average effective absorption coefficient for NO_2.

REFERENCES

1. Tuesday, C. S. The Atmospheric Photooxidation of Trans-Butene -2 and Nitric Oxide. In: Chemical Reactions in the Upper and Lower Atmosphere, Interscience, New York, N. Y. (1961).

2. Pitts, J. N., Jr., J. K. S. Wan, and E. A. Schuck. Photochemical Studies in an Alkali Halide Matrix. I. J. Am. Chem. Soc. 86:3606 (1964).

3. Thomas, M. D., L. H. Rogers, J. A. MacLeod, R. C. Robbins, R. C. Goettelman, and R. W. Eldridge. Automatic Apparatus for Determination of NO and NO_2 in the Atmosphere. Anal. Chem. 28:1810-16 (1956).

4. Bufalini, J. J., and E. R. Stephens. The Thermal Oxidation of Nitric Oxide in the Presence of Ultraviolet Light. Intern. J. Water Pollution. 9:123-28 (1965).

5. Leighton, P. A. Photochemistry of Air Pollution, Academic Press, New York, N. Y. (1961) p. 54.

6. Korth, M. W. Dynamic Irradiation Chamber Tests of Automotive Exhaust. U. S. Public Health Service Publ. No. 999-AP-5 Cincinnati, Ohio (1963) p. 9.

7. Leighton op. cit., p. 55.

8. Leighton, op. cit., p. 29.

9. Leighton, op. cit., p. 27.

10. Pitts. J. N., Jr., J. M. Vernon and J. K. S. Wan. A Rapid Actinometer for Photochemical Air Pollution Studies. Intern. J. Air Water Pollution 9:595-600 (1965).

11. Hall, T. C., Jr., and F. E. Blacet. Separation of the Absorption Spectra of NO_2 and N_2O_4 in the Range of 2400 5000A. J. Chem. Phys. 20:1745 (1952).

Table 3-1. ULTRAVIOLET RADIATION IN LOS ANGELES

Date[a]	Midpoint of exposure interval (TST)	k_d, NO_2, 10^{-3}/sec	I_o, NO_2 b	I_o, NO_2 c	(Acid) $_t$, 10^{-3} moles/l	I_o, ONBA b	I_o, ONBA c
Oct 6	0850	1.33	0.57	32.5	0.84	0.99	56.4
	1050	2.75	1.18	67.3	1.26	1.48	84.4
	1250	1.63	0.70	39.9	1.58	1.85	105.0
	1450	1.32	0.56	31.9	1.21	1.42	80.9
Oct 16	0835	3.34	1.43	81.5	1.17	1.37	78.1
	1035	7.37	3.15	180.0	1.64	1.92	109.0
	1235	4.40	1.88	107.0	1.70	1.99	113.0
	1435	5.87	2.51	143.0	1.41	1.65	94.0
Oct 18	0835	3.18	1.36	77.5	0.84	0.99	56.4
	1035	6.10	2.61	149.0	1.51	1.77	101.0
	1235	5.58	2.39	136.0	1.04	1.22	69.5
	1435	2.95	1.26	71.8	1.01	1.19	67.8
Oct 20	0835	2.88	1.23	70.1	1.13	1.33	75.8
	1035	1.02	0.44	25.1	1.70	1.99	113.0
	1235	6.13	2.62	149.0	1.51	1.77	101.0
	1435	1.73	0.74	42.2	1.17	1.37	78.1
			avg. 1.539			avg. 1.519	

[a] No data taken October 12.
[b] 10^{16} photons/sec-cm^2.
[c] Watts/m2 (assuming average energy at 350 nm).

Table 3-2. ULTRAVIOLET ABSORPTION CHARACTERISTICS OF PYREX

nm	T, 1 mm	A, 1 mm	Weight [a]	Weighted A
300	0.34	0.468	0.003	0.0014
310	0.55	0.260	0.026	0.0068
320	0.71	0.149	0.055	0.0082
330	0.80	0.097	0.089	0.0086
340	0.86	0.065	0.093	0.0060
350	0.88	0.055	0.103	0.0057
360	0.89	0.050	0.106	0.0053
370	0.90	0.046	0.127	0.0058
380	0.90	0.046	0.121	0.0056
390	0.91	0.041	0.114	0.0047
400	0.91	0.041	0.163	0.0066
			1.000	$\bar{A} = 0.0647$

[a] From Leighton (8) Table 8, 40 degree zenith angle (normalized from 300 to 400 nm).

Table 3-3. TRANSMITTANCE OF PYREX FLASK

Relative annular flux area	i	r	T_r	avg. $w = W_o$ av cos r
0	0	0	0.9608	1.50
0.1	18° 26'	12° 13'	0.9605	1.55
0.2	26° 34'	17° 25'	0.9599	1.59
0.3	33° 13'	21° 30'	0.9583	1.63
0.4	39° 14'	25° 03'	0.9556	1.68
0.5	45° 00'	28° 15'	0.9506	1.73
0.6	50° 46'	31° 14'	0.9418	1.78
0.7	56° 48'	34° 03'	0.9252	1.84
0.8	63° 26'	36° 46'	0.8920	1.91
0.9	71° 34'	39° 25'	0.8085	1.98
1.0	90° 00'	42° 01'	0	
			$\overline{T}_r = 0.8833$	$\overline{w} = 1.719$

Table 3-4. NO_2 ABSORPTION COEFFICIENT

λ, A	T_λ 0.001 in. Mylar	α_λ, NO_2 1 / mole - cm	ϕ_λ(est.)	Weight	Weighted ($\alpha_\lambda T_\lambda \phi_\lambda$)
3000	0	0	0.98	0.003	0
3100	0	57	0.97	0.021	0
3200	0.65	78	0.96	0.045	2.19
3300	0.80	98	0.95	0.074	5.51
3400	0.83	119	0.94	0.077	7.15
3500	0.85	136	0.93	0.085	9.14
3600	0.86	149	0.92	0.088	10.38
3700	0.87	158	0.92	0.105	13.28
3800	0.88	163	0.90	0.100	12.91
3900	0.89	167	0.84	0.094	11.74
4000	0.90	171	0.67	0.134	13.82
4100	0.91	167	0.09	0.174	2.38
				1.000	$\overline{\alpha} = 88.5$

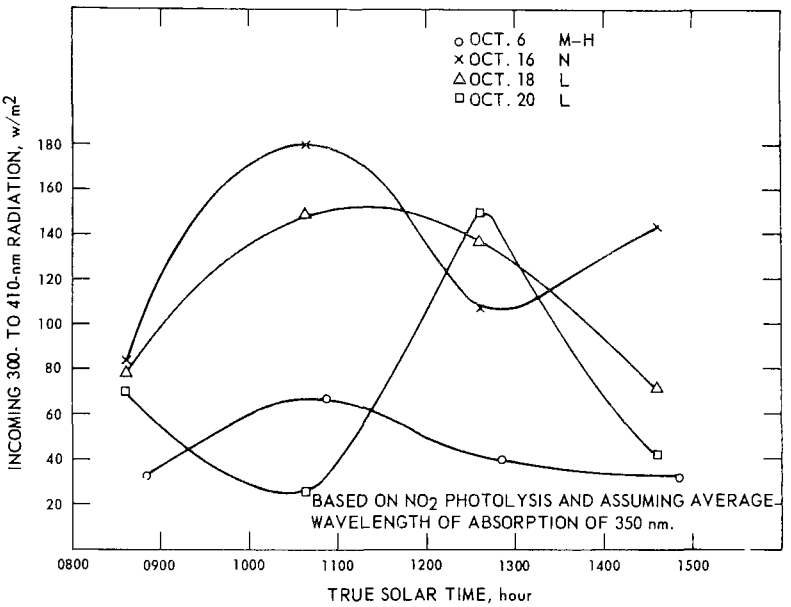

Figure 3-1. Incoming 300- to 410-nm radiation as function of time of day for various days of smog.

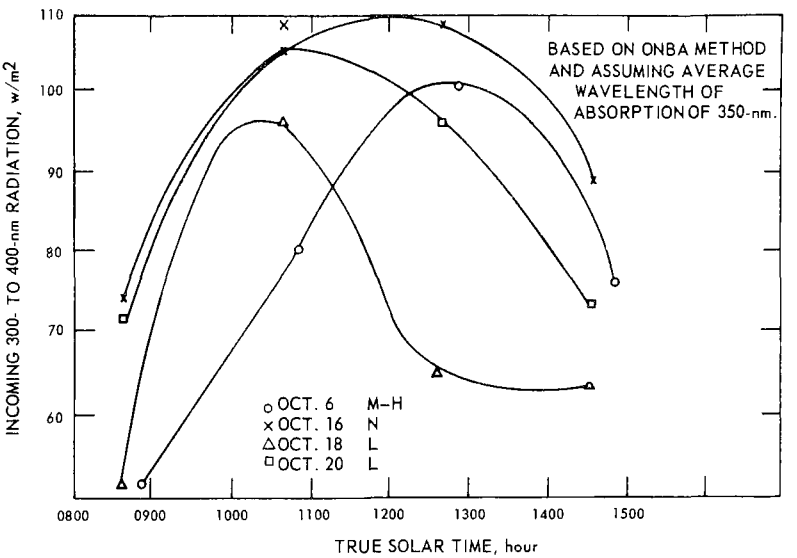

Figure 3-2. Incoming 300- to 400-nm radiation as function of time of day for various days of smog.

University of California at Riverside

4: PHOTOCHEMICAL MEASUREMENTS

R. N. McCormick, J. M. Vernon, J. N. Pitts, Jr.

Department of Chemistry
University of California at Riverside

The relative intensity values and ratios of direct and reflected intensities obtained during the cooperative ultraviolet study for the Los Angeles basin were arrived at by using a special sensitized actinometric paper impregnated with o-nitrobenzaldehyde *(1)*. Upon exposure to the wavelength range 300 - 400 nm in sunlight the photoisomerization of o-nitrobenzaldehyde (1) o-nitrosobenzoic acid (2) proceeds in gaseous, solution, and solid state with a quantum yield of 0.5, which is independent of the exciting wavelength in the prestated range of approximately 300 to 400 nm.

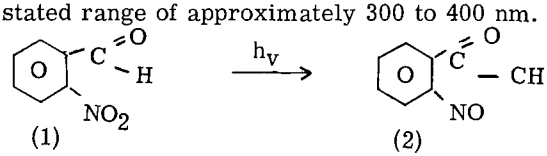

(1) (2)

Since sunlight received by the earth's lower atmosphere contains negligible radiation shorter than 300 nm, this o-nitrobenzaldehyde actinometer offers an advantage over many others in that its effective range corresponds almost precisely with the distribution of ultraviolet radiation present in the lower atmosphere. Furthermore, because of the simplicity of the procedure, the apparatus, and the calculations the technique is well suited to the program. In this method the assumption is made that the quantum yield for the rearrangement remains constant at 0.5 in the impregnated paper. Since this method is applied only to relative measurements, the exact quantum yield value is not important.

The sensitized papers were prepared by uniformly wetting 5.5-centimeter discs of filter paper with 0.5-milliliter portions of a 0.5 o-nitrobenzaldehyde solution in ethanol-water and allowing the treated papers to dry in the dark (approximately 2 hours drying time). Once dry, the sensitized papers were stored in a dark place and all further handling was done in a dark room, away from direct lighting. The sensitized papers are stable for extended periods if kept dry and in the dark.

The apparatus for analyzing exposed papers consisted of a Beckman Model G pH meter and an Ag/Ag-C1 combination electrode

(single unit, one electrode built within the other). The exposed papers were eluted with 20-milliliter portions of 1:1 ethanol-water, and the pH was determined after it had stabilized (about 20 minutes). Readings were reproducible within ±0.01 unit. With the measured pH value, relative ultraviolet intensity can be computed from equation (1), which is simply the total number of acid molecules formed divided by the exposure time.

$$Ir = \frac{\left\{\left[\frac{(H^+)^2}{Ka} + (H^+)\right] - (Hb^+)\right\} V}{t} \qquad (1)$$

I_r = relative ultraviolet intensity, Eins/min per unit area

K_a = dissociation constant for o-nitrosobenzoic acid in 1:1 ethanol-water = 3.2×10^{-5}

H^+ = hydrogen ion concentration calculated from measured pH

H_b^+ = hydrogen ion concentration from an unexposed sample paper = 1.90×10^{-7}

V = eluted solution volume = 0.020 l

t = exposure time, min

The sensitized papers were exposed first upward from atop the roof of the Air Pollution Control District Laboratory in downtown Los Angeles to measure the ultraviolet intensity penetrating through the atmosphere to approximately ground level, and second from an airplane flying at preassigned altitudes over the downtown vicinity. Two exposures were made at each level. One was upward to measure the incoming radiation from above and the other downward to measure the reflected radiation from below.

To allow for manipulation of the sensitized papers outside of the aircraft while in flight, the papers were sandwiched between two 1/16-inch polymethyl-methacrylate sheets (transparent to below 300 nm). The upward exposures were accomplished by manually holding the sample above and in front of the leading edge of the wing. For downward exposures a simple mechanical shutter device was mounted behind the wing support strut and was manually operated and reloaded from within the cabin of the aircraft. A similar shutter device was used to expose the samples from atop the laboratory roof. Every means was employed to keep the papers in the dark. All handling time was kept to a minimum while the papers were prepared and exposed.

RESULTS

The pH data and exposure times for the paper strips at B' elevations corresponding to the four flight intervals for the 5 flight days, are summarized in Table 4-1, which includes data from measurements on the laboratory rooftop at the Los Angeles measurement site. These results are reduced to values of average energy absorped per unit time by the sample strips during the exposure period given in Table 4-2. Ratios of outgoing to incoming radiation were calculated and are given in Table 4-3.

In the summary of results the most significant values are the ratio of intensities and the relative intensities, and not the stated intensities. Thus, the stated intensities are expressed in Einsteins per minute for the sample area (11.8 cm^2) without reduction to a unit area. Likewise, the value for energy per unit time was not converted to watts. This conversion would normally require a summation over the wavelength region of sensitivity, which varies with wavelength. Furthermore, an absolute value of the radiation incident on the sensor could not be calculated because data are not available to account for the efficiency with which the incident radiation is absorbed and to what extent it enters into the chemical reaction under various conditions of exposure and other functioning parameters. If approximations are to be made and assumptions tested, conversion of Einsteins per minute to watts is suggested at the average wavelength of 367 nm.

The variations of incoming and outgoing radiation for the 2 days of extreme conditions, i.e., moderate-to-heavy smog (October 6) and no smog (October 16) are shown as a function of elevation (Figures 4-1 and 4-2) and as a function of time (Figures 4-3 and 4-4). Ratios of outgoing to incoming radiation as function of elevation for various days of smog are shown for the mid-morning flight (Figure 4-5) and the late afternoon flight (Figure 4-6); they are also shown as a function of time for various days of smog for the lowest (Figure 4-7) and highest (Figure 4-8) elevation interval.

REFERENCE

1. Pitts, J. N., Jr., J. M. Vernon, and J. K. S. Wan. A Rapid Actinometer for Photochemical Air Pollution Studies. Intern J. Air Water Pollution 9:595-600 (1965).

Table 4-1. pH VALUES /EXPOSURE TIME (min) FOR INCOMING AND OUTGOING 300-TO 400-nm RADIATION

Exposure interval (TST)	Elevation, thousands of feet						
	Ground	1-1.5	2.6-3.0	5.6-6	1-1.5	2.8-3.2	5.6-6
	Incoming				Outgoing		
Oct 6							
0830-0930	3.87/15	4.04/5	4.06/5	4.07/5	4.42/10	4.33/10	4.30/10
1030-1130	3.83/15		3.98/4	3.98/4		4.09/15	4.18/10
1230-1330	3.79/15		3.98/4	3.96/4		4.12/15	4.11/15
1430-1530	3.95/14		4.14/4	4.14/4		4.28/15	4.20/15
Oct 12							
0800-0900	5.54/2	5.14/2	5.08/2	5.32/1	5.06/8	4.86/8	4.71/8
1000-1100	5.06/2	4.69/2	4.52/2	4.53/2	4.92/8	4.68/8	4.58/8
1200-1300	4.22/4	4.33/2	4.23/2	4.24/2	4.64/8	4.72/3	4.63/3
1400-1500	4.48/4	4.75/1	4.58/1	4.52/1	4.93/3	4.74/3	4.65/3
Oct 16							
0800-0900		5.05/1	5.32/1	5.48/1	5.97/3	6.11/3	6.26/3
1000-1100	4.24/4	4.46/2	4.42/2	4.60/1	5.33/8	5.61/3	5.57/3
1200-1300	4.19/4	4.67/1	4.66/1	4.33/2	5.97/3	5.92/3	5.08/8
1400-1500	4.53/4	5.07/1	4.80/2	4.64/2	6.48/3	5.96/3	5.32/8
Oct 18							
0800-0900	4.91/4	5.04/1	5.21/1	5.29/1	5.50/8	5.91/3	5.44/8
1000-1100	4.25/4	4.55/1	4.50/1	4.35/2	5.71/3	5.16/8	5.18/8
1200-1300	4.42/4	4.70/1	4.54/1	4.52/1	5.56/8	5.20/8	4.97/8
1400-1500	4.63/4	5.41/1	4.84/1	4.66/1	6.28/3	5.67/3	5.49/3
Oct 20							
0800-0900	5.56/2	5.18/2	5.55/2	5.76/2	5.72/8	5.92/8	6.46/3
1000-1100	4.75/2	4.33/2	4.78/2	4.77/2	5.96/3	5.54/8	5.41/8
1200-1300	4.68/2	4.67/2	4.53/2	4.50/2	6.24/3	5.64/8	5.40/8
1400-1500	5.01/2	5.06/2	4.90/2	4.66/2	6.45/3	5.75/8	5.32/8

Table 4-2. INCOMING AND OUTGOING 300- TO 400-nm RADIATION

Exposure Interval (TST)	Elevation, thousands of feet						
	0.35 (Rooftop)	1.1-1.5	2.6-3.0	5.6-6.0	1.1-1.5	2.6-3.0	5.6-6.0
	Incoming (10^{-7} Einsteins/min-area)				Outgoing (10^{-8} Einsteins/min-area)		
Oct 6							
0830-0930	9.39	13.9	12.9	12.4	16.6	23.0	25.7
1030-1130	13.7		22.4	22.4		38.4	40.5
1230-1330	13.0		24.4	22.4		34.1	35.4
1430-1530	6.72		11.8	11.8		18.5	25.0
Oct 12							
0800-0900	0.294	0.869	1.03	1.06	2.72	4.87	7.80
1000-1100	1.09	3.32	5.84	5.64	4.08	8.13	11.8
1200-1300	8.69	11.5	16.7	16.1	9.78	20.0	26.9
1400-1500	3.37	5.50	9.48	11.7	10.6	18.8	25.2
Oct 16							
0800-0900		2.24	1.06	0.692	0.614	0.403	0.246
1000-1100	8.03	7.20	8.30	8.92	1.29	1.64	1.82
1200-1300	9.62	7.10	7.33	11.5	0.614	0.700	2.57
1400-1500	0.117	0.678	2.36	3.91	0.096	0.633	1.33
Oct 18							
0800-0900	0.840	2.31	1.43	1.15	0.820	0.726	9.62
1000-1100	7.74	10.6	12.6	10.7	1.26	2.06	1.94
1200-1300	4.15	6.46	10.9	11.7	0.700	1.84	3.53
1400-1500	2.01	0.834	4.14	7.39	0.230	1.40	2.25
Oct 20							
0800-0900	0.280	0.778	0.288	0.163	0.455	0.263	0.107
1000-1100	2.75	2.14	2.50	2.58	0.633	0.737	1.04
1200-1300	3.42	3.55	5.64	6.26	0.263	0.565	1.07
1400-1500	1.26	1.09	1.74	3.67	0.113	0.422	1.32

Table 4-3. RATIO OF OUTGOING TO INCOMING 300- TO 400-nm RADIATION AT VARIOUS ELEVATIONS

Exposure interval (TST)	Elevation thousands of feet		
	1.1-1.5	2.6-3.0	5.6-6.0
Oct 6			
0830-0930	0.119	0.178	0.207
1030-1130		0.171	0.181
1230-1330		0.152	0.145
1430-1530		0.157	0.212
Oct 12			
0800-0900	0.313	0.473	0.736
1000-1100	0.123	0.139	0.209
1200-1300	0.085	0.120	0.167
1400-1500	0.193	0.198	0.215
Oct 16			
0800-0900	0.027	0.038	0.036
1000-1100	0.018	0.020	0.020
1200-1300	0.009	0.010	0.022
1400-1500	0.014	0.027	0.034
Oct 18			
0800-0900	0.035	0.051	0.084
1000-1100	0.012	0.016	0.018
1200-1300	0.011	0.017	0.030
1400-1500	0.028	0.033	0.030
Oct 20			
0800-0900	0.058	0.091	0.066
1000-1100	0.030	0.029	0.040
1200-1300	0.007	0.010	0.017
1400-1500	0.010	0.024	0.036

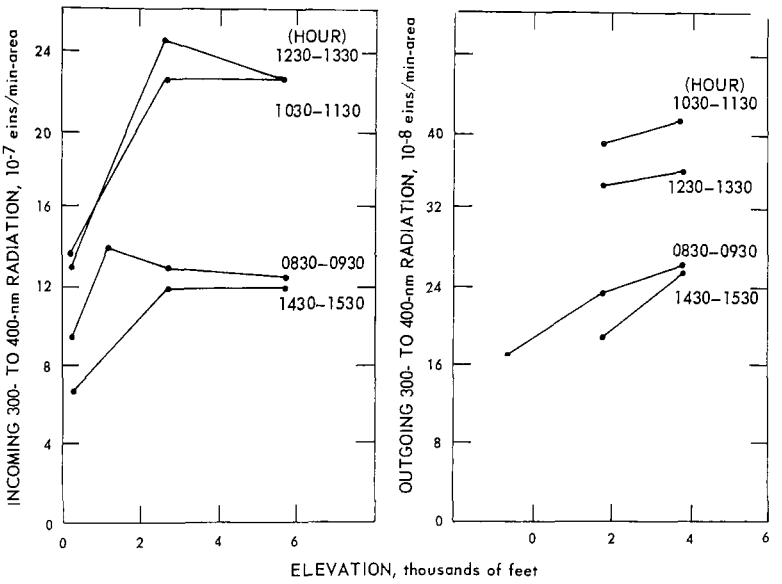

Figure 4-1. Incoming and outgoing radiation as function of elevation over Los Angeles for different times of day, October 6 (M-H smog).

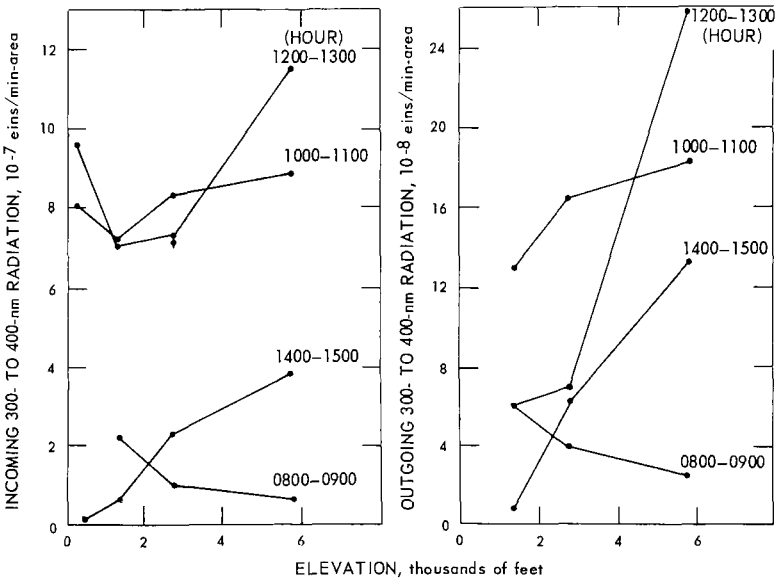

Figure 4-2. Incoming and outgoing radiation as function of elevation over Los Angeles for different times of day, October 16 (no smog).

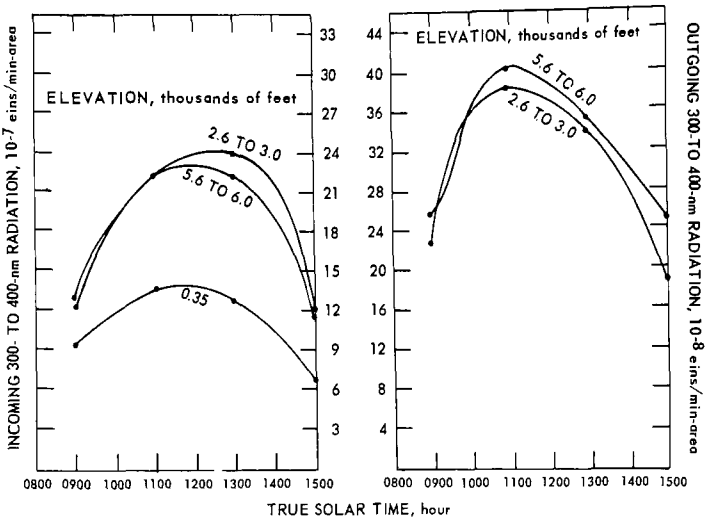

Figure 4-3. Incoming and outgoing radiation as function of time for various elevations over Los Angeles, October 6 (M-H smog).

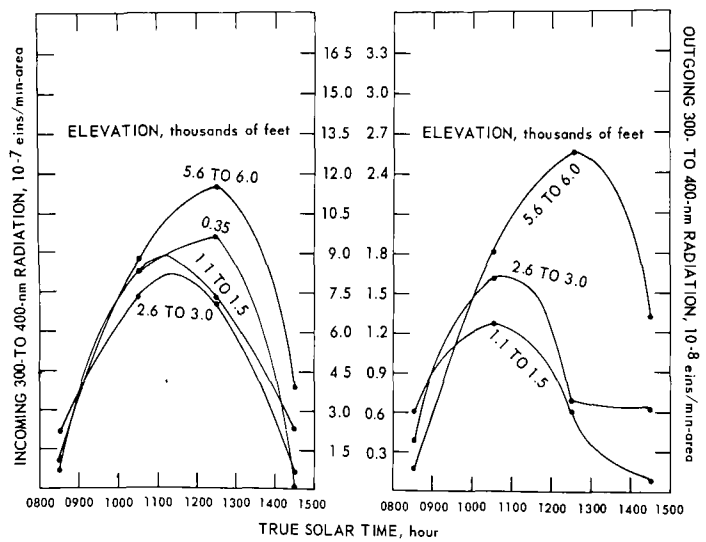

Figure 4-4. Incoming and outgoing radiation as function of time for various elevations over Los Angeles, October 16 (no smog).

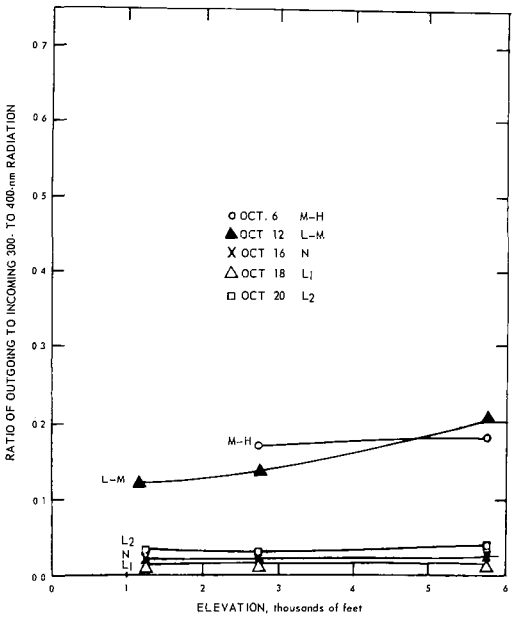

Figure 4-5. Ratio of outgoing to incoming radiation as function of elevation in time interval 1000 to 1100 for various days of smog.

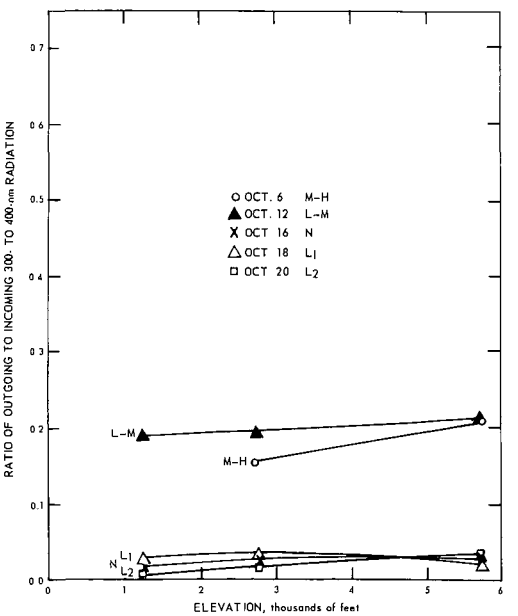

Figure 4-6. Ratio of outgoing to incoming radiation as function of elevation in time interval 1400 to 1500 for various days of smog.

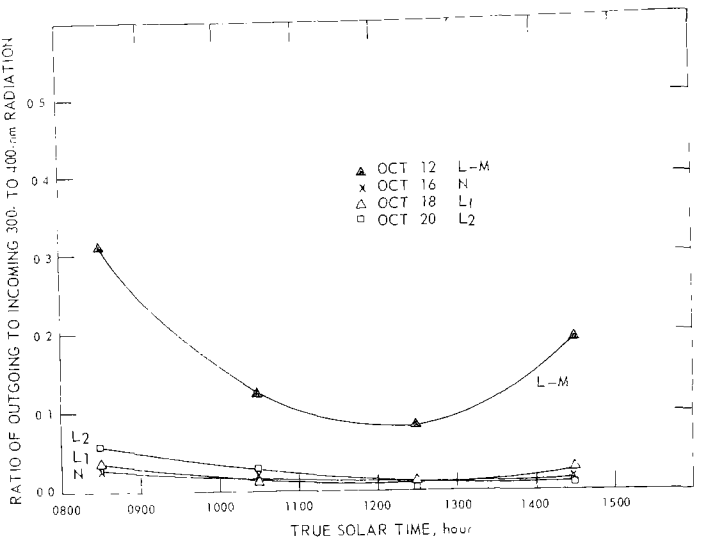

Figure 4-7. Ratio of outgoing to incoming radiation at 1,000 to 1,500 feet as function of time of day for various days of smog.

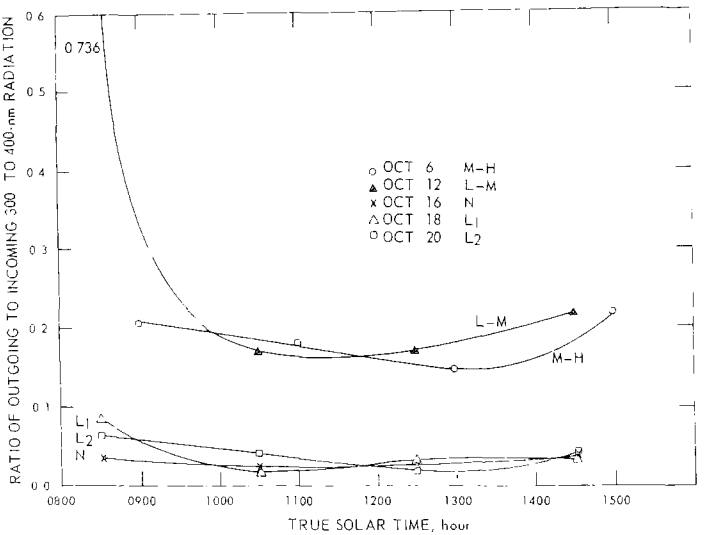

Figure 4-8 Ratio of outgoing to incoming radiation at 5,600 to 6,000 feet as function of time of day for various days of smog.

The Pennsylvania State University

5: PHOTOSENSITIVE PLASTIC MEASUREMENTS

Hans Neuberger

The Pennsylvania State University
Department of Meteorology

Under Grant No. WBG-46 by the U. S. Weather Bureau to The Pennsylvania State University *(1, 2)*, a method was developed for integrating UV irradiance from sun and sky by means of small plates of PLEXIGLAS*, type "G" of 0.03-inch thickness. These plates transmit wavelengths from about 340 nm upwards. Under exposure to UV transmittance decreases in the spectral range from 340 to 410 nm with a maximum response at about 355 nm (Figure 5-1). This transmittance change is due to photochemical action by wavelengths of $\leq$345 nm.

The method of using these PLEXIGLAS plates [abbreviated P(.03G)] has been standardized as follows:

1. Plates 3-1/2 inch square and 3/4 inch thick are exposed horizontally on the shiny side of a piece of household aluminum foil, which by its reflection enhances the degradation of transmittance due to UV irradiance. Exposure period is ordinarily from sunrise to sunset for determination of the UV dose for a whole day.

2. Degradation is evaluated by means of an optical densitometer, the DENSICHRON by W. M. Welch Manufacturing Co. with blue probe (S-4) covered by a Corning (CS 7-37) ultraviolet filter; the light source is a clear-glass 150-watt, 120-volt tungsten light bulb (straight filament coil). The spectral response of this apparatus covers the range from 320 to 395 nm with a broad maximum between 360 and 370 nm (Figure 5-2).

3. The optical density of P(.03G) is measured before and after exposure, the density difference being proportional to the UV dose that caused the increase in optical density. For improved accuracy in measurements, the plates are scored with a knife or stylus and broken into four pieces, which are than stacked on top of each other for density measurement. The reading accuracy of the Densichron meter is $\pm$0.005 dimensionless density units.

*Registered trade name of an acrylic plastic by Rohm and Haas Co.

4. The P(.03G) plates were calibrated by means of the NBS secondary irradiance standard QM-52 (1,000 watt); the irradiance was restricted to UV wavelength naturally occurring in sun and sky light by use of a Corning (CS 0-54) filter, which transmits from 300 nm upwards. With this filter the effective emission of the lamp in the range from 300 to 345 nm, to which Plexiglas is responsive, amounted to 0.134 watt/m^2 of UV.

5. The degradation of P(.03G) is independent of simultaneous irradiance of visible and infrared radiation; it is unaffected by very high or very low temperatures in dark storage and is stable in dark storage, after exposure, for several weeks. Over a storage period of a year additional spontaneous degradation (which does not take place in unexposed plates) amounts to less than 10 percent.

6. The degradation is greater for exposures to a given UV dose at high temperatures than at low temperatures (Figure 5-3). For this reason, the measured density changes must be corrected to a standard temperature, arbitrarily set at 113°F, which is above normally occurring air temperatures and at which calibration was carried out. The measured density changes are converted to UV doses by the formula:

$$I(UV) = 300 \triangle D_4 \left[1 + 0.00794(113 \quad T^{\circ}F)\right] ,$$

Where I(UV) is the UV dose in w-hr/m^2, 300 is the calibration factor, $\triangle D_4$ is the density change of stacks of four plates due to UV irradiance, and $T^{\circ}F$ is the average plate temperature during exposure. The average air temperature during exposure has been found to provide a reasonable estimate of the plate temperature.

7. The optical density change is a practically linear function of the UV dose well beyond the values experienced on clearest midsummer days. The accuracy of I(UV) is ±15 percent or better.

P(.03G) was exposed on the Los Angeles laboratory rooftop according to the standard procedure described above. The plates were later evaluated for degradation at the Pennsylvania State University laboratory by measuring the optical density changes by the standard methods. The results are given in Table 5-1.

Agreement between measurements by P(.03G) method and those by the filter phototube method for integrating UV radiation in the range of wavelengths from 300 to 345 nm, is within ±15 percent, which is considered to be the attainable accuracy of the plastic method.

REFERENCES

1. Neuberger, H., and D. R. Cochran. Integration of Ultraviolet by Plastics, Final Report. Prepared for U.S. Department of Commerce, Weather Bureau. The Mineral Industries Experiment Station, College of Mineral Industries, Pennsylvania State University, University Park, Pa. (October 31, 1965).

2. Neuberger, H. H. and D. R. Cochran, Ultraviolet Dosimetry by Plastics. J. Appl. Meteorol. 5(3) :358-63. (June 1966.)

Table 5-1. INTEGRATED ULTRAVIOLET IRRADIANCE (300 to 345 nm) MEASURED BY PHOTOSENSITIVE PLASTIC[a]

Exposure interval (TST)	Expos. time, hr	Average temp, °F	Density change ($\triangle D_4$)	Irradiance (Plexiglas), w-hr/m^2	Irradiance (filter phototube),[b]	Difference relative to filter-phototube data, %
Oct 6 0720 /1620	9	75	0.155	60	59.7	0.5
Oct 12 0705 /1620	9.25	70	0.145	58	54.4	6.6
Oct 16 Sample lost in high winds						
Oct 18 0650 /1620	9.5	70	0.13	52	59.1	-12.0
Oct 20 0720 /1620	9	86	0.16	58	66.5	-12.8

[a]Plexiglas, type G, 0.03-inch thick.
[b]Data by R. Stair and J. Nader (Section 2) reduced to same wavelength range and exposure time of P(.03G) plates.

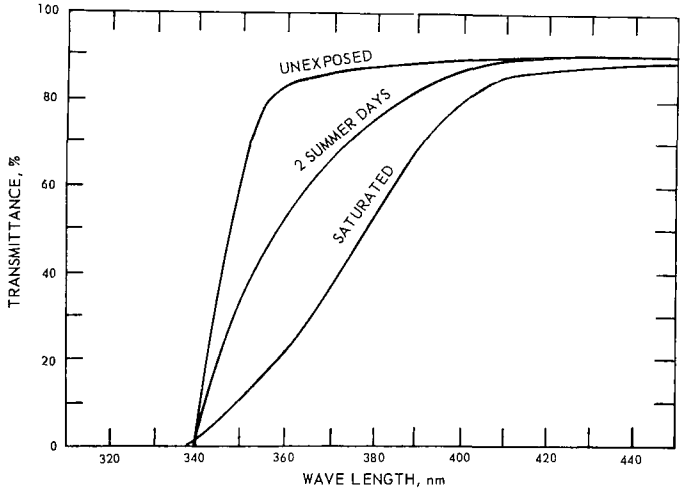

Figure 5-1. Transmittance of Plexiglas 0.07 in. thick.

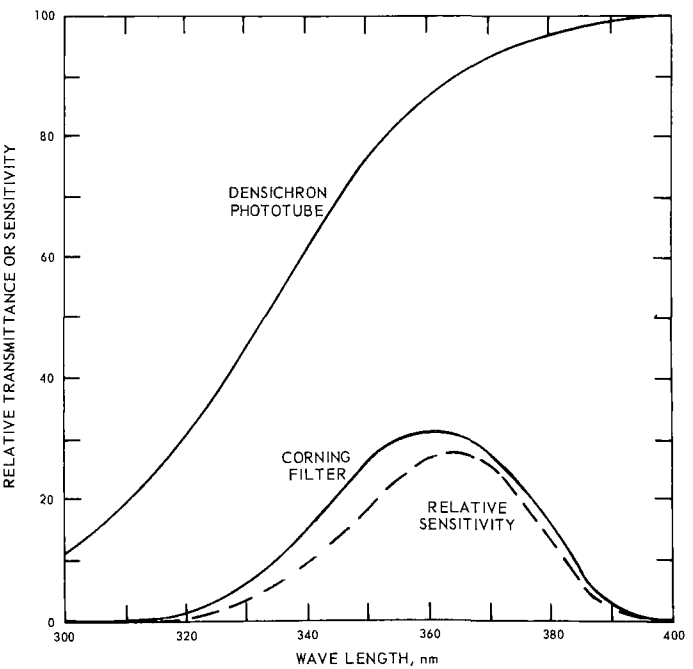

Figure 5-2. Sensitivity of filter and phototube.

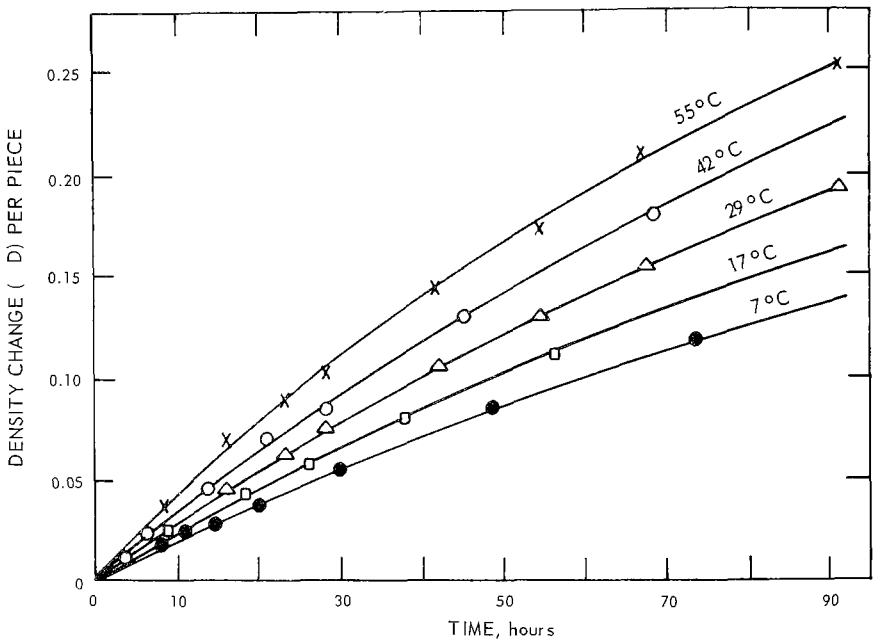

Figure 5-3. Degradation of Plexiglas (.03G) at different temperatures.

Public Health Service

6: PHOTOCHROMIC GLASS MEASUREMENTS

Jerome P. Flesch and John S. Nader
National Center for Air Pollution Control

INSTRUMENTATION AND METHOD

Photochromic glass developed by Corning Glass Co. possesses some unusual optical properties that were utilized in a prototype development of a simple, inexpensive monitor of incident ultraviolet radiation. Megla *(1)* has reported some of the important properties of this glass. The glass contains suspended silver halide microcrystals, which decompose upon exposure to radiation between 320 and 420 nm and which produce a visible darkening effect (optical density). The glass becomes clear upon removal of the activation energy. Some of the properties of the glass that bear on this application are: (1) the amount of darkening is proportional to the amount of incident radiation within a prescribed optical density range; (2) the cycle of darkening and clearing with introduction and removal of activation energy is repeatable, and the response time to both effects is quite rapid; (3) clearing (bleaching) also depends upon the temperature (thermal bleaching) and upon the incidence of long wavelength (550-650 nm) radiation (optical bleaching).

In principle a prototype UV monitor would consist of the photochromic glass as the UV sensor and a simple transmissometer to accurately monitor the optical density of the sensor. Absolute calibration would be required to convert transmittance data to absolute values of incident UV radiation. Data required for such a calibration include: (1) spectral response of the glass in terms of optical density change per unit incident energy as a function of wavelength over the range of activation; (2) the effects of thermal and optical bleaching as functions of temperature and wavelength; and (3) the response of the sensor as a function of angle of incidence of activating radiation.

To evaluate the principle of operation of a photochromic-glass sensor of UV radiation in the field, we constructed a prototype device (Figure 6-1) and placed it at the Los Angeles measurement site, beside the Eppley UV sensors.

The prototype instrument had a motor-driven turntable (1/2 rpm) to permit measurement of; (1) the incident light from the transmissometer light source through a clear opening in the turntable; (2) the zero reference level through an opaque portion of the turntable; and (3) the

transmittance each of duplicate sample specimens of photochromic glass exposed to incident UV radiation. A recorder provided continuous data on the transmissometer measurements throughout the day.

RESULTS

The transmissometer data were reduced to half-hour average values of transmittance tabulations for the 5 flight days. Calibration data were not available to permit reduction of the transmittance data to absolute values of incident UV radiation. The transmittance data were corrected for the attenuation (15%) by the unactivated glass and converted to optical density values (Table 6-1). Data shown in Figure 6-2 (for sensor No. 1) indicate the variation of UV radiation in terms of optical density as a function of time and its relative variation for the two days of extreme smog conditions (none too heavy). These results were not corrected for bleaching or for angular response characteristics of the glass sensors.

REFERENCE

1. Megla, G. K. Optical Properties and Applications of Photochromic Glass. Appl. Optics. 5: 945-60 (1966).

Table 6-1. AVERAGE FOR 30-MINUTE INTERVALS OF OPTICAL DENSITY DATA FROM PHOTOCHROMIC GLASS UV SENSOR

Midpoint of 30-minute interval (TST)	Oct 6		Oct 12		Oct 16		Oct 18		Oct 20	
	No. 1	No. 2	No. 1	No. 2	No. 1	No. 2	No. 1	No. 2	No. 1	No. 2
0745	0.30	0.31							0.26	0.27
0815	0.32	0.32			0.32	0.33	0.33	0.34	0.31	0.31
0845	0.32	0.32			0.39	0.40	0.37	0.37	0.33	0.32
0915	0.33	0.33	0.32	0.31	0.44	0.43	0.38	0.38	0.33	0.32
0945	0.33	0.33	0.33	0.31	0.46	0.46	0.39	0.37	0.32	0.32
1015	0.32	0.32	0.33	0.32	0.48	0.48	0.38	0.38	0.32	0.32
1045	0.32	0.33	0.34	0.32	0.49	0.48	0.38	0.39	0.28	0.28
1115	0.32	0.31	0.35	0.34	0.49	0.49	0.38	0.38	0.25	0.27
1145	0.33	0.33	0.37	0.37	0.50	0.49	0.36	0.37	0.26	0.27
1215	0.34	0.35	0.36	0.35	0.49	0.49	0.35	0.35	0.28	0.30
1245	0.33	0.34	0.36	0.35	0.48	0.48	0.35	0.35	0.28	0.30
1315	0.36	0.38	0.36	0.35	0.49	0.49	0.33	0.33	0.26	0.29
1345	0.39	0.40	0.36	0.36	0.47	0.47	0.33	0.32	0.25	0.28
1415	0.39	0.39	0.37	0.37	0.47	0.47	0.35	0.34	0.25	0.26
1445	0.37	0.38	0.38	0.38	0.50	0.49	0.37	0.36	0.24	0.25
1515	0.36	0.37	0.39	0.39	0.50	0.48	0.39	0.37	0.26	0.27
1545	0.37	0.37	0.40	0.39	0.50	0.48	0.40	0.38	0.26	0.26
1615	0.36	0.35	0.39	0.38	0.49	0.48	0.40	0.38	0.25	0.25
1645			0.38	0.37	0.48	0.45	0.38	0.36	0.25	0.24
1715									0.23	0.21

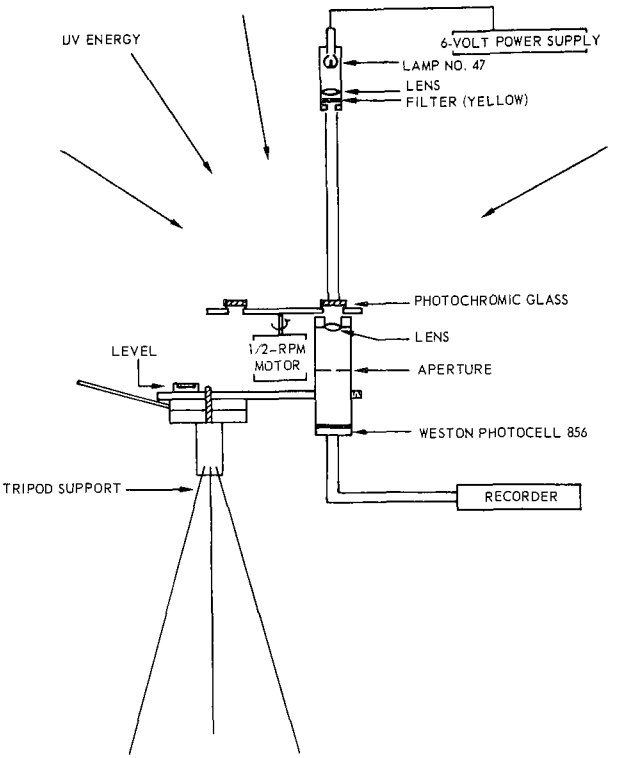

Figure 6-1. Schematic of photochromic-glass UV monitor.

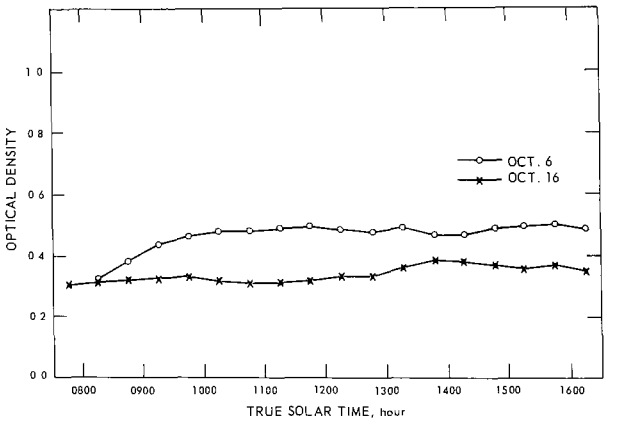

Figure 6-2. Relative UV measurements by photochromic glass in terms of optical density as function of time.

7: METEOROLOGICAL AND AIR QUALITY MEASUREMENTS

Robert J. Bryan and Robert E. Neligan*
Los Angeles County Air Pollution Control District

John S. Nader
National Center for Air Pollution Control

SAMPLING AND MEASUREMENT

Meteorological and air quality data were collected both at the laboratory in downtown Los Angeles and in the aircraft at various elevations over Los Angeles. All data from continuous stripcharts were reduced to 1-hour averages.

Methods by which these measurements were made at the laboratory are described in Appendix 7A. Air quality data are presented in Table 7-1 for carbon monoxide, total hydrocarbons, oxidant, nitrogen dioxide, nitric oxide, sulfur dioxide, and particulate soiling. Meteorological data, presented in Table 7-2 include values for temperature, relative humidity, wind direction and speed, 'weather,' sky cover, visibility, solar radiation, and turbidity coefficient *(1)*.

Air quality data obtained from the aircraft over Los Angeles are given in Tables 7-3 and 7-4. For these measurements samples were collected in aluminized Scotch-Pak bags, approximately 60 liters in volume. The samples were obtained by use of a 1/4-inch-diameter stainless steel tube, the outlet being positioned on the leading edge of the wing approximately 5 feet from the cabin. The sampling tube was led back through the wing into the cabin, where a quick-disconnect fitting was placed on the outlet. Flexible polyethylene tubing was connected to this outlet and the bag. The bags were filled by the ram action of the airplane flying through the air. Approximately 30 liters of sample were obtained in 3 to 15 minutes, depending upon the speed of the aircraft.

While samples were being taken aloft, a bag sample was also obtained from the roof of Station No. 1 (DOLA). The same size aluminized Scotch-Pak bags were used. The sample was collected by use of a DeVilbis pump, the diaphragm having been covered with a seal of aluminized Scotch-Pak film. Metering valves between the pump and

the bag were preset to allow for the collection of 50 liters of air during the period that the aircraft was over the Los Angeles Laboratory.

The bag samples from the aircraft were picked up at Cable Airport and brought to the laboratory. Immediately upon arrival at the laboratory, samples were withdrawn for NO_2 and hydrocarbon analyses. The samples had been in the bags approximately 3 hours.

Meteorological data from the aircraft were limited to temperature measurements, which are summarized in Section I, Figure 1-12.

ANALYSES

Nitrogen dioxide analyses were performed by the Griess-Saltzman method. Briefly the method consists of evacuating a 2-liter flask to a pressure of about 20 millimeters. Ten milliliters of full-strength reagent (5 g of sulfanilic acid, 140 ml of acetic acid, and 20 ml of 0.1% N-(1-naphthyl)-ethylenediamine dihydrochloride solution, diluted to 1 liter with water) were injected into the flask. The sample from the bag was allowed to expand into the evacuated bulb. It was then placed on a mechanical shaker and shaken for 15 minutes for color development; the absorbance of the solution was then read by a Beckman DU spectrophotometer.

The samples were analyzed for hydrocarbons by gas chromatography. Two-liter glass bulbs were evacuated to less than 0.1 millimeter of pressure, the bulbs connected to the bags, and the contents allowed to expand into the bulb. The bulbs were stored in a dark cabinet until the analysis was performed. Upon analysis, 1 liter of sample from the glass bulb was transferred to a freeze-out trap, immersed in liquid nitrogen, and packed with C-22 firebrick. The condensed sample was then charged to the Loenco Model APCD, two-stage gas chromatograph by heating the freeze-out trap. The sample first passed through a 6-foot, 1/4-inch-OD column of 15 percent BB thiodipropionitrile on 42-60 mesh firebrick, and then into the second column, a 14-foot, 1/4-inch-OD column of 20 percent di-n-butyl maleate on 42-60 mesh firebrick. As it exits from the second column the sample is split equally. One stream flows through a 4-inch, 1/4-inch-OD column of 20 percent mercuric perchlorate, then to the flame ionization detector; the other stream flows through a 4-inch, 1/4-inch-OD column of 20 percent polypropylene glycol on 42-60 mesh brick, then to a second detector.

With proper valving and flow controls, this system separates most hydrocarbons in the C_1 to C_6 range. The data are summarized in Table 7-4 as groups of hydrocarbons more or less relative to their photochemical reactivity. The contents remaining in the Scotch-Pak bags were inserted into the sampling lines of the MSA infrared carbon monoxide analyzer used for air monitoring. The sample was allowed to purge the IR cell fully, and a reading was taken after the instrument's response had come to equilibrium.

APPENDIX 7A

MEASUREMENT METHODS AND INSTRUMENTS USED AT LACAP LABORATORY

Carbon Monoxide - CO Analyzer, Mine Safety Appliance Co. This device measures the concentration of carbon monoxide on the basis of infrared absorption principles. Data are shown on a continuous chart with a linear scale.

Hydrocarbons - Flame Ionization Detector, Beckman Instrument Company. In this instrument the ionization flame is produced from a fuel mixture composed of 40 percent hydrogen and 60 percent nitrogen at a flow rate of 75 cubic centimeters per minute and a "breathing" air flow rate of 200 cubic centimeters per minute. These instruments read directly the hydrocarbon concentration in parts per million expressed as methane.

Oxidant - Beckman Instrument Co. The instrument consists of a continuous air-liquid contacting device and a recording colorimeter. It measures the total oxidant in the air by means of a chemical reaction involving the release of iodide from potassium iodide solution. Data are displayed on a continuous chart with a logarithmic scale.

Oxides of Nitrogen - NO/NO_2 Analyzer, Borman Engineering Co. This one instrument determines the separate atmospheric concentrations of two contaminants. The chart-trace sequence involves the recording of the NO_2 concentration for 2 minutes, followed by a 1-minute trace of NO, then repeating. The instrument consists of two air-reagent continuous contacting systems and a recording colorimeter. Saltzman's reagent is the reactant, and potassium permanganante is used to oxidize NO to NO_2.

Sulfur Dioxide - Thomas Autometer. The instrument absorbs sulfur dioxide in a wetted column, in which the sulfur dioxide is oxidized to sulfuric acid and the change in the electorlytic conductivity of the solution is determined. Reagents are dilute sulfuric acid and hydrogen peroxide. Data are displayed on a continuous chart with a linear scale.

Particulate Matter (K_m) - Chaney Autosampler. K_m values are measurements of the light-reflecting properties of filter samples of particulate matter. A sample of air is passed through a filter paper each hour of the day. One K_m unit represents that deposit of particulate matter that produces an optical density value of 0.1 when 1 cubic meter of air passes through 1 square centimeter of the filter.

Visibility - Defined as the greatest horizontal visual range averaged over one-half of the horizon circle. Visibility is measured by the distance at which it is just possible to see and distinguish prominent

objects or landmarks against the sky at the horizon. Although the measurement of visibility is therefore a subjective procedure, it can be done with great accuracy when the observer is provided with a sufficient number of identifiable objects at known distances.

Solar Radiation - Measured by means of an Eppley Pyranometer of the thermoelectric type. Radiation from the sun is allowed to fall on two concentric silver rings, the outer ring covered with magnesium oxide and the inner one covered with lamp black. The temperature difference between the rings is measured by a thermocouple and recorded in units of gram-calories per square centimeter per minute.

Turbidity Coeffecient - Calculated from measurements by Volz Sunphotometer *(1)*. The instrument is pointed at the sun to allow radiation to enter the lens opening in whose focal plane a diaphragm is located to limit the field of view to about 1 degree. The light is diffused by a ground-glass plate and passes through a filter combination that transmits a monochromatic beam with a peak transmission at 500 nm and a bandwidth of about 60 nm at 50 percent of peak transmission. The beam is incident upon a selenium photocell that gives a current output read on a microammeter. By means of a pivoted scale mounted on the instrument and appropriate alignment of the instrument for the sun's elevation, a measure of the sun's optical path length is determined.

Calculations of particle concentration averaged through the atmosphere above the ground can be made from the relationships *(2)*

$$N = 17.3 \times 10^6 \ B$$

and

$$M = 969 \ B$$

where N and M are the particle number and mass (μg) concentrations, respectively, per cubic meter in the size range 0.2 to 2.0 microns in diameter, and B is the turbidity coefficient.

REFERENCES

1. Volz, F. Photometer mit Selen-Photoelement zur Spektralen Messung der Sonnenstrahlung und zur Bestimmung der Wellenlängenabhängigkeit der Dunsttrübung. Arch. Meteorol. Geophys. Bioklimatol., Ser. B., 10(1): 100-31 (1959).

2. McCormick, R. A., and D. M. Baulch. The Variation with Height of the Dust Loading over a City as Determined from the Atmospheric Turbidity. JAPCA. 12:492-96 (1962).

Table 7-1. AVERAGE AIR QUALITY DATA FOR 1-HOUR INTERVALS

Midpoint of time interval (TST)	CO, ppm	HC (as methane), ppm	O_3, pphm	NO_2, pphm	NO, pphm	NO_x, pphm	SO_2, pphm	Particulate reflectance, Km units
Oct 6								
0550	23	10	2				4	11
0650	32	12	2				4	13
0750	28	9	3				4	11
0850	24	8	6	23	21	44	4	9
0950	23	7	10	32	7	39	4	9.5
1050	22	8	22	30	1	31	4	9.8
1150	17	4	25	25	1	26	2	5.8
1250	16	4	19				3	4.8
1350		3	18				2	4.0
1450	14	3	15				1	3.2
1550	15	3	14	6	1	7	2	3.8
1650	15	3	9	10	1	11	2	4.0
1750	14	3	3	14	1	15	2	3.2
Oct 12								
0550	22	8	2	15	20	35	1	
0650	35	12	2	15	25	40	1	
0750	37	14	3	19	46	65	2	
0850	34	16	5	25	40	65		5.1
0950	28	12	9	41	22	63		9.0
1050	23	9	15	38	5	43	1	6.9
1150	21	8	21	24	2	26	3	3.9
1250	19	6	26				1	2.0
1350	17	5	24				1	1.5
1450	17	4	22	8	1	9	1	1.3
1550	18	4	14	10	1	11	1	2.5
1650	18	4	11	12	1	13	1	0.9
1750	17	4	8	10	1	11	1	1.3
Oct 16								
0550	8	2	2	2	1	3	1	1.1
0650	8	2	2	2	1	3	1	0.9
0750	8	2	2	3	1	4	1	0.9
0850	8	2	3	3	1	4	1	0.4
0950	8	2	3	3	1	4	1	0.9
1050	8	2	4	3	1	4	1	0.8
1150	8	2	4	3	1	4	1	0.7
1250	9	2	4				1	0.9
1350	9	2	4				1	0.9
1450	8	2	4	3	1	4	1	0.9
1550	9	2	4	3	1	4	1	1.3
1650	10	2	3	3	1	4	1	1.3
1750	11	2	2	5	2	7	1	1.1

Table 7-1. AVERAGE AIR QUALITY DATA FOR 1-HOUR INTERVALS (Continued)

Midpoint of time interval (TST)	CO, ppm	HC (as methane), ppm	O_3, pphm	NO_2, pphm	NO, pphm	NO_x, pphm	SO_2, pphm	Particulate reflectance, Km units
Oct 18								
0550	15	6	1	10	20	30	1	4.4
0650	24	8	1	10	40	50	2	11.
0750	21	9	1	12	40	52	2	5.9
0850	17	5	2	14	20	34	2	3.4
0950		3	3	18	10	28		1.8
1050	13	3	8	12	2	14	1	2.5
1150	14	3	8	9	1	10	1	2.2
1250	13	3	18					1.3
1350	13	3	16					1.3
1450	13	3	8	8	1	9	1	0.9
1550	14	3	5	9	1	10	1	1.8
1650	13	3	5	14	2	16	1	1.6
1750	13	3	4	12	1	13	1	2.0
Oct 20								
0550	18	5	1	16	17	33	2	4.4
0650	25	7	1	10	34	44	2	5.6
0750	18	5	2	12	30	42	2	3.9
0850	17	5	3	16	18	34	2	4.1
0950	15	4	7	22	6	28	2	3.2
1050	18	5	18	24	1	25	2	2.7
1150	13	3	14	20	1	21	2	1.6
1250	13	3	15				1	1.3
1350	14	3	20				2	1.3
1450	15	3	17	8	1	9	3	1.6
1550	15	3	9	10	1	11	3	1.6
1650	17	3	5	14	1	15	3	2.2
1750	18	4	3	16	6	22	3	2.5

Table 7-2. METEOROLOGICAL DATA AT HOURLY INTERVALS

Time (TST)	Temperature, °F	Rel. humidity, %	Wind direction[a]	Wind speed,[a] mph	Weather[b]	Sky cover[b]	Visibility, miles	Solar radiation,[a] w/m^2	Turbidity coefficient[c]
Oct 6									
0520			NE	3					
0620	61	86	N	1				12	
0720	63	75	E	2	FHK	Clr	1.0	186	
0820	69	62	E	2	HK	Clr	0.8	349	0.260
0920	73	58	S	3	HK	Clr	0.8	500	0.330
1020	77	53	S	3	HK	Clr	0.5	581	0.510
1120	79	51	SW	6	HK	Clr	1.0	708	0.325
1220	81	48	SW	8	HK	Clr	2.0	743	0.237
1320	77	73	SW	8	HK	Clr	2.5	673	0.250
1420	76	74	SW	7	HK	PC	3.0	442	0.230
1520	75	76	SW	6	HK	PC	3.0	337	
1620	75	78	SW	7				163	
1720	73	85	S	7				12	
Oct 12									
0520			E	3					
0620	61	97	E	2					
0720	62	94	S	2	F	FC	0.5	93	
0820	65	94	S	3	F	Clr	0.5	209	0.580
0920	66	90	S	4	F	Clr	0.5	372	
1020	70	83	SW	6	HK	Clr	0.8	557	
1120	72	80	SW	5	HK	Clr	1.0	650	
1220	75	75	SW	6	HK	Clr	1.2	685	0.360
1320	78	69	SW	8	HK	Clr	1.0	650	
1420	74	80	W	8	HK	Clr	1.5	557	0.300
1520	72	85	W	8				372	
1620	69	95	W	8				209	
1720	66	99	W	5				23	
Oct 16									
0520			N	13					
0620	59	48	N	13				12	
0720	60	47	NW	13		Clr	25.	221	
0820	62	45	N	11		Clr	25.	395	0.037
0920	66	39	NW	10		Clr	25.	603	
1020	69	36	NW	9		Clr	25.	709	0.040
1120	71	33	W	10				778	
1220	72	36	W	10				755	
1320	71	36	SW	13				673	
1420	69	37	SW	16				488	
1520	70	37	W	14				302	
1620	67	50	W	11				70	
1720	69	43	NW	8					

[a]Averages for the 1-hour interval starting at the indicated time.
[b]F - fog, H - haze, K - smoke, Clr - clear, PC - partly cloudy cover, FC - full cloud cover.
[c]Reference 2.

Table 7-2. METEOROLOGICAL DATA AT HOURLY INTERVALS (Continued)

Time (TST)	Temperature, °F	Rel. humidity, %	Wind direction[a]	Wind speed,[a] mph	Weather[b]	Sky cover[b]	Visibility, mikes	Solar radiation,[a] w/m^2	Turbidity coefficient[c]
Oct 18									
0520			NE	4					
0620	57	74	NE	3				58	
0720	58	69	NE	3	HK	Clr	6.	163	
0820	59	68	NE	3	HK	Clr	3.	360	0.100
0920	65	60	E	3	HK	Clr	4.	511	
1020	71	52	SE	3	HK	Clr	5.	650	0.110
1120	74	39	SE	2	HK	Clr	5.	673	
1220	77	35	S	4	HK	Clr	4.	616	0.340
1320	77	35	SW	9	HK	Clr	4.	557	
1420	73	47	W	10	HK	Clr	5.	476	0.181
1520	71	51	SW	8	HK	Clr	6.	349	
1620	70	57	W	7				139	
1720	68	55	W	6					
Oct 20									
0520			N	4					
0620	68	47	NE	4					
0720	66	51	NE	7		Clr	10.	139	
0820	71	41	NE	4	HK	Clr	4.	349	
0920	78	36	NE	2	HK	Clr	4.	546	
1020	88	33	SW	4	HK	Clr	4.	650	
1120	90	29	SW	5	HK	Clr	5.	720	
1220	94	25	S	5		PC	8.	720	
1320	95	25	SW	6		PC	8.	639	
1420	95	25	W	7	HK	Clr	6.	487	
1520	93	25	W	9	HK	Clr	6.	291	
1620	90	27	W	6				128	
1720	88	28	W	3					

[a]Averages for the 1-hour interval starting at the indicated time.
[b]F - fog, H - haze, K - smoke, Clr - clear, PC - partly cloudy cover, FC - full cloud cover.
[c]Reference 2.

Table 7-3. AIR QUALITY DATA OBTAINED BY AIRCRAFT OVER LOS ANGELES

Time Interval (TST) / Elevation, 10^3 ft	CO, ppm	HC (as methane), ppm	HC (Carbon), ppm	NO_2, pphm
Oct 6 (M-H Smog)				
0835-0905/0.35[a]	24	3.7	8	23
/0.35[b]	21	2.96		61
0940/1.35	11	1.61		8
0950/1.8	9	1.66		3
1000/2.5	9	1.67		3
Oct 12 (L-M Smog)				
0835-0905/0.35[a]	34			25
/0.35[b]	29	5.63		58
0853-0906/1.35	14	2.51		13
0910-0918/1.8	10	1.75		6
0823-0834/2.5	8	1.60		6
Oct 16 (No Smog)				
0820-0850/0.35[a]	8	1.1	2	3
/0.35[b]	8	1.54		8
0853-0900/1.4	7	1.49		2
0838-0852/3.0	7	1.54		3
0821-0830/5.7	7	1.47		1
Oct 18 (L-Smog)				
0820-0920/0.35[a]	16	2.5	5	16
/0.35[b]	17	2.33		17
0854-0857/1.4	11	1.63		4
0907-0918/2.2	9	1.66		<1
0820-0829/5.7	9	1.48		<1
Oct 20 (L-Smog)				
0820-0920/0.35[a]	17	2.1	5	14
/0.35[b]	17	2.07		20
0856-0908/1.3		1.46		5
0838-0852/3.0	10	1.47		5
0820-0830/5.7	10	1.45		5

[a]Measurement made on air monitoring instruments at Laboratory.
[b]Measurement made from samples collected in bag at same location.

Table 7-4. GAS CHROMATOGRAPHIC DATA ON AIR SAMPLES OBTAINED BY AIRCRAFT OVER LOS ANGELES
(ppm)

Time interval (TST) / Elevation, 10^3 ft	Paraffins			Olefins			Acetylene	Aromatics	
	1-3C	4-6C	1-6C	Ethylene (2C)	3-5C	2-5C		Benzene	Toluene
Oct 6									
0835-0905/0.35	3.11	0.240	3.35	0.090	0.046	0.136	0.090	0.021	0.027
0940/1.35	1.64	0.047	1.68	0.011	0.004	0.015	0.009	0.007	0.011
0950/1.8	1.68	0.043	1.72	0.007	0.002	0.009	0.004	0.003	0.004
1000/2.5	1.50	0.010	1.51	0.003	0.003	0.006	0.003	0.003	0.006
Oct 12									
0835-0905/0.35	5.92	0.536	6.45	0.131	0.114	0.245	0.159	0.037	0.077
0835-0906/1.35	2.59	0.090	2.68	0.012	0.007	0.019	0.019	0.011	0.018
0910-0918/1.8	1.78	0.034	1.82	0.005	0.003	0.008	0.015	0.006	0.000
0823-0834/2.5	1.62	0.022	1.64	0.005	0.004	0.009	0.002	0.006	0.000
Oct 16									
0820-0850/0.35	1.56	0.050	1.61	0.013	0.012	0.025	0.013	0.011	0.000
0853-0900/1.4	1.50	0.021	1.52	0.003	0.002	0.005	0.005	0.005	0.000
0838-0852/3.0	1.48	0.017	1.50	0.003	0.003	0.006	0.002	0.004	0.000
0821-0830/5.7	1.55	0.017	1.57	0.003	0.003	0.006	0.002	0.005	0.000
Oct 18									
0820-0920/0.35	2.41	0.130	2.54	0.055	0.029	0.084	0.063	0.015	0.036
0854-0857/1.4	1.69	0.024	1.71	0.005	0.003	0.008	0.006	0.009	0.008
0907-0918/2.2	1.64	0.011	1.65	0.003	0.003	0.006	0.003	0.003	0.004
0820-0829/5.7	1.49	0.012	1.50	0.002	0.003	0.005	0.001	0.005	0.009
Oct 20									
0820-0920/0.35	2.14	0.109	2.25	0.049	0.032	0.081	0.054	0.016	0.024
0856-0908/1.3	1.47	0.033	1.51	0.005	0.008	0.013	0.006	0.004	0.016
0838-0852/3.0	1.48	0.021	1.50	0.002	0.003	0.005	0.002	0.006	0.012
0820-0830/5.7	1.46	0.009	1.47	0.002	0.003	0.005	0.001	0.004	0.007

8: DISCUSSION AND SUMMARY

The foregoing sections discussed physical and chemical methods of UV measurement and presented results of simultaneous measurements by these methods at one or more locations. The measurements represent incoming radiation above the smog envelope and at ground level, and outgoing radiation at various elevations within the smog layer. In this section, the editor attempts to relate the measurements to each other, wherever possible and to a limited extent. The methods of measurement and the properties of UV radiation in a smog environment are discussed. No effort has been made to be all-inclusive, and it is hoped that this initial effort will stimulate more work; many questions are provoked and left unanswered.

INCOMING RADIATION

UV Attenuation and Air Quality

Simultaneous measurement of incoming radiation by the filter-phototube sensors of NBS both on Mt. Wilson and in downtown Los Angeles permitted a calculation of the attenuation effects of the smog envelope on the vertically incident UV radiation as a function of time of day. The data of Table 2-3 were used to determine the ratio of Los Angeles values to Mt. Wilson values for corresponding times of day to give the data shown in Table 8-1 for the 5 flight days. A graphical presentation of these data in Figure 8-1 shows that ratio measurements: (1) eliminate the effect of the sun's elevation with time of day, which normally gives the cosine type curves appearing in Figures 2-8 and 2-9 with peaks at solar noon; and (2) give a measure of the attenuation of the vertical UV radiation by the intervening atmosphere between the elevations of 350 feet in downtown Los Angeles and 5,700 feet on Mt. Wilson. On the no-smog day the attenuation was fairly constant, averaging about 14 percent. On the light-to-moderate and moderate-to-heavy smog days the attenuation varied significantly through the day depending upon the incidence of smog conditions. A maximum of 58 percent was observed, about 4 times that on the no-smog day.

A large attenuation appears in the time interval from about 0915 to 1145 on the moderate-to-heavy smog day (October 6). Air quality and meteorological data during this period (Tables 7-1 and 7-2) show high levels of O_3, NO_2, and particulate, and very low visibility; peak values of pollutants and low values of visibility coincide with the peak attenuation at about 1030 TST. At this time the O_3 and NO_2 concentrations were 6 to 10 times those on the no-smog day and the visibility, which was 25 miles on the no-smog day, was only 1/2 mile.

The data in Table 2-2 for the M-H smog day were also converted to ratio values (Table 8-2) to determine whether the attenuation effects of the smog environment were possibly wavelength-dependent within the range from 310 to 390 nm. A plot of these data for the midmorning, noon, and midafternoon periods (Figure 8-2) shows no significant dependence of attenuation effects within this wavelength range. It is important to note that the instrumentation for these measurements, having wide apertures, measures a good deal of stray light and does not give the good resolution that true transmittance measurements provide.

Evaluation of Physical Methods

Ratios of measurements made with the Eppley wide-band sensor (Table 1-5) in downtown Los Angeles to those made with the NBS wide-band sensor (Table 2-3) at the same location were calculated to examine the responses of the instruments relative to each other. The average ratio among 90 values for the 5 days was 1.17, with a standard deviation of 0.03. These values indicate that the Eppley sensor, on the average, gave a value 17 percent higher than that of the NBS sensor. Possible differences in adherence to the cosine response should be considered, particularly at low angles of elevation. Extreme ratio values tended to occur early and late in the day, corresponding to low elevations of the sun.

Pyranometer data on solar radiation (Table 7-2) were plotted for the 5 flight days in Figure 8-3 for comparative evaluation with the corresponding UV data shown in Figure 1-7. Although the pyranometer data exhibit the same general trends relative to the smog environment as do the UV data, the resolution of attenuation and transmission peaks is significantly poorer. This would indicate that pyranometer data are not adequate for inferring information on attenuation effects in the UV range with any reasonable accuracy.

The photosensitive-plastic sensor was developed as a method of integrating UV radiation incident on small plates of PLEXIGLAS and is comparable to the filter-phototube sensor in being a horizontal-surface-type receiver. Results of comparison (Table 5-1), in which the filter-phototube data (Table 2-2) were integrated over the spectral response range of the PLEXIGLAS and for the period of exposure, show that the method is feasible for applications in the field, in which simple desimetric type measurements are desired. The attainable accuracy is within ±15 percent in the UV wavelength range from 300 to 345 nm.

The photochromic-glass sensor is essentially a horizontal surface sensor, very much like the Eppley sensor. Plots of UV radiation as a function of time (compare Figure 6-2 for the photochromic glass sensor with Figure 1-7 for the Eppley sensor) show that the photochromic glass sensor fails to provide resolution of peak intensity near solar noon or attenuation effects by smog. Possible factors that might contribute to these results and that need investigation are (1) deviation of sensor from cosine response; (2) spectral response; and (3) bleaching effects, which

may be directly related to time of day and tend to counteract the anticipated increase in UV radiation as a function of sun's elevation. Optical bleaching is most likely the important factor, whereas thermal bleaching would show less change since the temperature change through the day was within 10°F. Qualitatively, the data show the decreased UV radiation on the smog day as compared with the no-smog day, although they do not show correctly the relative variation within the same day.

Evaluation of Chemical Methods

The photochemical method described in Section 4 gives a measure of the UV radiation absorbed, but calibration data are not available to convert this information to absolute values of the incident UV radiation. Comparison of the data collected by this method (actinometer paper) with data collected by the Eppley sensor on the same laboratory rooftop leads to some very interesting observations.

Figure 8-4 is a plot of the relative incoming 300- to 400-nm radiation as a function of time of day for various days of smog; the plot is based on the actonometer paper measurements in Table 4-2. These data compare qualitatively with those of the Eppley sensor in Figure 1-7 with respect to the relative variations within a given day. Note, however, the inverse relationship between the two methods in the relative intensities for the no-smog day and the M-H smog day. In the Eppley data, the intensity of incoming radiation is greater on the no-smog day than on the M-H smog day. The actinometer paper absorbs significantly more energy on the M-H smog day than on the no-smog day, even though more energy is available on the no-smog day. Note, also, that the peak energy absorbed by the actinometer paper on the M-H day occurs within the time interval from 1030 to 1130. At about this time the corresponding Eppley data show a large attenuation effect. Data on outgoing radiation, discussed later in this section, show that the attenuation of incoming radiation on smog days corresponds to an increase in outgoing radiation; thus the data show that scattering is more of a factor than absorption in the overall attenuation effects.

These observations seem to indicate that the actinometer paper method may have a greater sensitivity to scattered radiation because of its geometrical response and/or its spectral response characteristics. Another possibility is that the smog environment may affect the photochemical response of the sensor. Some significant observations are that the actinometer paper method in its present method of application (1) does not give an absolute measure of incident UV radiation and (2) does not necessarily give a reliable measure of relative incident radiation levels.

The volumetric-type chemical actinometers described in Section 3 are used differently. The difference is essentially in the geometrical exposure and response of the sensors. First, we will compare the two o-nitrobenzaldehyde methods. The paper actinometer presumably acts

as a horizontal-surface-type sensor on which is incident radiation from all directions within a hemisphere, and the vertical components of these radiations are measured (assuming a cosine response sensor). The volumetric actinometer exposes the same reagent, as a solution in a spherical flask, to radiations from all directions about the sphere; in principle at least, all radiation is measured equally, independent of direction.

Since data obtained by the volumetric actinometer were calculated in terms of absolute energy of incident radiation, comparison with the corresponding absolute data obtained by the Eppley sensor is of interest. The volumetric data (Figure 3-2) seem to compare much more favorably with the Eppley data (Figure 1-7) than do the actinometer paper data with respect to variation of relative intensity as a function of time of day and various degrees of smoginess.

Note that the peak intensity measured by the volumetric actinometer on the no-smog day is about 115 w/m^2 as compared to about 36 w/m^2 measured by the Eppley sensor, a factor of a little over 3. These values bring out a very important point with respect to UV radiation available to a volume in space. The vertical component radiation measured by the Eppley sensor represents one of the six vector components (perpendicular to six plane surfaces of a cube) required to account for all the radiation incident on a volume in space. If the radiation were uniformly distributed with respect to all direction in space, then the volumetric measurement of incident radiation would be expected to be 6 times the vertical component measurement. For an anisotropic distribution, the factor will most likely be less than 6 if it is assumed that the incident vertical component approximates the horizontal components in magnitude. A calculation of the ratio of volumetric measurements to simultaneous horizontal plane measurements (Table 8-3) shows values for 4 of the 5 flight days ranging from 2.9 to 4.8. The ratios are lowest near solar noon, as might be expected since the vertical component (in the denominator) tends toward a maximum at noon.

OUTGOING RADIATION

Scattering Effects and Air Quality

Incoming radiation on Mt. Wilson was measured (filter-phototube sensor) simultaneously with measurement of outgoing radiation on the aircraft (filter-photocell sensor) at the same elevation of 5,700 feet. From these two sets of values we could calculate the scattering effect of the smog envelope on the vertically directed incident radiation (300 to 380 nm) as a function of time of day. The data of Table 2-3 and Figure 1-11 were used to calculate the ratios of outgoing to incoming radiation values. A plot of these ratio values in Figure 8-5 for the various days of smog shows a significant shift toward higher ratios for the smog days, higher by a factor of about 2. The outgoing radiation is a combined measure of the incoming radiation scattered by the polluted

medium and the radiation reflected from the ground level and transmitted through the polluted medium. The curve for the no-smog day is indicative of the reflectivity of the ground, averaging about 15 percent of the incident radiation and assuming negligible scatter from the relatively unpolluted medium. On the M-H smog day, the polluted medium causes a significant increase in the outgoing radiation, which averages about 24 percent of the incident radiation. Note what appears to be a buildup of pollution on October 18 (light smog); the ratio in the morning corresponds to that for a no-smog day at about 18 percent and increases gradually from mid-morning to noon, at which time it corresponds to the ratios for the relatively smoggy days (L-M and M-H) at about 23 percent while the value for the no-smog day has dropped to about 13 percent. This is generally consistent with the turbidity and visibility data in Table 7-2. However, in relating air quality data obtained at ground level to scattering at 5,700 feet, it is necessary to bear in mind that high scattering values can reflect a buildup of pollution in the upper layers of the atmosphere. This pollution in the upper layers may appear in the air quality data obtained at ground level at some time earlier or later, depending upon meteorological conditions near the ground and at the higher elevations.

Figure 8-6 shows the results of measurement of outgoing radiation with the sensor on the aircraft and the scattering effects of a polluted medium as a function of elevation over Los Angeles for various days of smog during the mid-morning flight interval (1000 to 1100 TST). These plots suggest an exponential relationship between outgoing radiation and elevation, as would be expected if the intervening medium between the aircraft and ground is treated as a variable scattering medium whose reflectivity is related to its concentration of particulate pollution (turbidity) and its thickness (elevation). The increased pollution on smoggy days displaces the curves toward higher outgoing radiation values. Curves for both morning and afternoon flights showed that values of outgoing radiation for the no-smog day are lower than those for any of the smog days. Values of outgoing radiation for the relatively heavy-smog days are higher than those for the no-smog day by a factor of approximately 2.

Data on ratios of outgoing to incoming radiation measurements made with the sensitized actinometer paper as a function of time for the 5600- to 6000-foot elevation interval (Figure 4-8) also show a significant increase in ratio values for the relatively heavy-smog days relative to the no-smog day. Note the comparison of these data with the corresponding data obtained with the physical sensors (filter photosensors, Figure 8-5). The chemical sensor tends to show a greater increase in the ratio values (a factor of about 6) for the M-H smog days than do the physical sensors (a factor of about 2). This is consistent with our earlier comments regarding what appears to be the abnormally high sensitivity of the actinometer paper method to scattered radiation.

SUMMARY

1. Incident and outgoing ultraviolet radiation (within the wavelength range from 300 to 400 nm) in the Los Angeles urban area was measured during 5 days with conditions ranging from no smog to moderate-to-heavy smog. Simultaneous UV measurements were made with physical and chemical detection systems; concurrent with these measurements, air quality and meteorological data were collected.

2. Absolute-energy data for radiation incident on a horizontal plane surface were obtained by the filter photocell and filter-phototube methods of detection. The filter-photocell method on the average gave a value 17 percent higher than that given by the filter-phototube method.

3. Incident 300 to 380 nm radiation on a no-smog day at an elevation of 5,700 feet peaked to a value of about 36.1 w/m^2 at solar noon. At an elevation of 350 feet near ground level this UV radiation measured simultaneously was 30.7 w/m^2. The attenuation through the day was relatively uniform, with a mean value of about 14 percent and a minimum of about 3 percent for unpolluted air. On a moderate-to-heavy smog day, the attenuation for the smog layer from 350 to 5,700 feet varied significantly through the day; peak attenuation was as much as 58 percent with a mean value of about 38 percent or almost 3 times that measured on the no-smog day.

4. Incident UV radiation was measured with nine narrow-band filters having 10-nm bandwidths and centered at every 10 nm starting with 310-nm wavelengths through 390 nm. Results of attenuation measurements through the moderate-to-heavy smog layer indicated that attenuation effects were not significantly dependent on wavelength within this range.

5. Pyranometer data indicated that such wide-band (300 to 2,500 nm) radiation measurements were not adequate for inferring accurate information on attenuation effects in the UV (300 to 400 nm) range.

6. The photochromic-glass sensor was inadequate for providing informative UV data. Results showed significant lack of resolution, which may be attributable to several factors requiring further study.

7. The photosensitive-plastic sensor used as a dosimeter gave a good quantitative measure of incident UV (300 to 345 nm) radiation with a calculated accuracy of about ± 15 percent when compared to the filter-phototube sensor.

8. The actinometer paper method in its present state of development does not give an absolute measure of incident UV (300 to 400 nm) radiation, and results of relative measurements were not reliable in the prototype system. The initial system is capable of refinement and further study that might overcome these obstacles. The high sensitivity of this method to scattered radiation associated with smog condi-

tions may be of unique value in monitoring incidence of smog or other smog-related measurements.

9. Measurements with the volumetric type of chemical actinometer (ONBA) were higher than those with the horizontal-plate type sensor by a factor ranging from 2.9 to 4.8, with a mean of 3.8

10. Outgoing radiation increased with elevation, tended to peak with time of day approaching solar noon, and increased on smoggy days. The ratio of outgoing radiation to incident radiation on relatively heavy-smog days was approximately twice the ratio for a no-smog day (0.23 to 0.13 at solar noon).

11. Data on the ratios of outgoing radiation to incident radiation measured by the actinometer paper method also reflected the increased outgoing radiation on smoggy days. This method showed a greater increase, indicating a higher sensitivity to scattered radiation than is provided by the filter photocell method.

Table8-1. RATIO OF INCOMING 300- TO 380-nm RADIATION IN LOS ANGELES (300 feet) TO INCOMING RADIATION ON MT. WILSON (5,700 feet), 1965

Midpoint of time interval (TST)	Oct 6	Oct 12	Oct 16	Oct 18	Oct 20
0715	0.69				
0745	0.63	0.54	0.76	0.72	0.81
0815	0.59	0.47	0.85	0.72	0.78
0845	0.57	0.43	0.88	0.71	0.83
0915	0.60	0.42	0.87	0.75	0.82
0945	0.51	0.47	0.98	0.78	0.80
1015	0.47	0.50	0.91	0.81	0.76
1045	0.45	0.53	0.88	0.80	0.73
1115	0.58	0.56	0.89	0.76	0.81
1145	0.66	0.56	0.88	0.67	0.81
1215	0.70	0.60	0.85	0.59	0.85
1245	0.70	0.69	0.87	0.57	0.80
1315	0.71	0.68	0.87	0.62	0.80
1345	0.70	0.77	0.91	0.59	0.72
1415	0.74	0.73	0.88	0.59	0.80
1445	0.86	0.69	0.85	0.67	0.81
1515	0.66	0.65	0.77	0.65	0.71
1545	0.71	0.65	0.68	0.70	0.75

Table 8-2. RATIO OF INCOMING RADIATION IN LOS ANGELES (350 FEET) TO RADIATION ON MT. WILSON (5700 FEET) ON OCTOBER 6 AT INDICATED WAVELENGTH (nm)

Midpoint of time interval (TST)	310	320	330	340	350	360	370	380	390	Average
0715	0.82	0.66	0.64	0.68	0.65	0.67	0.68	0.66	0.66	0.68
0745	0.54	0.61	0.59	0.58	0.61	0.62	0.63	0.60	0.60	0.60
0815	0.59	0.57	0.57	0.56	0.58	0.59	0.59	0.57	0.56	0.58
0845	0.48	0.55	0.54	0.54	0.56	0.56	0.58	0.56	0.55	0.55
0915	0.50	0.55	0.55	0.54	0.57	0.56	0.58	0.57	0.56	0.55
0945	0.44	0.48	0.48	0.49	0.50	0.49	0.51	0.50	0.49	0.49
1015	0.38	0.45	0.45	0.45	0.47	0.47	0.48	0.47	0.44	0.45
1045	0.36	0.42	0.42	0.42	0.45	0.45	0.48	0.47	0.47	0.44
1115	0.48	0.52	0.53	0.54	0.57	0.58	0.61	0.62	0.61	0.56
1145	0.54	0.60	0.61	0.61	0.65	0.66	0.69	0.63	0.63	0.62
1215	0.58	0.64	0.64	0.60	0.69	0.69	0.72	0.71	0.70	0.66
1245	0.60	0.65	0.66	0.66	0.70	0.70	0.73	0.71	0.70	0.68
1315	0.62	0.66	0.66	0.66	0.70	0.71	0.73	0.71	0.71	0.68
1345	0.62	0.69	0.69	0.69	0.67	0.66	0.70	0.67	0.66	0.67
1415	0.63	0.64	0.65	0.65	0.68	0.71	0.74	0.71	0.70	0.68
1445	0.75	0.78	0.78	0.79	0.80	0.83	0.88	0.86	0.89	0.82
1515	0.67	0.62	0.60	0.60	0.63	0.63	0.64	0.62	0.62	0.63
1545	0.78	0.67	0.66	0.66	0.69	0.70	0.73	0.70		0.70

Table 8-3. RATIO OF VOLUMETRIC MEASUREMENTS TO CONCURRENT HORIZONTAL PLANE MEASUREMENTS

Midpoint of exposure interval (TST)	Average UV radiation, w/m^2		Ratio
	ONBA (Table 3-1)	Eppley (Table 1-4)	
Oct 6			
0850	56.4	14.4	3.9
1050	84.4	19.1	4.3
1250	105.	30.1	3.5
1450	80.9	19.2	4.2
Oct 16			
0835	78.1	17.9	4.4
1035	109.	32.8	3.3
1235	113.	34.5	3.3
1435	94.0	24.5	3.8
Oct 18			
0835	56.4	14.3	4.0
1035	101.	28.9	3.5
1235	69.5	22.6	3.1
1435	67.8	17.2	4.0
Oct 20			
0835	75.8	15.7	4.8
1035	113.	26.3	4.3
1235	101.	34.4	2.9
1435	78.1	20.0	3.9

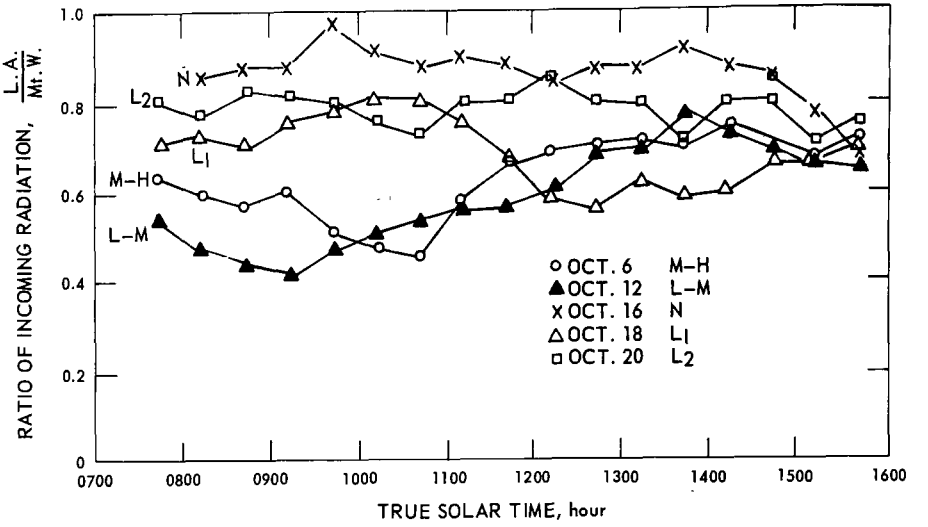

Figure 8-1. Ratio of incoming 300- to 380-nm radiation at Los Angeles to that at Mt. Wilson for various days of smog.

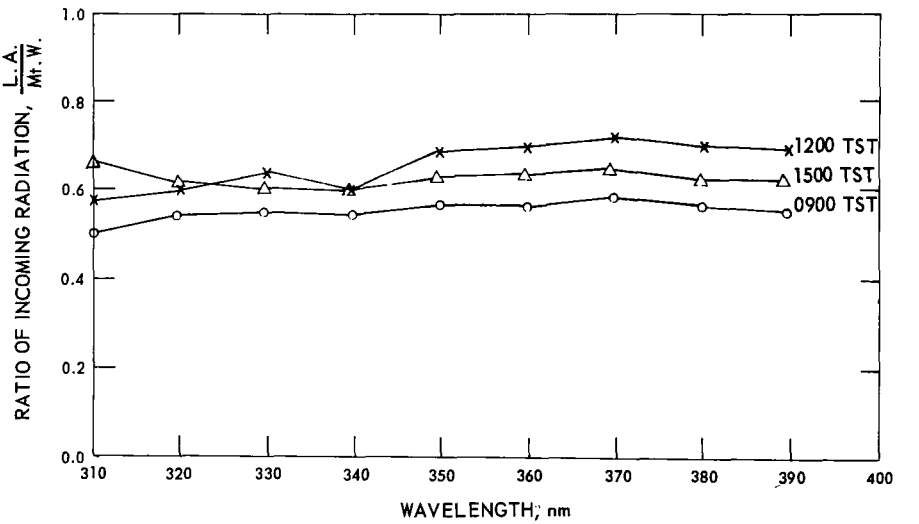

Figure 8-2. Ratio of incoming radiation at Los Angeles to that at Mt. Wilson as function of wavelength for different times of day on Oct. 6, 1965.

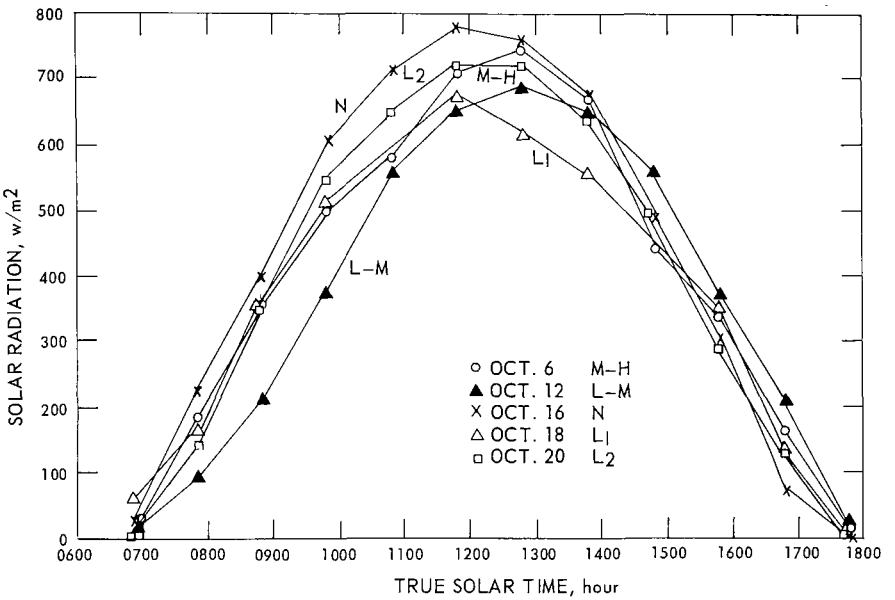

Figure 8-3. Average solar radiation measured with pyranometer for 1-hour intervals in Los Angeles.

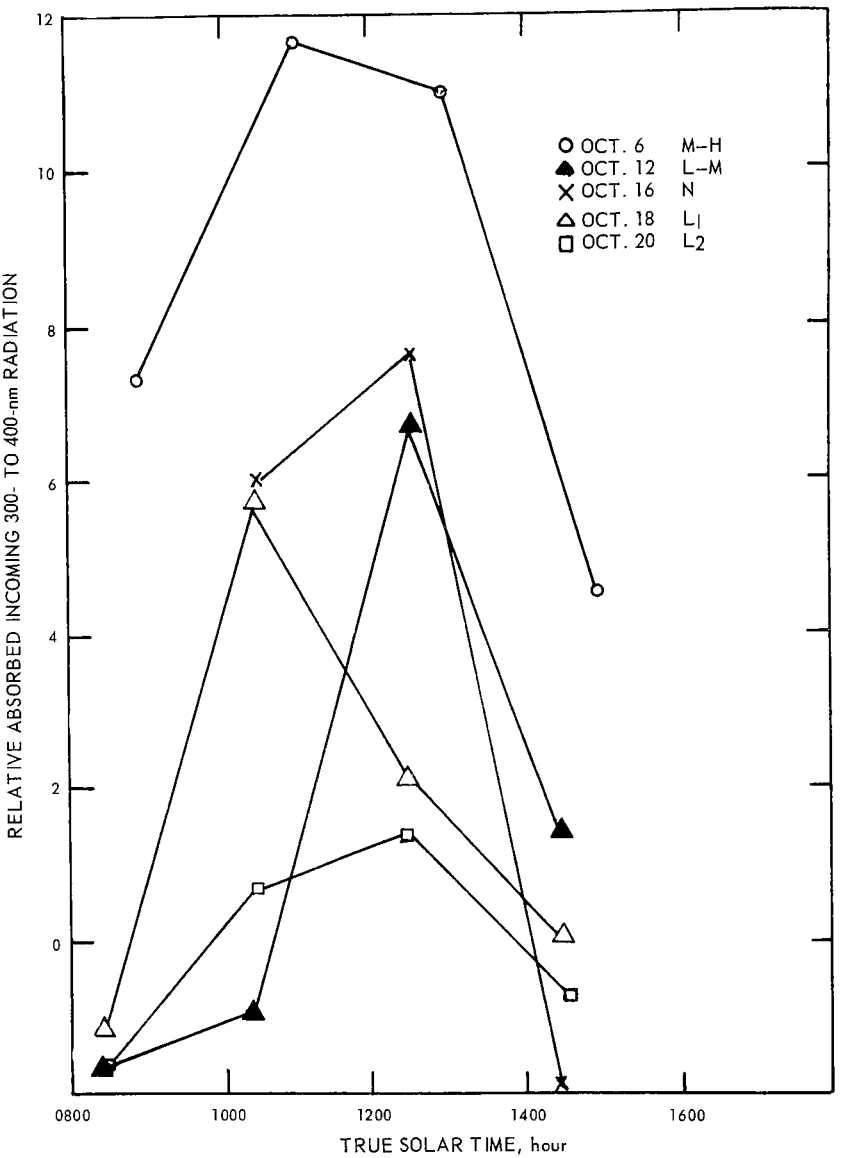

Figure 8-4. Relative absorbed incoming radiation measured with ONBA filter paper at Los Angeles laboratory site.

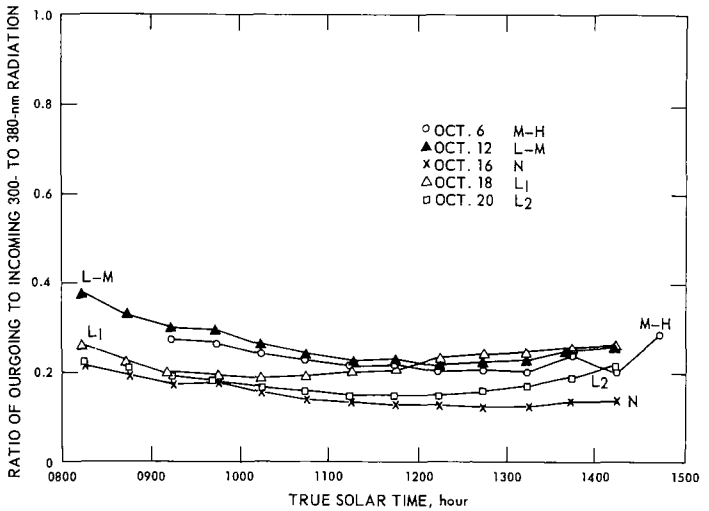

Figure 8-5. Ratio of outgoing (from aircraft) to incoming 300- to 380-nm radiation at elevation of 5,600 to 6,000 feet (Mt. Wilson).

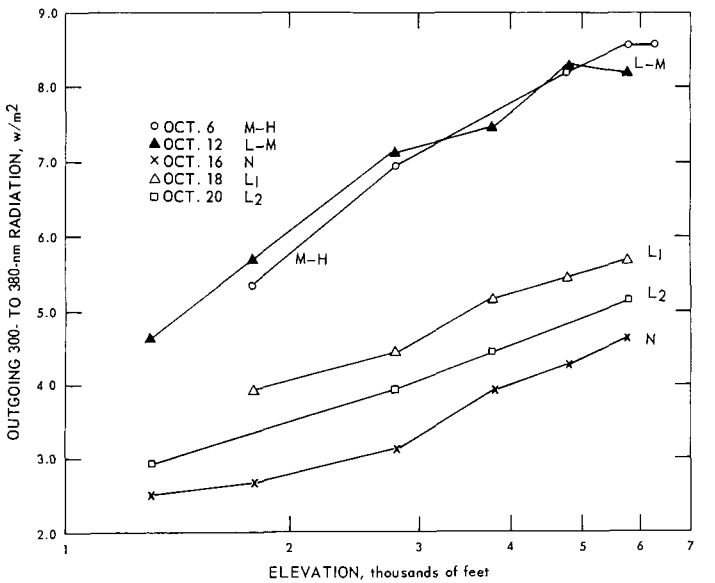

Figure 8-6. Outgoing radiation as a function of elevation over Los Angeles for various days of smog for the time interval 1000 to 1100.

☆ U. S. GOVERNMENT PRINTING OFFICE : 1968 O - 291-029

BIBLIOGRAPHIC: Nader, John S. Pilot study of ultraviolet radiation in Los Angeles, October 1965. PHS Publ. No. 999-AP-38. 1967. 91 pp.

ABSTRACT: Several research groups combined efforts to measure simultaneously the available ultraviolet radiation of the urban atmosphere of Los Angeles under representative environmental conditions. The study was planned to permit evaluation of possible methods of measuring the UV radiation important in photochemical reactions (in the range from 300 to 400 nanometers) and to obtain preliminary data on the UV radiation energy with respect to location, elevation, and time of day. Measurements were made on five days at various levels of air pollution ranging from no smog to moderate-to-heavy smog.

ACCESSION NO.

KEY WORDS:

Instrumentation

Measurements

Methodology

Ultraviolet Radiation

Photochemistry

Air Pollution

Smog

Ultraviolet Detection

BIBLIOGRAPHIC: Nader, John S. Pilot study of ultraviolet radiation in Los Angeles, October 1965. PHS Publ. No. 999-AP-38. 1967. 91 pp.

ABSTRACT: Several research groups combined efforts to measure simultaneously the available ultraviolet radiation of the urban atmosphere of Los Angeles under representative environmental conditions. The study was planned to permit evaluation of possible methods of measuring the UV radiation important in photochemical reactions (in the range from 300 to 400 nanometers) and to obtain preliminary data on the UV radiation energy with respect to location, elevation, and time of day. Measurements were made on five days at various levels of air pollution ranging from no smog to moderate-to-heavy smog.

ACCESSION NO.

KEY WORDS:

Instrumentation

Measurements

Methodology

Ultraviolet Radiation

Photochemistry

Air Pollution

Smog

Ultraviolet Detection

BIBLIOGRAPHIC: Nader, John S. Pilot study of ultraviolet radiation in Los Angeles, October 1965. PHS Publ. No. 999-AP-38. 1967. 91 pp.

ABSTRACT: Several research groups combined efforts to measure simultaneously the available ultraviolet radiation of the urban atmosphere of Los Angeles under representative environmental conditions. The study was planned to permit evaluation of possible methods of measuring the UV radiation important in photochemical reactions (in the range from 300 to 400 nanometers) and to obtain preliminary data on the UV radiation energy with respect to location, elevation, and time of day. Measurements were made on five days at various levels of air pollution ranging from no smog to moderate-to-heavy smog.

ACCESSION NO.

KEY WORDS:

Instrumentation

Measurements

Methodology

Ultraviolet Radiation

Photochemistry

Air Pollution

Smog

Ultraviolet Detection

This report is a compilation of data obtained by the several participants, with brief accounts of instrumentation and procedures. The instrumental sensors used to detect the UV radiation were filter photocell, filter phototube, photochemical sensors, photosensitive plastic, and photochromic glass. Air quality and meteorological data for the sampling periods are also presented. A discussion and summary relates the data obtained in measurements by the different methods and at the various locations.

This report is a compilation of data obtained by the several participants, with brief accounts of instrumentation and procedures. The instrumental sensors used to detect the UV radiation were filter photocell, filter phototube, photochemical sensors, photosensitive plastic, and photochromic glass. Air quality and meteorological data for the sampling periods are also presented. A discussion and summary relates the data obtained in measurements by the different methods and at the various locations.

This report is a compilation of data obtained by the several participants, with brief accounts of instrumentation and procedures. The instrumental sensors used to detect the UV radiation were filter photocell, filter phototube, photochemical sensors, photosensitive plastic, and photochromic glass. Air quality and meteorological data for the sampling periods are also presented. A discussion and summary relates the data obtained in measurements by the different methods and at the various locations.